Project Number: ME-RLN-0701

ASSEMBLY MACHINE SCRAP REMOVAL STATION REDESIGN

A Major Qualifying Project Report

submitted to the Faculty

of the

WORCESTER POLYTECHNIC INSTITUTE

in partial fulfillment of the requirements for the

Degree of Bachelor of Science

by

Michael Ardito	Kyle Cypher	Loren Gjata	Steven McHugh

Date: December 13, 2007

Approved:

_____

Professor Robert L. Norton, Advisor

Acknowledgements

Our MQP team would like to thank the following individuals from WPI and the Sponsoring Company for their dedication and help throughout the course of this project:

- Professor Robert Norton
- Charlie Gillis
- Jamie Ulery
- Neil Cicciu
- Jack Carrozzo
- Al Duchemin
- Joe Kodzis
- Tim Sweet
- Daniel LaBelle
- Ernie Chandler
- Adam Lane

Abstract

This project improved the function of a cam-driven station on an assembly machine at the sponsoring company. The station consisted of three systems working in conjunction with each other to remove excess material from an indexing conveyor. Before this redesign, the station had been experiencing reliability problems resulting in unprofitable down time. The goal of this project was to improve the reliability of the station by reducing the vibrations present in the system. Vibration was reduced by redesigning two cams, two shafts, and adding an air cylinder to remove play in a linkage. The baseline for analysis was established through dynamic modeling, finite element analysis, and experimental data collected on the machine. New designs for cams, shafts, and air cylinder were manufactured and installed. Tests of the new design showed a reduction of impacts and vibrations of between 55 and 60% as compared to the original design. The redesigned parts have been left on the production machine to accumulate long-term data on their improved function and reliability.

Executive Summary

The goal of this project was to redesign components of the excess material removal station in order to reduce machine down time, noise levels, and scrap. The vacuum system and the stripper system of this station were determined to have the most impact on machine down time and were redesigned.

The redesign process began with the creation of a lumped mass and stiffness model of each linkage of the system. Effective mass calculations were based on mass properties obtained from Pro/Engineer computer models of each link or other machine part. Effective stiffness calculations were based on hand calculations and finite element analysis utilizing SolidWorks. Using the effective mass and stiffness of the dynamic system as felt at the cam roller follower, program Dynacam analyzed the dynamic model and predicted vibration responses. Data was collected from the production machine using accelerometers, signal analyzer, linear variable differential transformer (LVDT), and pressure gages to verify the validity of the Dynacam models.

Accelerometer data indicated that the vacuum linkage was experiencing impact and over-travel not designed into that subsystem. The strategy for reducing the intended impact in the vacuum linkage was to reduce the velocity of the end effector before and at impact by redesigning the cam profile of the linkage. Accelerometer data also suggested that the over-travel experienced by the vacuum linkage was absorbed by a weak shaft acting as a torsion bar. The diameter of both the vacuum shaft and the stripper shaft were enlarged to increase the effective stiffness of the linkages and subsequently reduce vibrations. The frame holding the shafts was also redesigned to accommodate the new shafts. Impacts occurring due to loose tolerances in the stripper linkage were eliminated with the addition of an air cylinder to provide backward

pressure on the stripper slide and eliminate slack in the linkage. The cam for the stripper linkage was redesigned because the existing cam was an out-dated cycloidal design.

Additional accelerometer data was taken with the new cams, new shafts, and air cylinder to determine the effect of these changes on the performance of the station. Implementation on the station of the new cams alone resulted in virtual elimination of the impacts experienced by the vacuum linkage. The impacts seen on the stripper linkage due to loose tolerances were completely eliminated by addition of the air cylinder on the back of the slide. The addition of the new shaft on the vacuum linkage reduced its vibrations but the new shaft for the stripper linkage caused vibrations greater than those with the new cam and air cylinder alone. The peak accelerations in both linkages were not increased with the addition of the new shafts.

Several recommended changes result from this project. It is recommended that the cams designed in this project be implemented on both the vacuum and stripper systems. For the stripper system, it is also recommended that a suitable bracket be manufactured to attach an air cylinder to the back of the slide as is currently present on the vacuum and stabilizer slides. It is recommended that the vacuum linkage shaft diameter be increased to 1 inch. It is recommended that the shaft for the stripper linkage should not be changed from its original diameter since doing so increased vibrations compared to the results obtained from the new cam and air cylinder alone, although both configurations were better than the original.

Table of Contents

List of Figures

List of Tables

1. Introduction

The sponsor company uses an indexing machine to load metal product into a traveling nest, weld metal product to a support piece, and unload the finished assemblies into a magazine. The process leaves a scrap piece on the nest, which is removed at the end of the conveyer line. When this scrap or "excess material removal" station fails to perform, the machine must be shut down and manually cleaned. This downtime is undesirable, and it is believed that a redesign of the excess material removal station will alleviate this problem. High levels of vibration and high speed impacts are most likely responsible for the system's misbehavior. The linkages and cams will be investigated to determine possible redesigns which will reduce impacts and vibration in this system.

Currently, the excess material removal station consists of three, synchronous, cam-driven linkages. These linkages move three sets of tooling which respectively qualify the position of the nest, remove the scrap piece, and unload it.

In order to perform this task, we began by creating several mathematical models and a CAD solid model of the station and its three synchronous cam driven linkages. We verified the validity of this model experimentally by doing accelerometer tests on the machine while it made product. Using these models and test data, we then identified the most problematic linkages and components of these linkages. These components were redesigned, and effects of the redesigned components were simulated using our mathematical models. Finally, we manufactured and installed the new components to experimentally verify that vibrations and impacts had been reduced.

In the following report, we will detail some background information on the excess material removal station. We will describe the methodology used to create and test our models,

as well as create and test our redesigned parts. We will then provide the results of our redesign, and, finally, provide further recommendations and conclusions.

2. Background

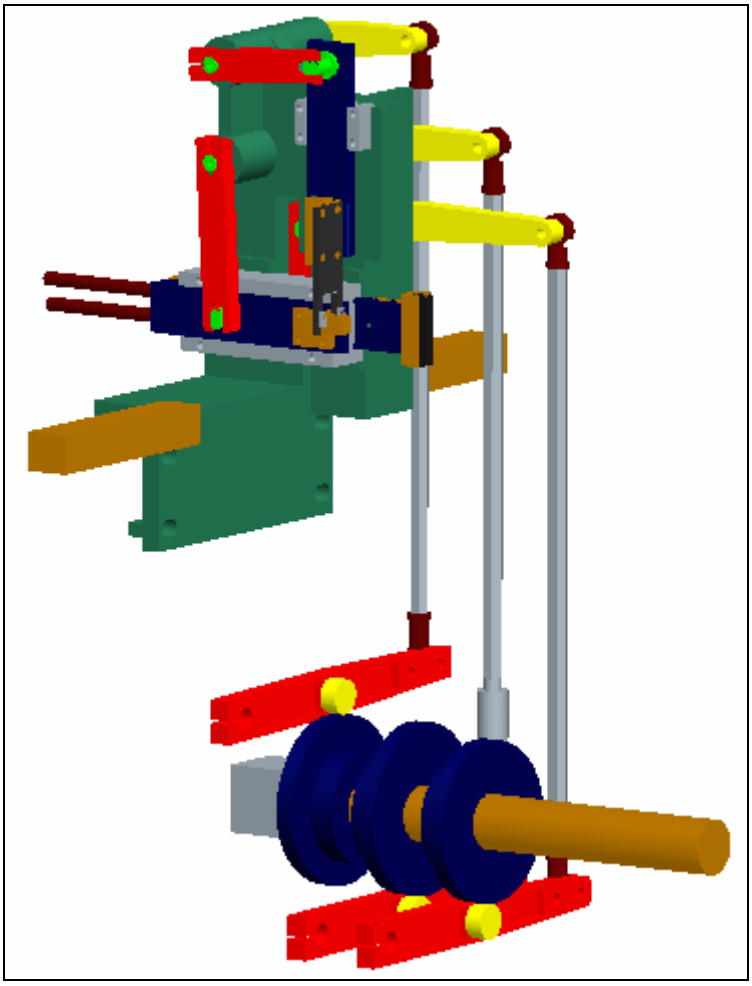

Figure 1: Removal Station

The removal station seen in Figure 1 is one station in an assembly machine whose function is to remove excess product material from the conveyer nest nest and drop it down a chute for recycling. It has been partially upgraded throughout the years to operate at higher speeds in order to meet increased product demand. The station consists of three systems, all of which were analyzed as part of this project. These systems are the Stabilizer mechanism, the Vacuum pickup mechanism, and the Stripper mechanism.

The stabilizer and vacuum systems interact directly with the nest, which is attached to an indexing conveyor. There are many nests attached to the conveyor. The removal station performs the same operations to each nest: stabilizing the nest, removing material with a vacuum head, and stripping material off the vacuum head. According to the engineers of the sponsoring company, the operation that is causing the most problems is removal of material from the nest with the vacuum head.

The vacuum system uses suction to remove the excess material from the nest. In order to successfully perform this operation, the vacuum head needs to be perfectly aligned with the nest. Because of the stop-and-go motion of the conveyor, the nest experiences vibrations that cause the nest sometimes to misalign with the vacuum head. The stabilizer system keeps the nest stationary by touching it (essentially like a brake). The third and last operation is to strip the material off the vacuum head after it has retracted from the nest. This operation is done by the stripper system that uses a two-pronged fork that passes in front of the vacuum head, stripping away the excess material and causing it to drop down a chute. Figures 2 and 3 show the assembly of the systems and the nomenclature used to describe the components.

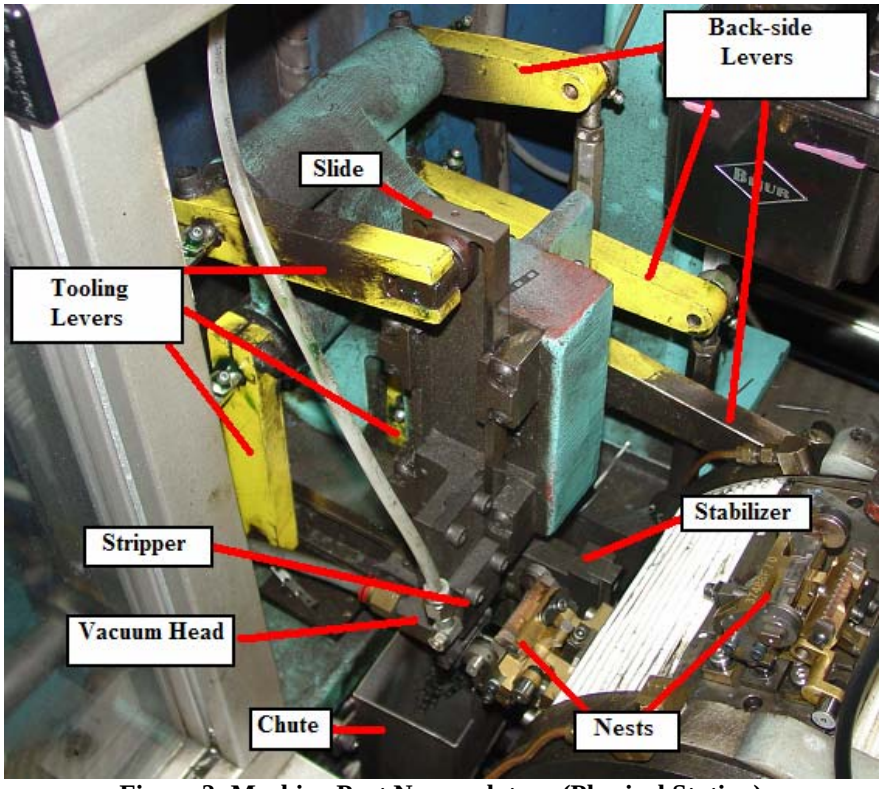

Figure 2: Machine Part Nomenclature (Physical Station)

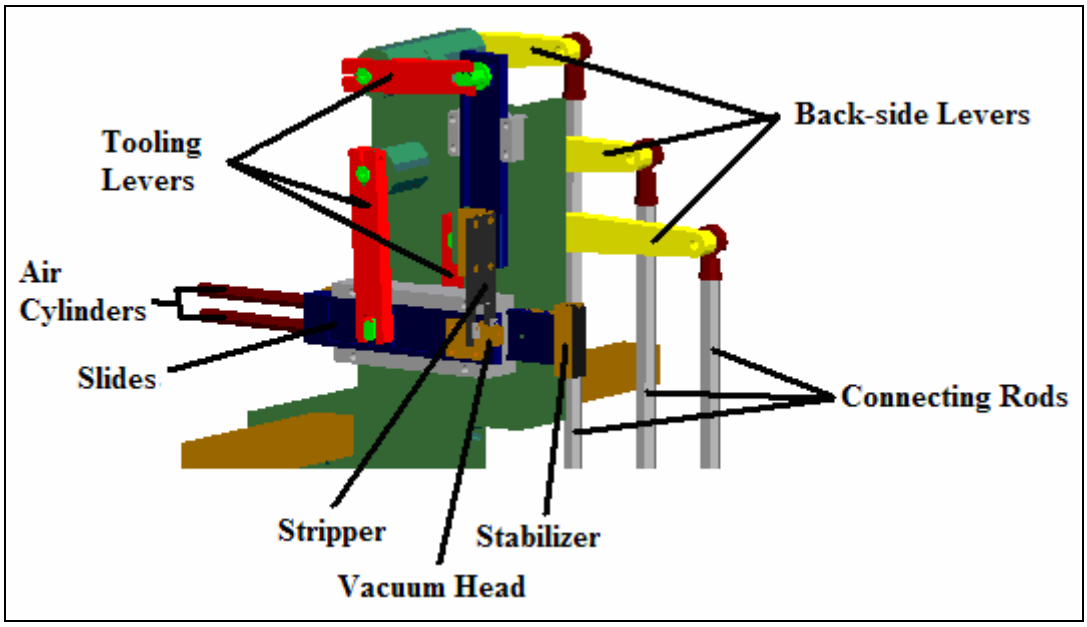

Figure 3: Machine Part Nomenclature (CAD Model)

The stabilizer system and the vacuum system motions are both horizontal while the stripper system motion is vertical. Each of the three systems is driven by a separate cam. When the nest is in position, the stabilizer moves forward in order to align and hold the nest in position.

Then the vacuum head moves forward to make contact with the excess material, which is held on the nest magnetically. The vacuum head uses suction to remove and hold the excess material. The vacuum head dwells momentarily against the nest and the excess material is suctioned onto the vacuum head before it backs away from the nest. As soon as the vacuum head leaves the nest, the stabilizer also moves back from the nest in order to allow the conveyor to move the next nest into position. As soon as the vacuum head stops for a dwell in its fully retracted position, the stripper begins its downward motion to push the excess material off the vacuum head and into a chute. While the stripping operation occurs, the stabilizer begins its forward movement again, the vacuum head follows soon after. Then the stripper begins its upward movement to get in position to repeat its operation.

2.1. Stabilizer System

The purpose of the stabilizer system, shown in Figure 4, is to align the nest and hold it steady while the vacuum head performs its operation. The movement of the stabilizer is horizontal. When the nest is in position, the stabilizer moves forward and contacts a metal plate called the carrier (a part of the nest assembly that attaches the nest to the conveyor belt). Because of the geometry of the end effector of the stabilizer, light contact with the carrier is enough to stabilize the nest. After the vacuum head leaves the nest, the stabilizer also moves backward and away from the carrier. The conveyor then moves the next nest into position. The process then repeats with the stabilizer moving forward toward the carrier.

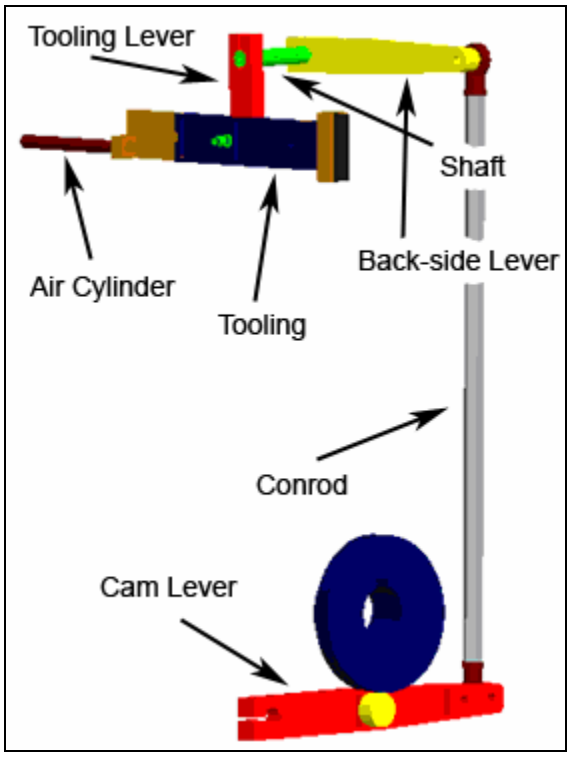

Figure 4: Stabilizer System

The cam for this system is a single-dwell 3-4-5-6 Polynomial. The dwell corresponds to the time when the end effector is contacting the carrier. Cam rotation causes the cam lever to move up and down which in turn causes the back-side lever of the stabilizer system to move up and down via a connecting rod. An air spring is attached to the cam lever which serves to keep the follower in contact with the cam. The connecting rod has ball joint bearings at each end because the movement of the levers is not purely vertical; they trace an arc as they move up and down.

The shaft connects the back-side lever to the tooling lever, as seen in Figure 4. These two levers are offset by 90°, converting the vertical motion of the back-side lever to the horizontal motion of the tooling lever. The tooling lever is slotted and connected via a pivot pin to a slide which holds the end effector. This pivot pin is necessary because the motion of the slide is purely horizontal while the motion of the lever traces an arc. The slide moves inside of a slide housing

to ensure horizontal motion. An air cylinder is attached to the back of the slide with the piston up against the slide housing to provide backward pressure on the slide connection. The reason for this forward pressure is to compensate for any clearances in the many links and joints of this system. A small pressure on the slide connection gets rid of any looseness that might be present between the pivot pin and the tooling lever when the movement changes direction, thereby eliminating backlash.

The existing stabilizer system has a better cam design than either of the other two systems. It is believed that this cam has been redesigned once in the past because its design differs markedly from that of the other two cams.

2.2. Vacuum System

The purpose of the vacuum system, shown in Figure 5, is to remove the excess product material from the nest. The movement of the vacuum head is horizontal. This system's operation is similar to that of the stabilizer system except its function is different. It moves forward until it touches the nest and dwells for a short period of time to ensure that proper suction is created between the excess material and the vacuum head. Light contact with the nest is sufficient to create suction. Then the vacuum head moves backward away from the nest and dwells again to allow the stripper system to remove the material from the vacuum head. Then it repeats the operation starting with the vacuum head moving forward into the nest.

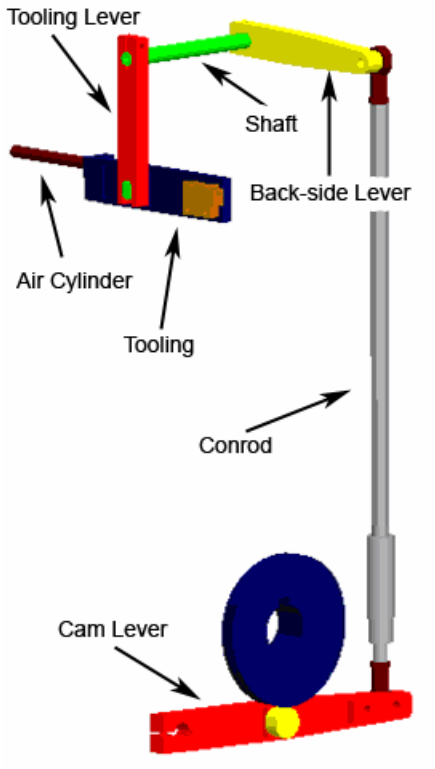

Figure 5: Vacuum System

The vacuum linkage is made up of the same type of links as the stabilizer system. The cam for this system is a double-dwell cycloidal. The cam lever is attached to a ground link at one end and on the other end to an air spring that ensures contact between the cam and the follower. Also attached to the cam lever is a connecting rod that contains an air cylinder. This is the only system of the machine that has an air cylinder in series with the connecting rod. The air cylinder is constantly extended during normal machine function but it can be depressurized to allow the operator to clear any jams. The connecting rod that includes the air cylinder is connected to the cam lever and the back-side lever in the same fashion as it was for the stabilizer system. This connecting rod also has ball-joint bearings which allow for the arc motion of the levers.

The vertical motion of the cam lever and its back-side lever is converted to a horizontal motion through a shaft in the exact same fashion as the stabilizer system with a 90° offset between the back-side lever and the tooling lever as seen in Figure 5. The tooling lever is slotted

and connects via a pivot pin to a slide which contains the end effector. This slide has an air cylinder connected on the back which provides backward pressure in order to eliminate any looseness due to tolerances between the pivot pin and the tooling lever.

Originally, on this machine the end effector of this linkage performed its function mechanically instead of using suction. This original design created many problems especially at higher running speeds, so the mechanical end effector was replaced with a vacuum head. The original vacuum head contained a valve to turn suction on and off to remove or release the excess material, respectively. Problems arose as small metal particles were occasionally being sucked into the valve, preventing the valve from performing its proper function. The design was changed to a vacuum head with continuous suction and mechanical stripping as presently installed. The cam for this linkage is a double-dwell cycloidal motion which leaves considerable room for improvement.

2.3. Stripper System

The purpose of the stripper system, shown in Figure 6, is to remove the excess product material from the vacuum head. This is accomplished using a two-pronged tool which moves vertically up and down. During the downward motion, the end effector catches the excess material and strips it off the vacuum head, breaking the suction of the vacuum and causing the material to fall down a chute. The downward motion of the stripper occurs while the vacuum system is at its back dwell. The upward motion of the stripper occurs while the vacuum head is moving forward into the nest.

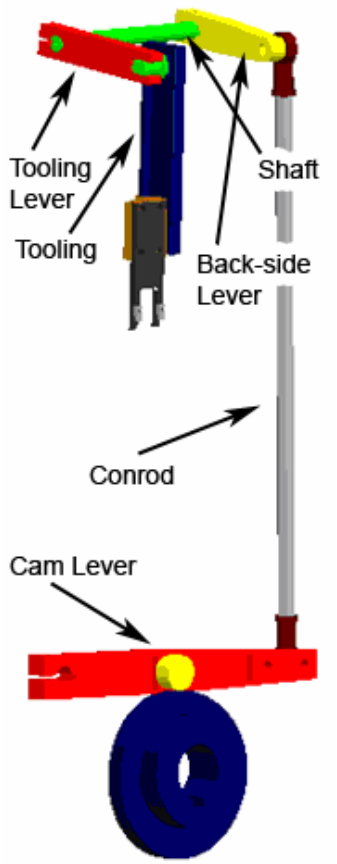

Figure 6: Stripper System

The stripper linkage contains the same type of components as the other two systems. It differs from the other systems in its movement, the length of the links, and its end effector. Another difference between the stripper and the other two systems is the location of the cam lever. The cam lever is located above the cam for the stripper system while for the other two systems it is located below the cam. The location of the cam lever shortens the length of the connecting rod for the stripper system. The connecting rod connects the cam lever and the back-side lever in the same fashion as in the other systems.

The up and down movement created by the cam is not converted to a horizontal movement in the case of the stripper system. The shaft is still present connecting the back-side lever to the tooling lever but the two levers are oriented in the same direction so the movement stays vertical. There is still a slot on the tooling lever where a pivot pin connects this lever to the

slide. The slide for the stripper system does not contain an air cylinder like the slides of the other two systems. The fact that this slide does not contain the air cylinder causes vibration problems for the stripper system as will be seen.

3. Goal Statement

The excess material removal station has been responsible for machine down time on a regular basis. This station's reliability needs to be improved in order to reduce down time. It is likely that the vacuum system within the excess material removal station is causing the reliability problem. However, all linkages need to be evaluated in order to identify problems and redesign if necessary. Since vibrations anywhere in the system may also cause reliability problems, these should also be reduced or eliminated. The ideal design will result in the excess material being removed from the nest every time and collected for recycling. In addition to improving reliability, noise levels of the machine should also be reduced if possible.

4. Modeling

In order to understand the machine and to effectively analyze it, we created several different models. We created a CAD model using Pro/Engineer in order to better understand the motions of the machine and how the different linkages interact with each other. The CAD model also served to provide mass properties of all the modeled parts based on their geometry and material. In addition to the CAD model we created motion models using Dynacam. One of these models produced the motion of the cam follower without considering the rest of the linkage. This model was called the theoretical motion model.

Because, in reality, all the links have mass and will deform under loading, the motion of the end effector will differ slightly from the motion of the cam follower. To account for the

masses and the deformations of the links, a dynamic motion model was created which took into account the effective mass and stiffness of all links as felt at the roller follower.

4.1. Theoretical & Dynamic Motion Models

To analyze the motion of the linkage, we needed to create models of the follower's motion, and these models could then be converted into the motion of each link. The theoretical motion model describes the motion of the cam follower without considering the rest of the linkage. The dynamic motion model describes the motion of the cam follower when taking into account the mass and spring constants of the linkages it is attached to. Dynacam was used to analyze these models. The displacement, velocity, and acceleration output of the models was exported from Dynacam and converted into graphs against degrees for every 0.125 degree.

4.1.1. Theoretical Motion Model

The theoretical motion model for the existing systems was created by taking the information on the cam drawings, such as the timing diagrams, and creating the existing profile functions in Dynacam. For the cycloidal cams, this process was done by simply creating the appropriate number of dwell, rise and fall segments, setting the rise and fall segments to "Cycloid Full," and inputting the angular displacement of the follower. For the polynomial cam, we created the appropriate number of dwell and polynomial segments and input seven boundary conditions, including the angular displacement of the follower. Dynacam then computed the cam profiles and the motion of the follower.

4.1.2. Dynamic Motion Model

The spring constants for the links were found by using finite element analysis (FEA) software, in SolidWorks specifically. For the simple levers, the tooling and back levers for all

linkage trains, the end on the shaft was fixed and a dummy force was applied where the conrod was connected. The point where this dummy force was applied was offset laterally from the center of the link so that twist of the lever was taken into account. The FEA software found the resultant displacement from the applied force. The spring constant was the applied force divided by this displacement.

Finding the spring constant of the cam levers was more involved because of their complex loading conditions. Moving along the cam lever, the levers are connected to a bearing on one end, then the cam roller, then the cam spring, then the connecting rod (conrod) on the opposite end. The loading setup is shown in Figure 7. We were interested in the spring constant of the lever for a given force applied on the lever at the point where the conrod connects to it. In order to find the spring constant at the conrod we first ran the FEA without any force on the conrod, only the spring force calculated by its pressure preload, and the constraints of the bearing and the roller to find the displacement. Then we ran the FEA with a realistic force applied on the conrod pin, the resultant displacement was noted. The spring constant from the perspective of the force applied on the conrod was calculated as the conrod force divided by the change in displacement of the conrod point (the displacement found with an applied conrod force minus the displacement found without a conrod force).

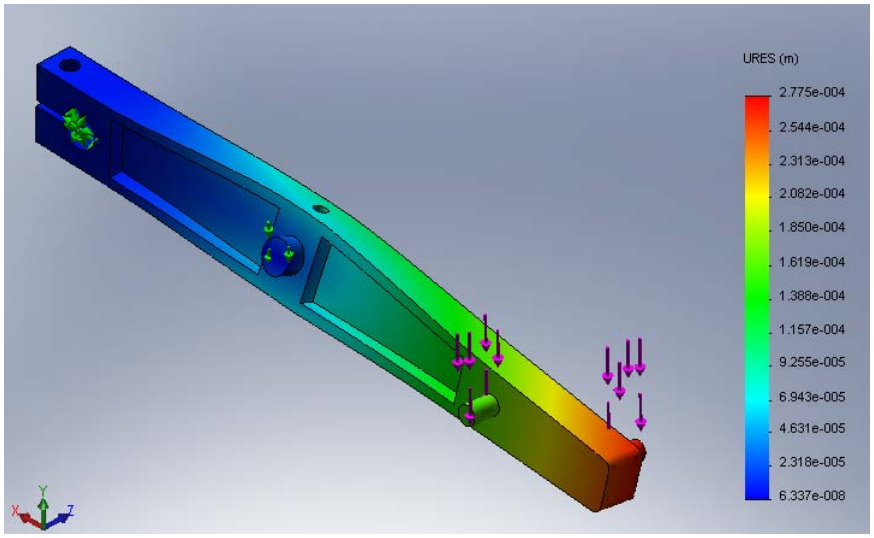

Figure 7: FEA of Cam Lever

The spring constants of the conrod, shafts, and tooling were calculated manually because of their simplicity or, in the case of the tooling, irrelevance.

These spring constants were combined in series and with the correct lever ratios, where appropriate, to find the overall spring constant of the entire linkage train, for each of the three systems of links. The individual components' spring constants were multiplied by the relevant lever ratios to find the stiffness of each link at the follower.

The lumped mass model was found by combining the effective masses of each link in the linkage train. The actual mass and moment of inertia of each link was found using the pro/Engineer model. We performed a mass properties analysis of the individual parts after setting the correct density for the material properties in pro/Engineer and creating/selecting a coordinate system in the correct place, usually about a connecting axis for the levers. The effective mass of each lever was found by dividing the link's mass moment of inertia by the squared length of the lever (pivot to pivot). The effective mass of links, like the tooling and the conrod, that translate in a straight line (or nearly a straight line) is their actual mass. These effective masses were

combined with the proper lever ratios for the levers on the shaft and the cam lever to find the overall effective mass for each of the three linkage trains.

4.2. CAD Model

To run FEA on all the parts and understand how the linkages run, we needed to develop a CAD model. We used drawings for the frame and all the moving parts at our station to design these parts in pro/Engineer. Additionally, we used Dynacam to create the profiles for the cams and exported them into a text file that we then imported into pro/Engineer. For all the parts we defined the appropriate material properties, specifically mass density, depending on the material specified on the drawings. We then chose the dynamic connections to most accurately reflect reality. We added a servo motor to each cam and defined the speed based on the parts-per-minute of the machine we did our testing data on.

4.3. Experimental Data

In order to determine the validity of our models, we performed tests that measured the time domain and frequency domain linear spectra of the accelerations for each linkage. We then compared these to the values calculated by our simulations in Dynacam and also analyzed them to determine the areas most in need of redesign. We measured acceleration and linear spectra data for the tooling, cam, and back-side levers of each linkage train. In order to compare simultaneous motions of different linkages, we had to synchronize the time domain data manually with machine zero by visual comparison with the theoretical cam profile. We acquired this data using a Hewlett-Packard dynamic signal analyzer, model number 35670A.

Using Dytran accelerometers, model #'s 3055B4 and 3055B1, we measured the acceleration close to the conrod connection of the cam levers and back-side levers, and on or near the tool of the tooling levers. From Figure 8, we can see the placement of accelerometers.

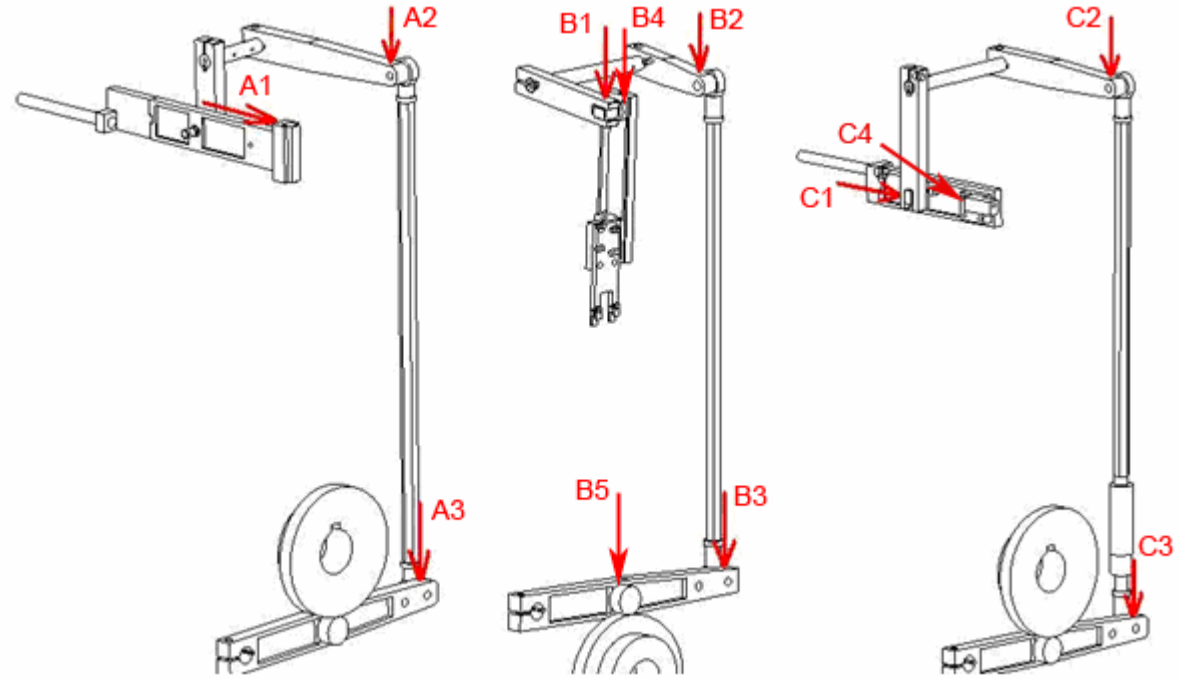

Figure 8: Stabilizer, Stripper, and Vacuum Accelerometer Placements

The accelerometers measured in real time taking 4096 acceleration measurements and 1600 frequency measurements over a 0.500 second interval. We averaged over 10-25 cycles for most of our data in order to reduce noise. For some tests we were able to use a peak of the acceleration curve to ensure that the measurement triggered at the same point in the cycle each time. This trigger, however, often proved to be unreliable, and we collected the remainder of the test data using a Turck inductive proximity sensor, part number Ni4U-EG08-AP6X-V1131, which was placed at an arbitrary lever arm on the machine that moves synchronous with the measured linkages. The proximity sensor outputs a signal to the data analyzer when metal is within 4 mm of the probe. As the metal lever arm moved in and out of range of the sensor, a

pulse was sent to the data analyzer at the same point in each cycle. This was then used as the trigger to line up our cycle averages.

4.4. Graphs of Theoretical & Dynamic Motions with Experimental Data

We combined the experimental data collected with the graphs of the theoretical and simulated dynamic motions with two purposes in mind. First of all, these embedded graphs allowed us to compare what the linkages should be doing with what they were actually doing. Secondly, these embedded graphs proved that our theoretical and dynamic motion models reasonably matched our experimental data, which justified using our theoretical and dynamic models to analyze new designs.

To create these graphs we began by transforming the experimental data to match the graphs of the theoretical and dynamic motion models. The first thing we did to transform the data was to determine the direction the accelerometer's motion in relation to the direction of the cam follower's motion. We determined the direction of accelerometer's motion based on what side of a lever it was on. A direction vector that travels from the bottom to the top of the accelerometer is positive motion according to its frame of reference. If the direction of the accelerometer's motion was the opposite of the direction of the cam follower's motion, then all the experimental data for that set was multiplied by negative one. The second thing we did to the data was to center it about zero. To do this we found the average of the data and subtracted it from all the values. This was necessary because the piezoelectric accelerometers do not give an accurate DC value.

The motion output from Dynacam is the acceleration of the cam follower in deg/sec^2. However, the output of the experimental data is in g's of acceleration, measured at specific locations on each of the nine levers at which we took data. To find the displacement in meters

we first calculated the projected distance from the axis of rotation of the specific lever to the position of the accelerometer on it. We then multiplied this value by the conversion to radians (π/180) to get meters per degree. This constant was then divided by 9.81 m/sec^2 to obtain g*sec^2/deg. Finally, all of the Dynacam output was multiplied by this conversion factor to obtain the theoretical and dynamic accelerations in g's. Additionally, all displacement and velocity data from Dynacam, also in degrees, were multiplied by the meters per degree constant to obtain appropriate graphs. This process was repeated for all nine of the tested levers.

The motion output from Dynacam is not measured from machine zero, but rather references zero degrees from the starting point of the cam function. Moving all theoretical and dynamic motion curves to machine zero allows the three linkages to be lined up in time. Therefore, we needed to subtract the starting angle of the cam from 360 and start the graph at that degree value of the Dynacam output and end at that value plus 360. This method is displayed in Figure 9.

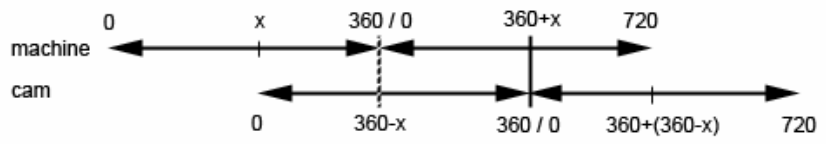

Figure 9: Phase Shift Diagram

The next step was to line up the experimental data with the theoretical and dynamic motion curves by also shifting the experimental data to machine zero. The zero acceleration points are the easiest to recognize in the experimental data because that is where the acceleration goes from some magnitude to zero. Therefore, we shifted the data by finding the difference on the time scale between the first zero acceleration point in theoretical motion curve and the matching zero acceleration points in the experimental data. The experimental data was then shifted forward or backward from time zero by this difference. To shift backward from zero the

experimental data was actually shifted forward by the time for one cycle minus the difference found.

Once the data had all been properly shifted to machine zero, we checked to make sure that our theoretical and dynamic models matched the experimental data. A good example of the models and data matching is seen in the graph labeled Figure 10.

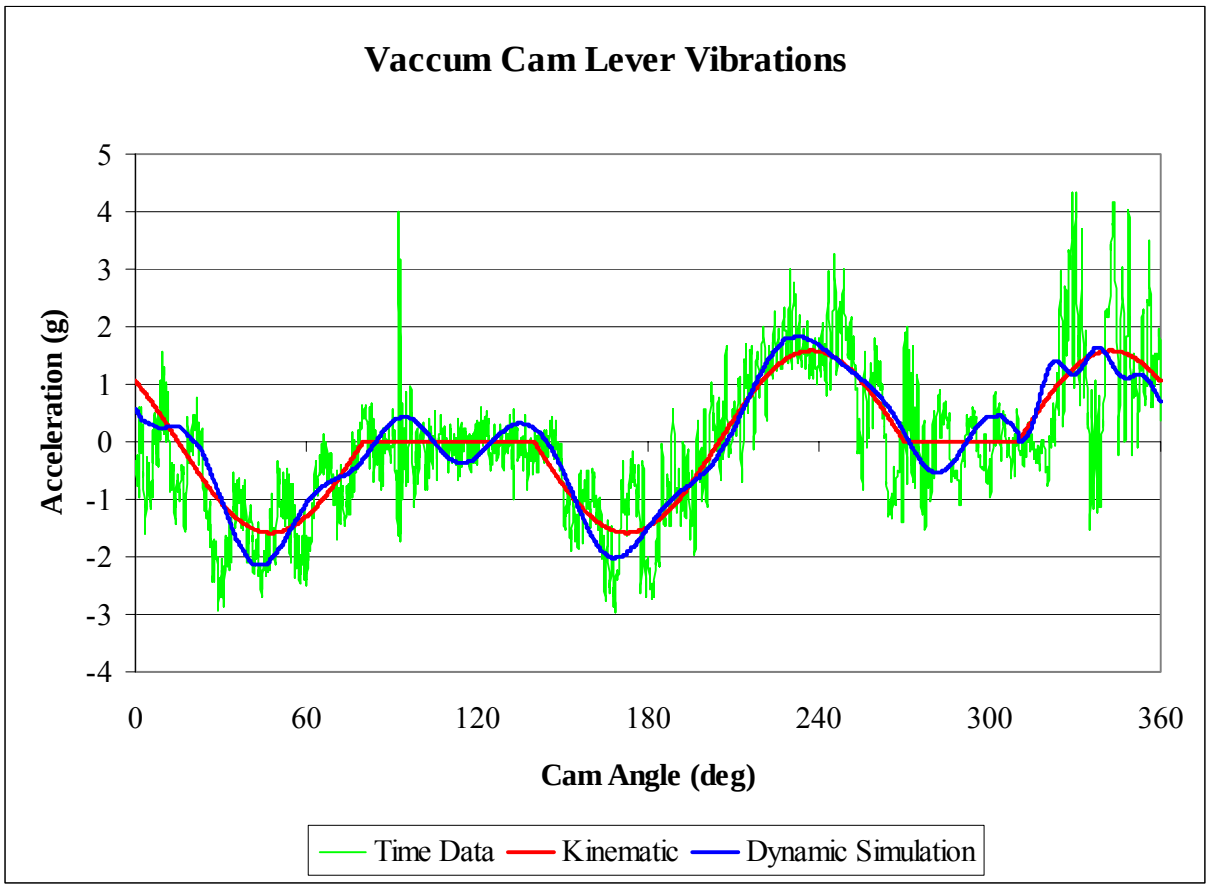

Figure 10: Vacuum Cam Lever Vibrations (C3 in Figure 8)

One indication of the match is that the theoretical and dynamic model curves pass through the fluctuating experimental curve. Another indication is that the theoretical and dynamic model curves transition from negative to positive at about the same time as the experimental data. Establishing that the experimental data matches the theoretical and dynamic data justifies using the theoretical and dynamic models to evaluate iterations of our improved designs.

5. Analysis

An extensive analysis of the machine was performed using the gathered experimental data and the computer models. All aspects and components of the station were analyzed, including cams, shafts, air cylinders, end effectors, and levers. The analysis consisted mostly of comparing gathered experimental data to data obtained from computer models. These comparisons served to identify areas for improvement as well as to verify that our models were an accurate representation of the actual machine. Several conclusions were drawn from the experimental data, calculated data, and observations.

5.1. Cam Motions Are Not Ideal

In the existing design, the stripper cam and the vacuum cam used cycloidal rises and falls which, though easy to calculate and machine, are not ideal for reducing acceleration, and offer no control over the interiors of the s-v-a-j curves. In addition, the cam profiles have large discontinuities in jerk that cause large vibrations which can be seen in both the dynamic simulations from Dynacam and in the accelerometer test data. Likely, these cam profiles have not been redesigned from the original cams.

5.1.1. Vacuum Cam

Our test data shows that the vacuum linkage strikes the nest far earlier than intended. This impact can be seen as a large spike in acceleration that is marked in Figure 11.

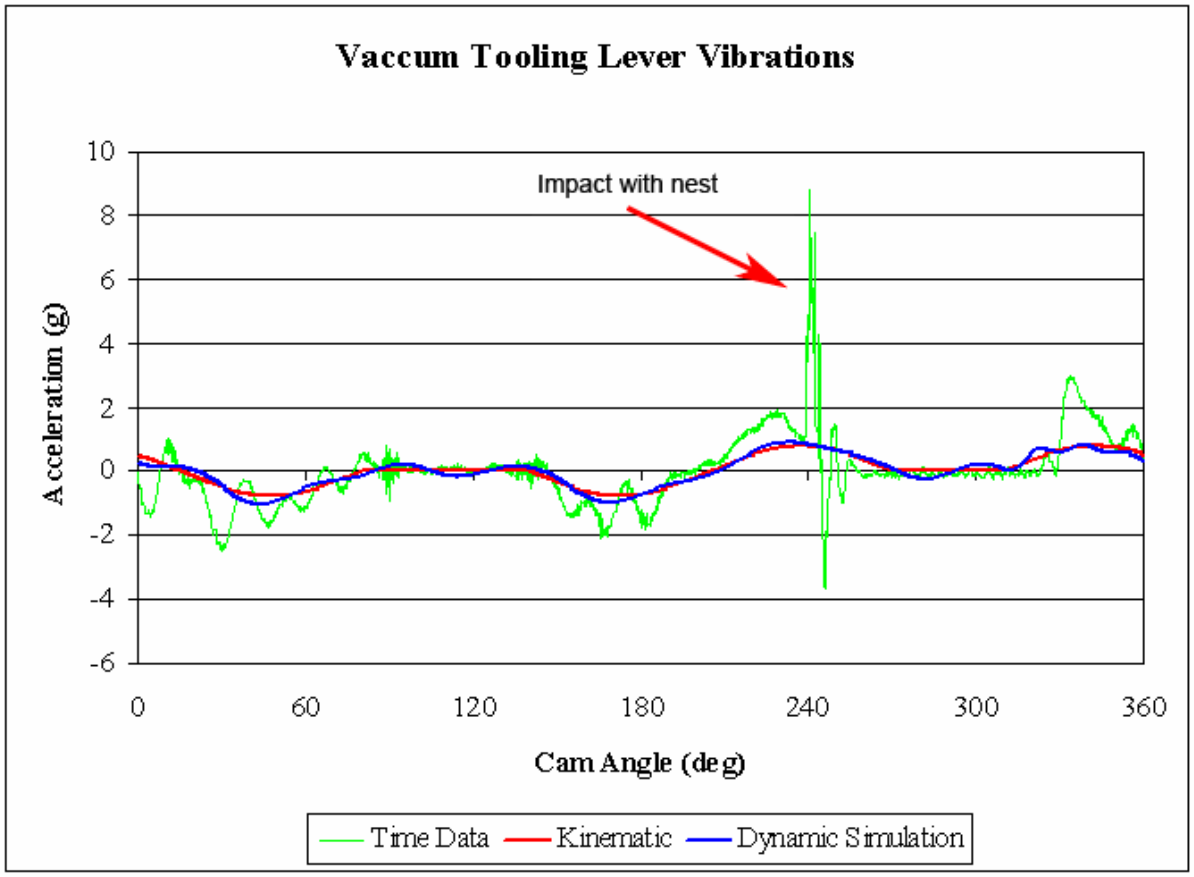

Figure 11: Vacuum Tooling Lever Vibrations (C1 in Figure 8)

As the impact occurs while the cam is still in the midst of a fall, the velocity at impact is quite high and we can see this impact ringing out through the dwell of the vacuum linkage, as well as showing up as minor vibrations in the stabilizer linkage. These vibrations that were transferred through the nest can be seen in Figure 12. Originally, we believed the impact was intended to occur before the dwell with a resulting over-travel. Upon further review of the mechanic's set up manual for the excess material removal station, we discovered that the design intent is for the vacuum tooling to hit the nest exactly at the beginning of the dwell, as only a light touch is needed to form a vacuum seal. However, this does not appear to occur in practice.

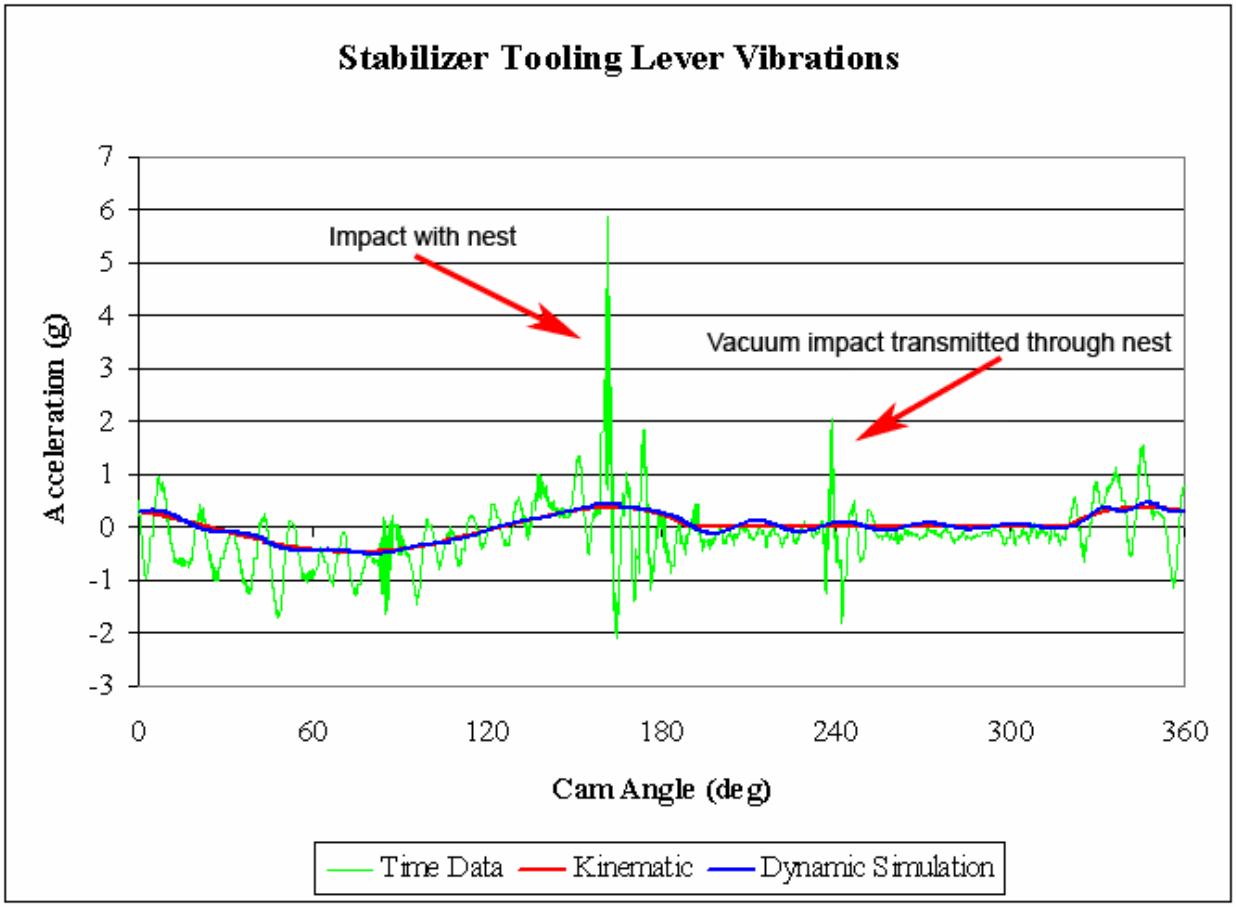

Figure 12: Vacuum Impact with Nest Translated to the Stabilizer (A1 in Figure 8)

5.1.2. Stripper Cam

The stripper cam has an asymmetric rise-fall motion with no dwell and uses cycloidal motions on both rise and fall, which is less than optimal. Its acceleration curve also has unnecessary returns to zero which cause unnecessarily large accelerations and increased vibrations.

5.1.3. Stabilizer Cam

The stabilizer cam has a polynomial function profile and lower peak accelerations than the other two cams. In addition, the stabilizer linkage has a much shorter (thus stiffer) shaft reducing its vibrations in comparison to the other two linkages.

5.2. Shafts Are the Weakest Components

The CAD model created in Pro/Engineer provided us with the masses and mass moments of inertia of every component on the machine that was modeled. This enabled us to calculate the effective mass of the system at the cam follower. However, to determine the stiffness of each link on the machine, we completed a finite element analysis (FEA) on all the levers, including the cam levers, using the CAD program Solidworks. This process is described in section 4.1.2. Table 1 summarizes the masses, spring constants (or stiffnesses), and the effective masses and effective spring constants at the follower for the moving components of all three linkages.

Table 1: Effective Masses and Siffnesses of System Components

Name	*Weight (lb)*	*Mass (kg)*	*Stiffness (lb/in)*	*Stiffness (N/m)*	Eff Mass at Follower (kg)	Eff Stiffness at Follower (lb/in)
Stabilizer Lever Nest Plate Square	2.00	0.91	17,409	3,048,780	4.51	86,381
Stabilizer Slide Lever	0.67	0.31	141,197	24,727,992	0.21	96,437
Stabilizer Shaft	0.29	0.13	713	124,900	0.66	3,539
Stabilizer Cam Lever	2.41	1.09	8,461	1,481,790	5.42	41,984
Stabilizer Connecting Rod	1.06	0.48	336,262	58,890,000	2.38	1,668,532
Stabilizer Tooling	2.48	1.13	3,935,903	689,300,000	0.77	2,688,222
Stabilizer Effective Mass and Stiffness	**14.19**	**6.44**	**3,036**	**531,700**	**13.94**	**3,036**
Extractor Lever M3372HR	1.82	0.82	25,843	4,525,890	4.23	132,574
Extractor Slide Lever	1.17	0.53	31,564	5,527,920	1.69	100,880
Extractor Shaft	0.57	0.26	532	93,230	1.32	2,731
Extractor Cam Lever	2.35	1.06	6,772	1,186,060	5.46	34,742
Extractor Connecting Rod	0.91	0.41	430,020	75,310,000	2.11	2,206,003
Extractor Conrod Air Cylinder	0.36	0.16	1,132	198,200	0.83	5,806
Extractor Tooling	2.08	0.94	3,935,903	689,300,000	3.02	12,579,146
Extractor Effective Mass and Stiffness	**21.68**	**9.84**	**1,709**	**299,300**	**18.66**	**1,709**
Stripper Lever	0.93	0.42	56,975	9,978,050	2.38	320,084
Stripper Slide Lever	0.97	0.44	56,523	9,899,030	3.21	411,830
Stripper Shaft	0.60	0.27	1,826	319,800	1.53	10,259
Stripper Cam Lever	2.13	0.97	5,589	978,888	5.42	31,402
Stripper Connecting Rod	1.45	0.66	316,163	55,370,000	3.69	1,776,202
Stripper Tooling	1.84	0.84	3,935,903	689,300,000	6.09	28,676,989
Stripper Effective Mass and Stiffness	**27.35**	**12.40**	**7,383**	**1,293,000**	**22.32**	**7,383**

Looking at the stiffnesses in Table 1, it is immediately apparent that the shafts are the least stiff of the links. This low stiffness makes the shafts prime targets for improvement. If we look at the combined effective stiffness of each linkage, “Stabilizer Effective Mass and Stiffness” for example, we see that the value 3036 lb/in is smaller than any of the stiffnesses of the other links except for the stiffness of the shaft. This suggests that the shaft is contributing the

most to reducing the overall stiffness. If the shaft stiffness can be improved, then the overall system stiffness will also be improved. From the data in Table 1, we can also conclude that improving the stiffness of the other links would improve the overall stiffness slightly, but it would still be limited by the low stiffness of the shaft. Thus, if we want to increase the overall stiffness of the mechanism, we need to increase the stiffness of the shaft. Increasing the stiffness of the cam lever (the next least stiff component) or any other lever would not be the best solution because it would have little impact on the overall stiffness.

Increasing the stiffness of a shaft is relatively easy considering the relation of the shaft's diameter to its stiffness. The shaft's stiffness is proportional to its diameter to the fourth power; so if we increase the diameter of the shaft, the stiffness will go up by that factor to the fourth power. We can easily see this if we look at the formula for the stiffness of a shaft in torsion below.

$$k_t = GJ/L$$

k_t is the torsional spring constant for a shaft, G is the shear modulus of the material, J is the polar moment of inertia of the shaft, and L is the length of the shaft.

The polar moment of inertia J is given by

$$J = \pi D^4/32$$

where D is the outer diameter of the shaft. Combining the two equations, we get

$$k_t = G\,\pi D^4/32L$$

From this final equation, it is immediately apparent that a small change in the diameter of the shaft will yield a very large change in stiffness given that the length and the material of the shaft are not changed.

5.3. Vacuum Shaft Acts as a Spring

The vacuum shaft was found to function as a spring to absorb the over-travel present in the machine as a result of improper set up. The spring constant of the shaft is smaller than those of the other links and the measured accelerometer data shows over-travel present when the vacuum head touches the nest. This over-travel is absorbed by the weaker spring which is the shaft.

5.3.1. LVDT data

Our model for the effective mass and stiffness of the vacuum linkage was not complete without including the stiffness of the air cylinder within the connecting rod. To calculate this stiffness, we used the following formula:

$$k = A\Delta P/\Delta X$$

where k is the stiffness, A is the area of the piston (1 inch diameter), ΔP is the change in pressure inside the cylinder, and ΔX is the displacement of the piston inside the cylinder.

The change in pressure and the displacement were measured on the machine using a pressure transducer and a linear variable differential transformer (LVDT). An LVDT consists of a magnet and an induction coil. By measuring the current passing through the coil, we can obtain the velocity of the magnet and integrate it to find the displacement. For our experiments we used a Trans-Tek model #243-0000 LVDT as shown in Figure 13.

Figure 13: Trans-Tek LVDT

The thin cylinder is the magnet probe that moves freely in the larger cylinder, which contains the coil and circuitry. To measure the displacement of the air cylinder, our strategy was

to attach the magnetic probe to the connecting rod and the LVDT body to the air cylinder. The challenge was to attach the LVDT to the air cylinder and the connecting rod in a way that eliminated all movement except for vertical motion. The probe needs to be aligned with the LVDT in order to give accurate readings and both needed to be securely attached to the air cylinder and connecting rod so that they followed the air cylinder's and connecting rod's movement exactly. To accomplish this attachment, we designed two brackets as illustrated in Figure 14.

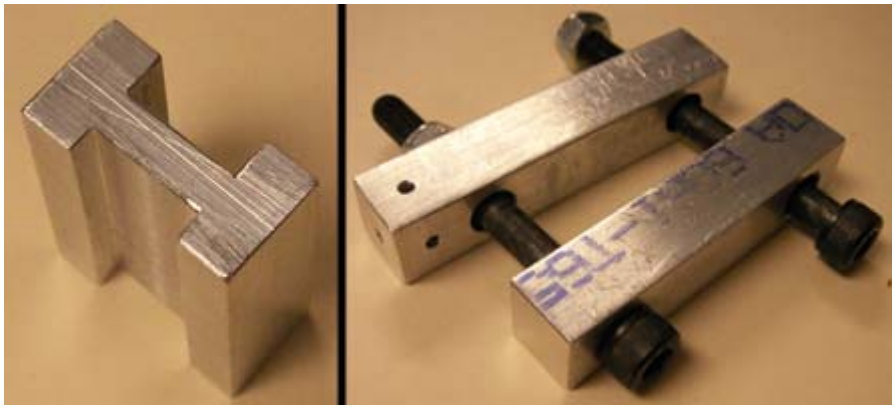

Figure 14: LVDT Mounting Bracket

The piece with an "I" cross-section was placed between the LVDT and the air cylinder, so that the two cylinders could be hose-clamped together. The bracket was placed around the hexagonal connecting rod, and the probe, a thin rod, went in a hole located in one of the clamps. A set screw kept the probe from sliding inside the hole.

The data from the LVDT and the pressure transducer were recorded by an HP dynamic signal analyzer. To ensure that each data set began at the same point in time, a proximity probe trigger was used. We conducted three tests averaging 14 to 25 sets of data. It was immediately apparent, even before the data was analyzed that the air cylinder was compressing very little. The data showed that the maximum displacement of the piston inside the cylinder was 28.7 μin. This displacement was very small and could have easily been attributed to the compression of the

rubber stop in the air cylinder. This find was surprising given the amount of over-travel that the vacuum tooling has. This over-travel was due to improper set up of the conrod which was adjusted too long. High-speed video of the movement of the air cylinder was recorded and reviewed to verify that there was little to no displacement of the piston inside the air cylinder. There was no visible displacement but this conclusion is highly subjective. Further investigation was needed.

5.3.2. Shaft is Half as Stiff as Air Cylinder

The LVDT data was used to obtain the spring constant of the air cylinder. Once these calculations were complete, the results yielded an explanation of the surprising observation that the air cylinder was not compressing. The stiffness data given in Table 2 shows that the vacuum shaft stiffness (labeled “Extractor shaft” in the table) is significantly lower than the stiffness of the air cylinder. This fact suggests that the over-travel of the vacuum tooling is absorbed by the shaft deflecting in torsion instead of the air cylinder because the shaft is the weakest spring.

Table 2: Effective Masses and Siffnesses of System Components

Name	Weight (lb)	Mass (kg)	Stiffness (lb/in)	Stiffness (N/m)	Eff Mass at Follower (kg)	Eff Stiffness at Follower (lb/in)
Stabilizer Lever Nest Plate Square	2.00	0.91	17,409	3,048,780	4.51	86,381
Stabilizer Slide Lever	0.67	0.31	141,197	24,727,992	0.21	96,437
Stabilizer Shaft	0.29	0.13	713	124,900	0.66	3,539
Stabilizer Cam Lever	2.41	1.09	8,461	1,481,790	5.42	41,984
Stabilizer Connecting Rod	1.06	0.48	336,262	58,890,000	2.38	1,668,532
Stabilizer Tooling	2.48	1.13	3,935,903	689,300,000	0.77	2,688,222
Stabilizer Effective Mass and Stiffness	**14.19**	**6.44**	**3,036**	**531,700**	**13.94**	**3,036**
Extractor Lever M3372HR	1.82	0.82	25,843	4,525,890	4.23	132,574
Extractor Slide Lever	1.17	0.53	31,564	5,527,920	1.69	100,880
Extractor Shaft	0.57	0.26	532	93,230	1.32	2,731
Extractor Cam Lever	2.35	1.06	6,772	1,186,060	5.46	34,742
Extractor Connecting Rod	0.91	0.41	430,020	75,310,000	2.11	2,206,003
Extractor Conrod Air Cylinder	0.36	0.16	1,132	198,200	0.83	5,806
Extractor Tooling	2.08	0.94	3,935,903	689,300,000	3.02	12,579,146
Extractor Effective Mass and Stiffness	**21.68**	**9.84**	**1,709**	**299,300**	**18.66**	**1,709**
Stripper Lever	0.93	0.42	56,975	9,978,050	2.38	320,084
Stripper Slide Lever	0.97	0.44	56,523	9,899,030	3.21	411,830
Stripper Shaft	0.60	0.27	1,826	319,800	1.53	10,259
Stripper Cam Lever	2.13	0.97	5,589	978,888	5.42	31,402
Stripper Connecting Rod	1.45	0.66	316,163	55,370,000	3.69	1,776,202
Stripper Tooling	1.84	0.84	3,935,903	689,300,000	6.09	28,676,989
Stripper Effective Mass and Stiffness	**27.35**	**12.40**	**7,383**	**1,293,000**	**22.32**	**7,383**

We concluded that the shaft was acting as a torsion bar absorbing the over-travel of the vacuum tooling. Engineers who were involved in the original design of the machine declared that the shaft was never meant to absorb over-travel. It was obvious to us that this shaft needed to be stiffened to the point where it was at least stiffer than the air cylinder.

5.3.3. Vacuum Shaft Recoil

To understand what causes the spikes seen in the accelerometer data taken for the vacuum system, we plotted the experimental data in time phase with the theoretical acceleration data as seen in Figure 17. Figures 15 and 16 are included to further clarify what is happening with the motion at the time of these acceleration spikes.

The accelerometer data for the vacuum showed an expected spike in acceleration indicating the impact of the vacuum head with the nest as seen in Figure 17. By plotting the accelerometer data in the same phase as the theoretical acceleration data and looking at the

timing diagram, it was verified that the impact seen in the recorded data matched the timing where the vacuum head touched the nest.

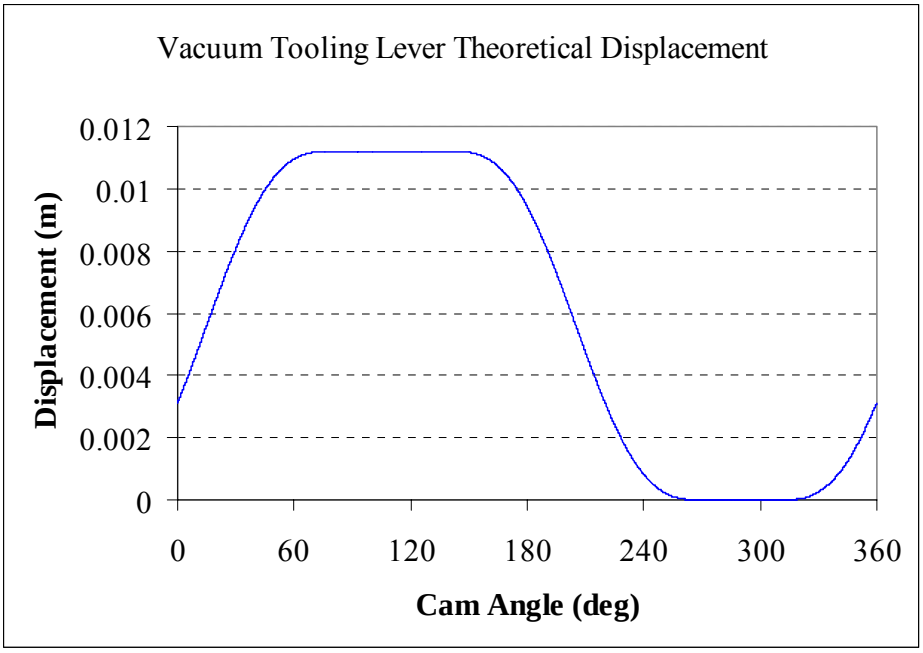

Figure 15: Theoretical Vacuum Tooling Displacement

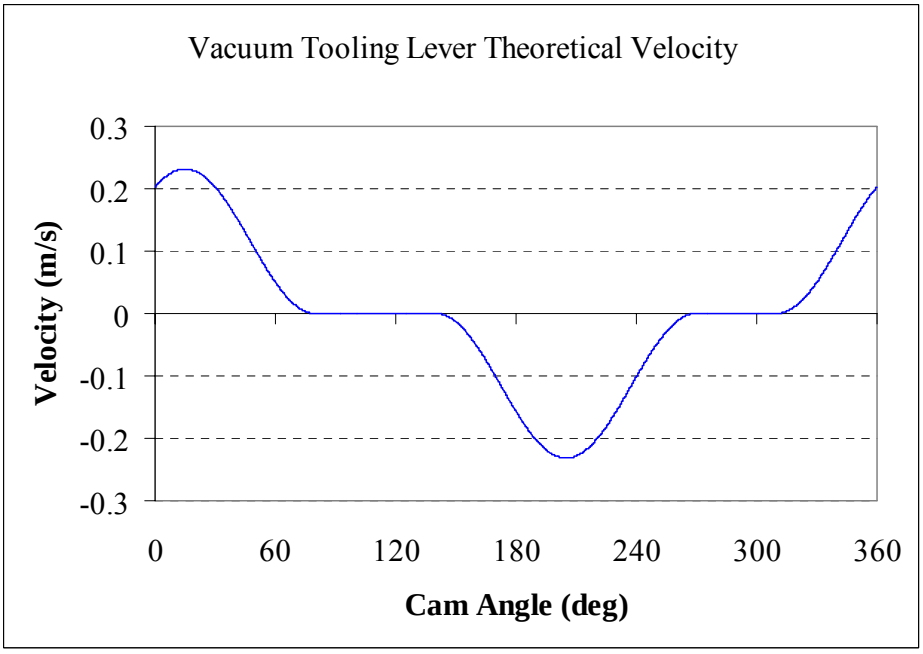

Figure 16: Theoretical Vacuum Tooling Lever Velocity

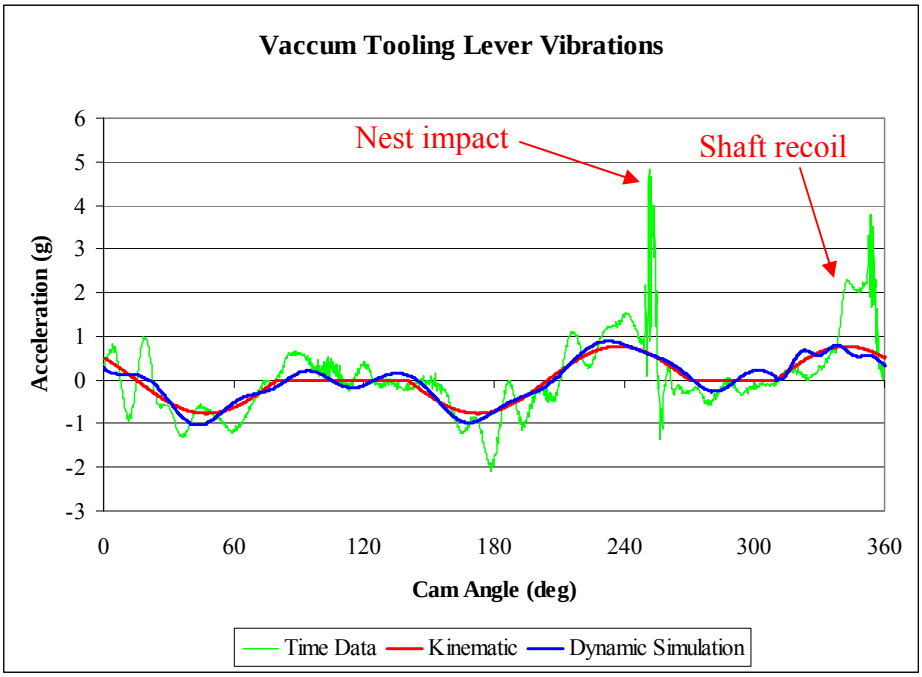

Figure 17: Vacuum Tooling Lever Vibrations

Figure 17 shows a spike in acceleration which suggests that an impact occurs right before the vacuum head enters the dwell. This impact is the vacuum head touching the nest. There is another spike in acceleration occurring when the vacuum head leaves the nest. We believe this spike is caused by the shaft recoiling as the vacuum head leaves the nest. We have already concluded that the shaft absorbs the over-travel of the vacuum head, which results in the shaft twisting. As the vacuum head leaves the nest, the shaft untwists which causes vibrations as seen by the second spike in acceleration on Figure 17.

The peak accelerations seen in the above graph can be reduced in different ways. The first spike, which is the vacuum head impacting the nest, can be minimized by reducing the velocity of the vacuum head before, and as, it touches the nest. To achieve this, the vacuum cam needs to be redesigned. The second spike which is the shaft untwisting can be eliminated completely by stiffening the shaft so that it does not twist. The shaft should be made stiffer than

the air cylinder on the connecting rod so that the air cylinder absorbs the over-travel instead of the shaft absorbing it.

5.4. Air Cylinder Needed on Stripper Tooling

We hypothesized that the spikes seen in the accelerometer data taken on the stripper linkage, displayed in Figure 18, are the result of play in the linkage, particularly in the pivot pin/slide interface and the pivot pin/tooling lever interface. There are no deliberate, built-in impacts in this stripper mechanism.

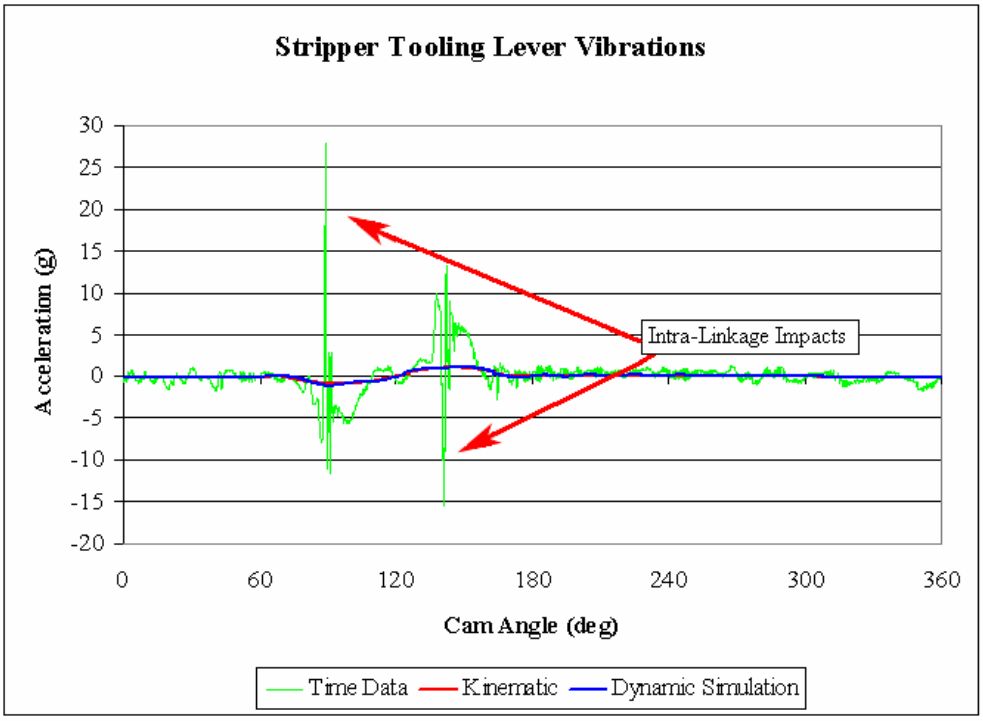

Figure 18: Stripper Tool Side Lever Vibrations (B1 in Figure 8)

We analyzed the slack between the tooling and the tooling lever by putting accelerometers on each component individually, as shown in Figure 19.

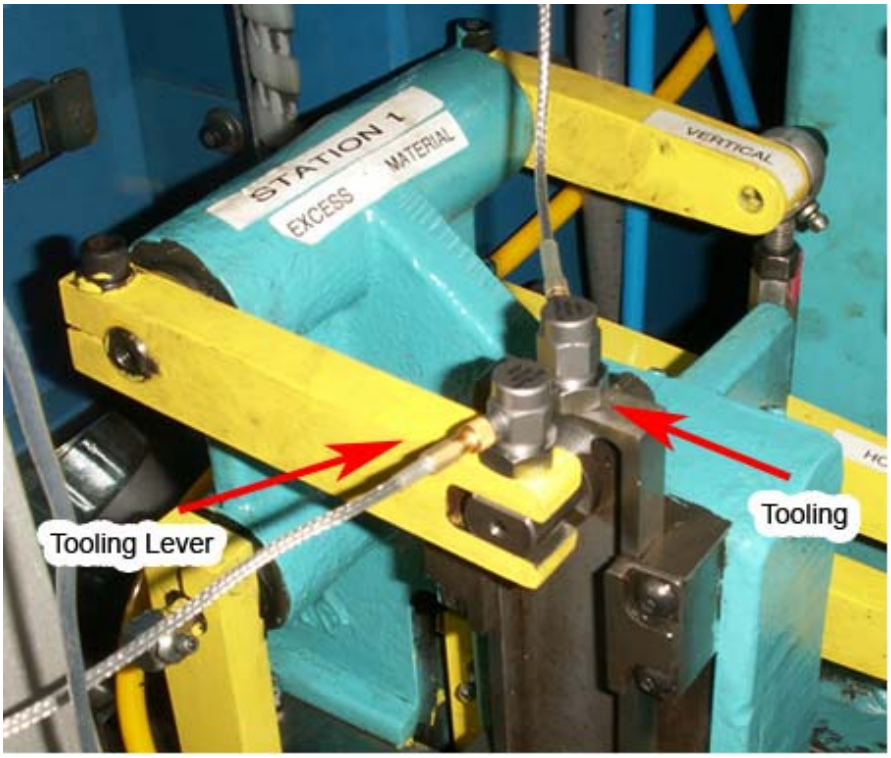

Figure 19: Stripper Tooling and Tooling Lever Accelerometer Placement

It was apparent from the graph of the time data that the tooling and the tooling lever had different motions, as seen in Figure 20.

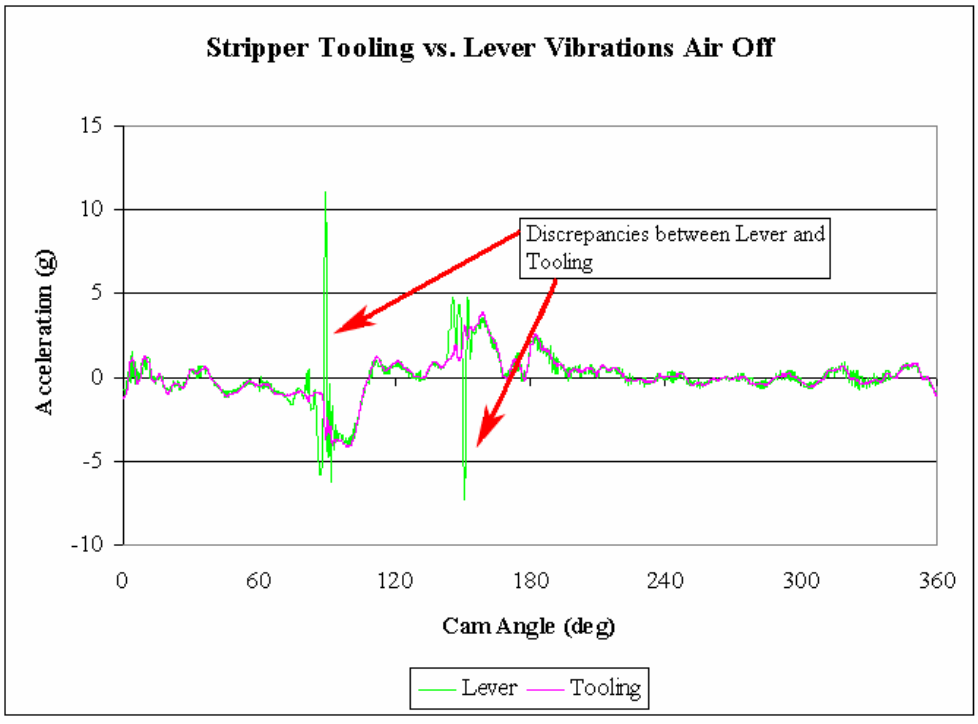

Figure 20: Stripper Tooling vs. Lever Vibrations (B4 & B1 in Figure 8)

The vacuum and stabilizer linkages have air cylinders on the back of the slides which exert force on the slides; these take up the clearance in the linkage in one direction all the time. The stripper does not have an air cylinder, thus when the acceleration of the stripper changes direction, i.e. from positive to negative, the 1 mm of clearance in the linkage is taken up in the other direction, causing an impact to occur when the other end of the backlash clearance is hit. This was our theory for the impacts seen in Figure 18.

In order to verify that it was the air cylinders that were keeping the vacuum and stabilizer linkages from showing similar impacts, we ran the vacuum system with and without its air cylinder connected. As with the test on the stripper linkage, we put accelerometers on the tooling lever and on the tooling itself. The results of the test with the air cylinder connected are shown in Figure 21.

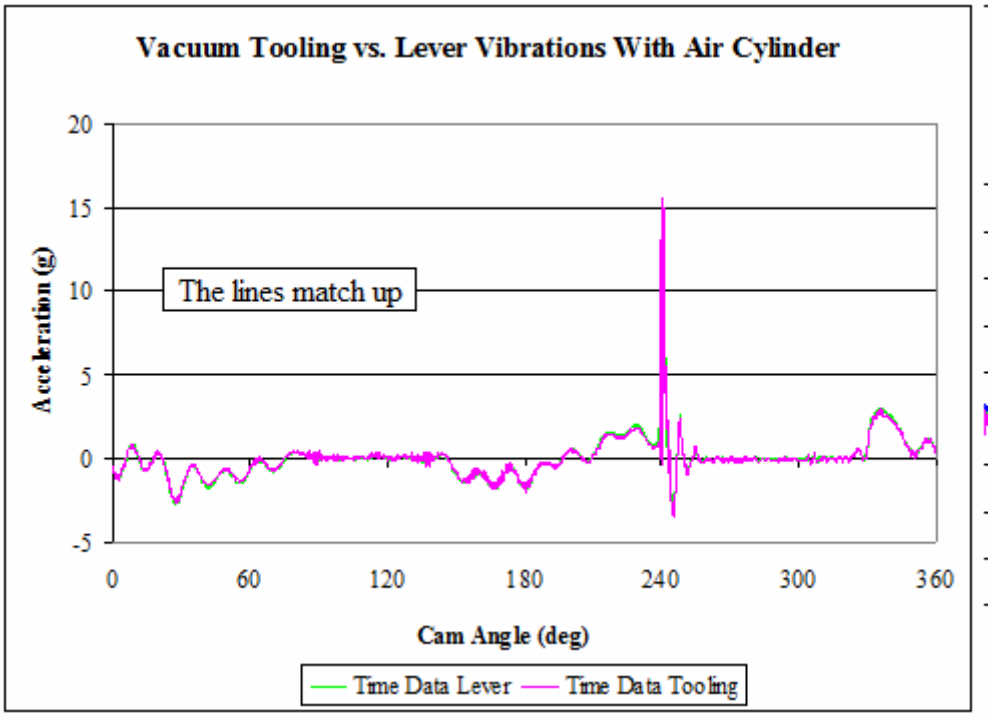

Figure 21: Vacuum Tooling vs. Lever Vibrations with Air Cylinder (C4 & C1 in Figure 8)

The graphs are nearly identical thus the play in the joint does not seem to be affecting the vacuum system when the air cylinder is connected. The results of the test without the air cylinder connected are shown in Figure 22.

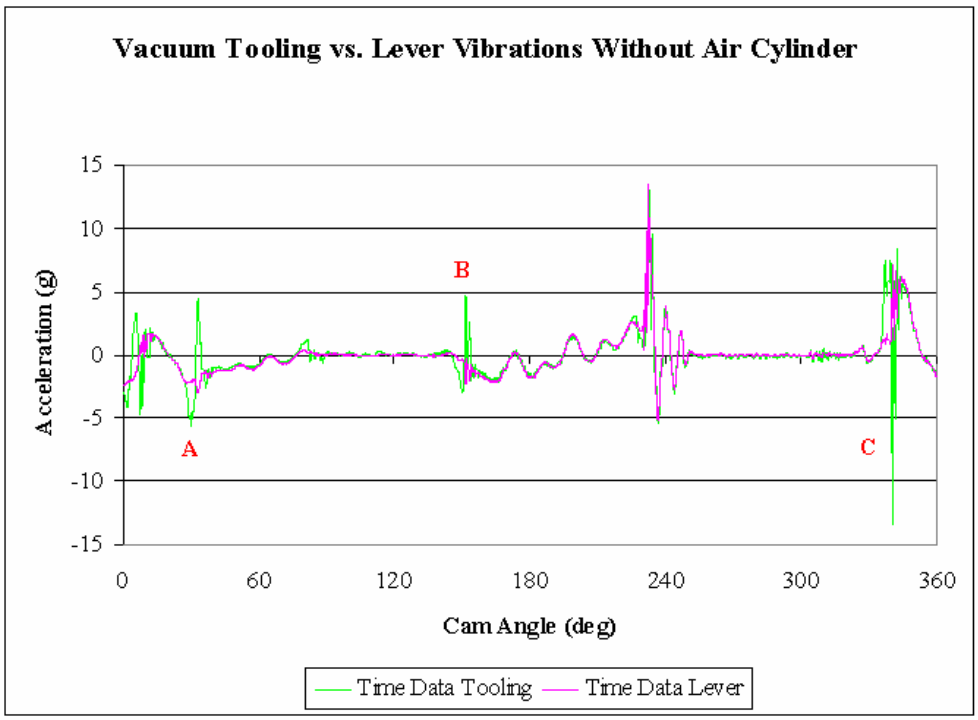

Figure 22: Vacuum Tooling vs. Lever Vibrations without Air Cylinder (C4 & C1 in Figure 8)

The accelerations are much different and the differences are most prevalent when the acceleration changes direction from positive to negative or vise versa at points A, B and C. With the air hose to the cylinder disconnected, the cylinder's internal retraction spring retracted it. Therefore it was not impacting the slide housing, which would interfere with our obtaining accurate results. When the hose was disconnected, there was a similar amount of slack in the vacuum linkage as in the stripper linkage, 1 to 1.5 mm. There was no slack in the vacuum linkage with the air hose connected.

Excessive clearances of the pivot pin are partially responsible for these impacts due to slack. There is approximately 1 mm of slack in the stripper linkage in the machine on which we did our testing. This machine's slack is representative of all the machines. The pivot pin in the

machine was smaller than shown on the drawings but the hole for the pin in the slider was also smaller than shown on the drawings. The maximum clearance of the pivot pin/slide interface according to the drawings is 0.063 mm, the measured clearance of the actual parts is 0.07 mm. Even for a new pivot pin, which we acquired and measured, the clearance is 0.06 mm. The clearance of the lever/pin interface according to the drawings is 0.038 mm, the actual is 0.06 mm. With a new pin the clearance was measured as 0.04mm.

The slack was not due to wear because the pivot pin and slide hole were not visibly worn, and the tooling side lever was only worn minimally, as shown in Figure 23. Thus, the parts are not manufactured correctly according to the drawings, and more importantly the clearances are too large. If the clearance were reduced, it would reduce the severity of the impacts seen in the data. Approximately 85% of the slack in the whole linkage train is in the tooling lever/pivot pin and pivot pin/slide interfaces.

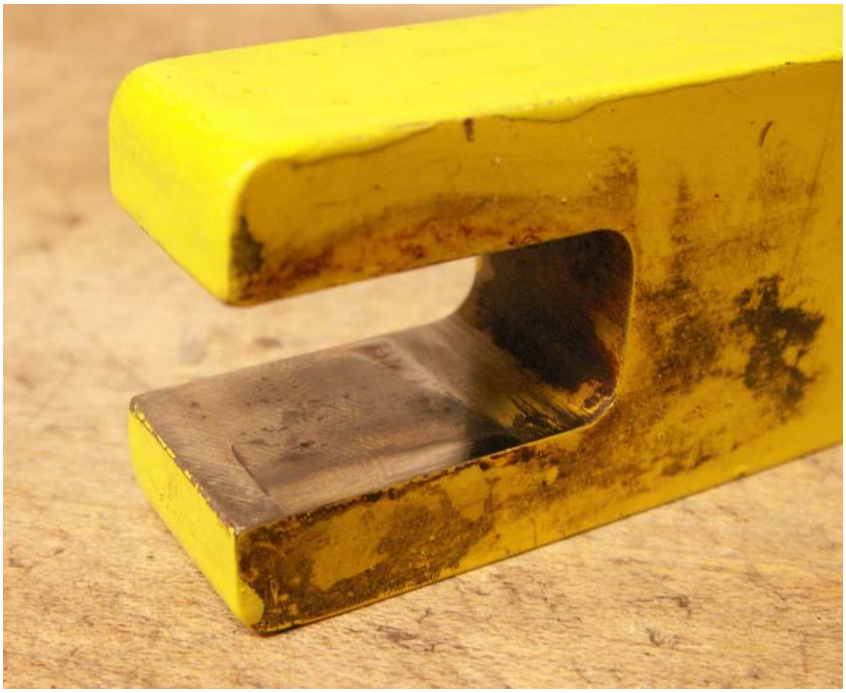

Figure 23: Stripper Tooling Lever Wear

One method of eliminating/reducing the acceleration peaks is by eliminating the slack in the linkage by having better fits between parts and tighter tolerances, but this is not practical or cost effective. The precision required to manufacture the pivot pin such that there would be minimal clearance is greater than can be accomplished without significant cost. Furthermore, as the tools wore they would need to be re-sized to eliminate or minimize slack.

Alternatively, an air cylinder could be mounted on the back of the slide to keep the play taken up in one direction. It does this by applying a pressure against the slide by pushing it away from the top of the slide housing against which the piston rod will rest, like the vacuum and stabilizer air cylinders. Such an air cylinder entirely eliminates the slack in the linkage and any intra-linkage impacts. Having greater precision pivot pins is only a partial, temporary fix because these pins would have to be replaced often due to wear; it will reduce the magnitude of the intra-linkage impacts, but an air cylinder would eliminate them. Additionally with an air cylinder mounted on the back of the slide, the components of the linkage would not have to be replaced as often because the air cylinder can compensate for slack resulting from wear.

It is not strictly necessary to have an air cylinder on the back of the stripper slide because, unlike the vacuum and stabilizer linkages which have impacts between tooling and nest, the stripper system does not have any such external impacts. Furthermore, its precise placement at any given moment is not that important. Its motion of stripping the product off the vacuum can be accomplished with a high degree of imprecision. Adding an air cylinder to the stripper slide would increase the forces exerted on the joints thereby possibly increasing the rate of wear and, consequently, the costs of running the machine. However, the air cylinder may in fact decrease tool wear because it will eliminate the intra-linkage impacts. In any case, the worn components

can be used for longer with the air cylinder, making the possibility of higher wear much less relevant.

6. Redesign

Based on our analysis, we pinpointed several areas in need for improvement and redesign. One area for improvement was increasing the stiffness of the Vacuum and Stripper shafts. The Stabilizer shaft was not chosen for redesign because it was found to be functioning adequately and was not presenting any problems.

Other areas requiring improvement are the Stripper and Vacuum cams. The original design of these two cams used cycloidal segments and we felt that their design can be significantly improved. The Stabilizer cam was not chosen for redesign because its design is satisfactory.

6.1. Shaft Redesign

The shafts were found to need an increased diameter to increase the stiffness. There were limits to how large we could make the shafts. The shafts are located inside a cast frame and the holes in the casting could not be made so large that we risked the frame failing. We were limited further by the bushings that go around the shafts. These bushings have a larger outer diameter (OD) than the diameter of the shaft and the holes in the casting must be large enough to accommodate the bushing. A further limitation was the available bushing sizes provided by the supplier. The frame's outer diameter around the shafts is 1 3/4 (44.45 mm), the inner diameter of the frame's bushing mounts is 1 7/8 (22.22mm), for a 5/8 shaft. The company's bushing supplier, Carr Lane has bushings with ODs of 1, 1 1/4, and 1 3/8 inches, for an inner (and thus shaft)

diameter of 3/4, 7/8, and 1 inch, respectively.[1] The next size bushing has an OD of 1 ¾ thus it would be too large because the frame's outer diameter around the shaft is 1 3/4 inch.

6.1.1. Shaft Frame Factor of Safety Calculations

The forces exerted on the frame by the shafts were found by multiplying the effective mass at the pivot of the end of the levers attached to the shafts by the peak accelerations measured with the accelerometers and signal analyzer, plus the force exerted on the tooling by the air cylinders on the back of the vacuum and stabilizer slides.

Using these forces we calculated the stresses exerted on the frame by the shaft through the bushing, based on tearout and tension failure. With the current shafts and frame dimensions the safety factors for normal loading were all around 80. Changing the frame to accommodate the largest shaft (1 inch diameter) meant that the inner diameter of the frame was changed to 1 3/8 inches. Still the safety factors were quite high, around 30. For all these calculations we used the endurance strength, which was calculated with the correction factors for fatigue failure. The von Mises stress was also found using SolidWorks FEA function, a screen capture of a deformed FEA modeled frame is shown in Figure 24. The results confirmed that the assumptions made to find the von Mises stress using MathCad were reasonable and accurate enough.

[1] http://www.carrlane.com/Catalog/index.cfm/27225071F0B221118070C1C512A0A1F0900101B0300105 43C1C0C16190D172D252A5E4B5E56

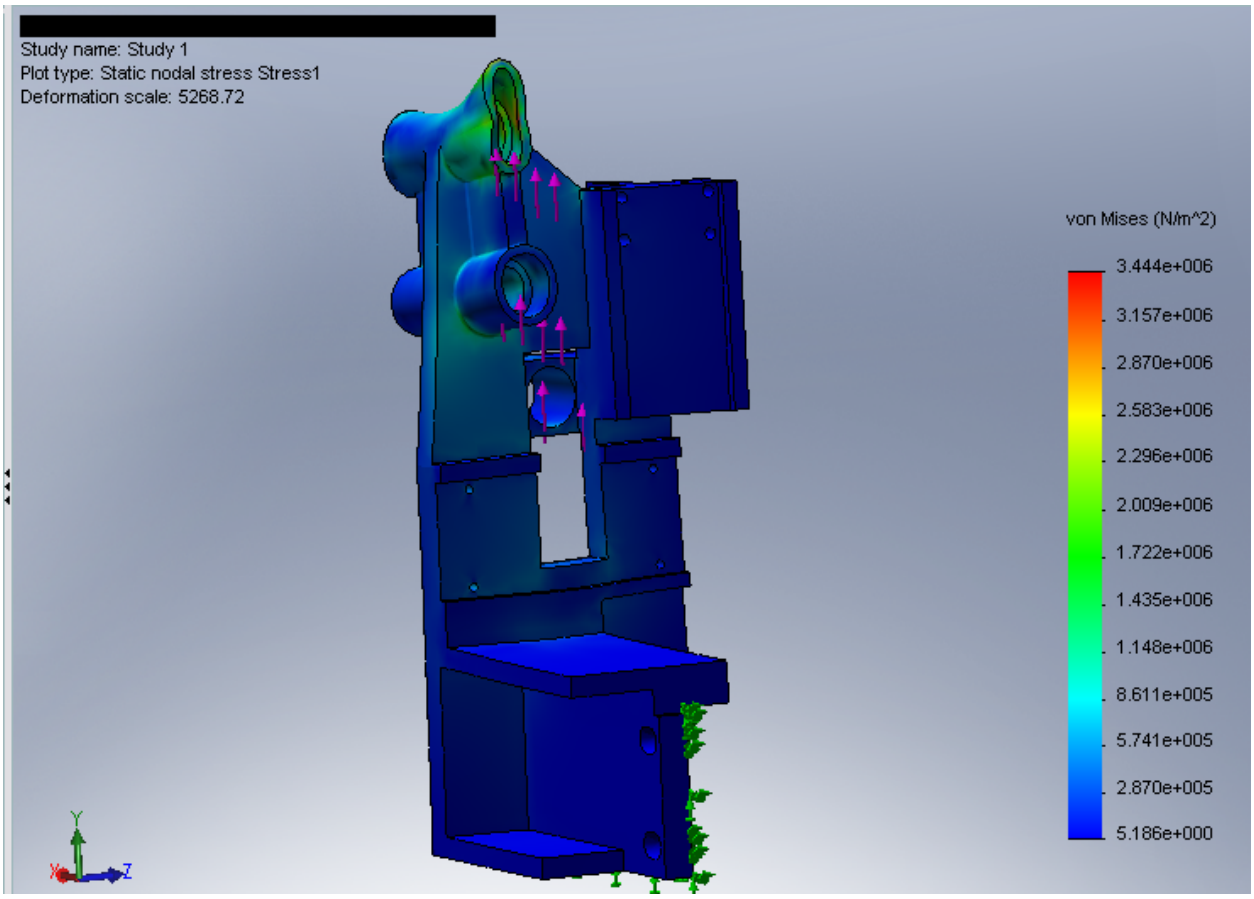

Figure 24: FEA of Frame

Because our accelerometer data was based on 25 cycles averaged, the peaks could potentially be much higher than the peaks shown in the data. If a given impact does not occur at the exact same time each cycle, either from tolerances in the machine or small triggering errors in the analyzer, the peak could be reduced significantly as was subsequently seen in our data when we used a more precise external trigger. Thus to make certain that the frame will not break with the new bored out shaft holes we increased the force to its maximum possible. The accelerometers we used were 100 g rated, we know that none of the measurements we took exceeded this because we would have seen errant data. Thus for a worst case scenario we set all the peak accelerations to 100 g. The resultant forces were applied to the MathCad file and SolidWorks FEA model in order to compute the von Mises Stresses for various loading conditions (vacuum accelerating inward/outward and all the forces upward/downward). The

highest von Mises stress resulted in a factor of safety of 3.1. Thus the frame is capable of supporting a 1 inch diameter for all shafts at impact accelerations of up to 100 g.

6.1.2. Shaft Diameter Selection

Table 3 : Stiffness Data for Shaft Diameter Options

linkage	shaft dia inches	shaft stiffness k.s at follower lbf/in	Linkage k.eff at follower lbf/in	% increase in k.eff overall vs. oringinal
Stripper	5/8	10340	7422	
Stripper	7/8	39660	15820	113%
Stripper	1	67650	18950	155%
Vacuum	5/8	2745	1714	
Vacuum	7/8	10530	3185	86%
Vacuum	1	17960	3641	112%
Stabilizer	5/8	3538	3036	
Stabilizer	7/8	13680	8344	175%
Stabilizer	1	23330	11160	268%

The frame can support a 1 inch shaft for all shafts, but that does not mean that we need a 1 inch shaft for each linkage. The stiffness of each linkage with the original 5/8, and new 7/8, and 1 inch diameter shafts and the percent increase in stiffness for each is shown in Table 3. The vacuum shaft is the weakest because of its comparatively long lever arms. The stripper shaft is strongest because it has two short levers on its ends. The Stabilizer shaft is stiffer than the vacuum shaft despite its slightly longer lever arm because it is about half the vacuum shaft's length.

We chose to use a 1 inch diameter vacuum shaft in order to make the air cylinder function as a spring (as was the original designer's intent as far as we can learn). There is such a small increase in overall system stiffness gained by changing the vacuum shaft diameter from 7/8 to 1 inch diameter because its effective stiffness value as seen at the cam follower is being held

down by the low stiffness of the air cylinder. Even though the overall spring constant of the system is only increased by 112% the actual system should perform much better than that increase implies because the cylinder is much highly damped (by friction only) than the shaft is, thus the vibrations seen should have smaller peaks and they should decay faster. The air cylinder in the conrod may have been intended only to prevent breaking parts when the nest spring is broken. When the nest spring is broken, the nest is deployed/closed, which would result in the vacuum head contacting the closed nest located approximately 1/4" away from where the head normally contacts the excess material. Even if this was the original intention in putting the air cylinder in the conrod, it will still be better to force the cylinder to function as a spring to absorb over-travel than have the shaft act as the spring. This is why we chose to use a 1 inch diameter shaft for the vacuum linkage.

Though a 7/8 shaft would have been adequate, we chose a 1 inch diameter shaft for the stripper linkage train because that size was convenient: a 1 inch shaft could be ordered to size from a supplier thus reducing the machining time required complete the shaft. The stripper linkage train, even with a 7/8 shaft, will be twice as stiff as it was with its original 5/8 diameter shaft. Furthermore it will be about four times stiffer than the vacuum linkage with its new 1 inch diameter shaft. We chose to leave the stabilizer shaft at its current 5/8 diameter. Increasing its diameter would increase its stiffness by 268% but it is unnecessary in this case. The stabilizer has the smallest tooling travel, has only a single dwell, has a shaft of approximately half the length of the stripper and vacuum shafts, and has the most modern, best designed cam of the three. For all these reasons the stabilizer linkage is the least vibrationally problematic. Boring the stabilizer shaft hole larger will take more time and money but provide minimal additional

benefit. If we chose to bore this shaft hole in addition to the other two, it would have made it less likely that the frame rework be done in time to allow testing.

The stabilizer linkage may also have over-travel, by design or improper setup, and the shaft can, and possibly does, function as a spring to absorb this small amount of over-travel. The machine we did our accelerometer testing on does not show a spike in acceleration like an impact or ringing, decaying vibration, on this linkage. This may also be due to the fact that the stabilizer is leaving contact with the nest slowly enough for the shaft to come out of torsion without the impact-like acceleration spikes seen in the vacuum linkage. Assuming that over-travel does not occur, which is probable, the stabilizer linkage shows no evidence of its shaft functioning as a spring, at least on the machine which we tested. If the conrod is setup too short however, then there will be over-travel and the forces could be significantly higher. This could result in increased wear on the conveyor components and stabilizer linkage and in an increased likelihood of parts breaking, if the shaft diameter was enlarged thereby removing it as a potential spring from the linkage. Therefore we chose not to replace the stabilizer shaft with a larger diameter shaft primarily because it would be costly and would not improve the system to a significant degree.

6.2. Cam Profile Redesign

The goal of the following cam redesigns is primarily to minimize the velocity at impacts and secondarily minimize the values of the acceleration of the cam follower. It is also desirable to minimize the fourth time derivative of position, sometimes called ping, in order to reduce vibrations. In order to create more effective cam profiles, we used B-splines. B-splines offer more control over the interior of the s-v-a-j curves which allowed us to reduce the velocity at impacts, B-splines also allow us to combine multiple segments into a single function which can

reduce peak accelerations and jerk. We did not substantially alter the timing diagrams of the cams, as such work would have required extensive redesign of the entire station.

6.2.1. Vacuum Cam

Figure 25 shows the original vacuum cam. It was a double dwell cam with a cycloidal rise and a cycloidal fall. Although both dwells were kept as is, the rise and fall were replaced with B-spline curves in order to better control the velocity at the time of impact. Although no hard stop is designed into the vacuum system, the vacuum head does contact the nest. Variances in set up, maintenance, and background noise will prevent the linkage from following the cam's theoretical profile exactly. To this end, we redesigned the cam to have a lower velocity for a longer time in the interval where it touches the nest in order to reduce the impact, even if it occurs earlier than expected. Although this decrease in velocity at impact comes at the price of increasing the acceleration everywhere else along the cam profile, the new peak accelerations are still not higher than the measured accelerations caused by impact. Although theoretical peak accelerations increase, this cost is well worth the benefit of reducing or even eliminating the impact.

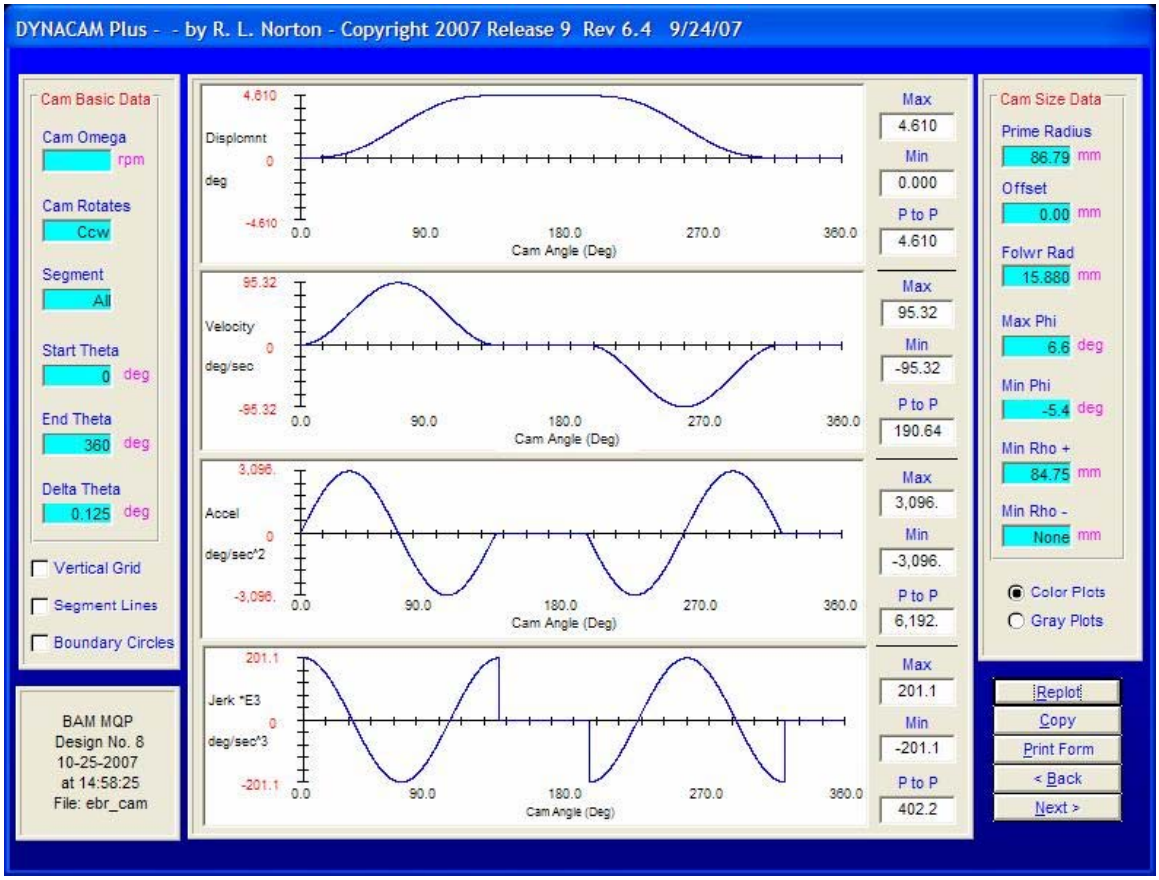

Figure 25: Original Vacuum Cam Parameters (s-v-a-j curves)

Because spline curves were used for the rise and fall segments, pseudo-dwells were considered to replace the true dwells of the initial profile. Both dwells, however, need to be precise in order for the linkage to function. No over-travel is intended as the vacuum head moves into the nest, so it is preferred that the vacuum does not move below zero displacement during the low dwell. In order for the stripper to meet with the vacuum precisely, a true dwell is also preferable for the high dwell.

In order to eliminate an impact force on the nest, the velocity of the vacuum head at the time of contact should be zero. For the existing cam, the velocity is zero at the intended point of impact, but the magnitude of the velocity rises quickly at even small displacements. The goal of the redesign was to create a more "robust" design by reducing the velocity of the vacuum head over a larger range of displacement to make allowances for some variance in the setup and

maintenance of the machine. This means that the vacuum will have to move to a lower velocity in the same amount of time, increasing the accelerations associated with the rise and fall of the cam. This is unfortunate but reducing the impact at contact is more important. Although the theoretical peak accelerations are higher, as seen in Figure 26, the vibrations are generally reduced. Looking at the dynamic simulation of our cam in Figure 27, we can see that the differences in accelerations are not as severe as it first appears.

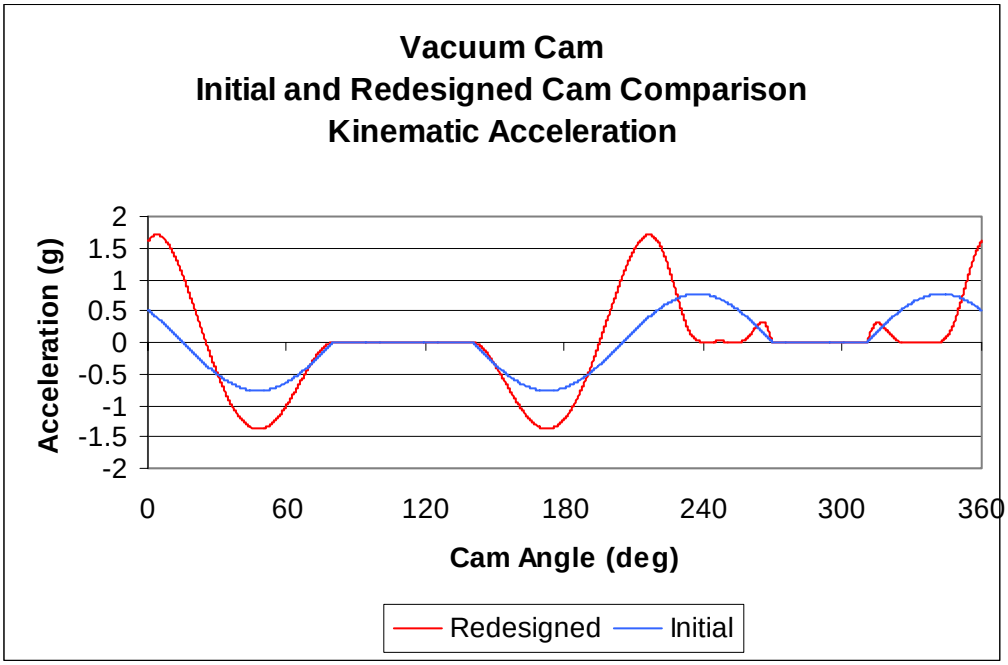

Figure 26: Redesigned vs. Original Vacuum Cam Theoretical Acceleration

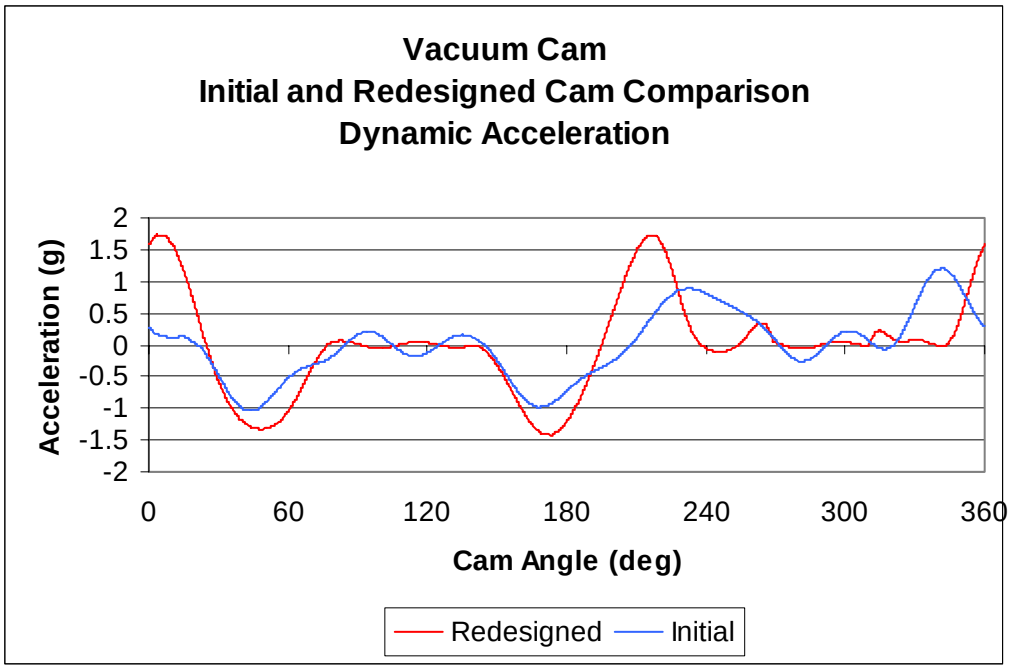

Figure 27: Redesigned vs. Original Vacuum Cam Simulated Dynamic Acceleration

We decided, given the air cylinder attached to the back of the vacuum tooling, which should eliminate most of the variance caused linkage slack, that a reasonable range over which to decrease the velocity would be 1 mm from the nest. This goal was achieved by using B-splines to replace the cycloidal fall and rise. Boundary conditions were chosen to ensure that the displacement of the tool would be 1 mm from the nest when the acceleration would be zero. A value for the velocity was chosen, and several iterations were designed and compared in order to determine the boundary conditions which would yield the lowest velocity over the entire range of displacement. Again, a splinedyne curve was used to reduce the accelerations and displacement error of the tooling.

As you can see in Figure 28, the redesigned cam does have a much lower velocity close to the nest.

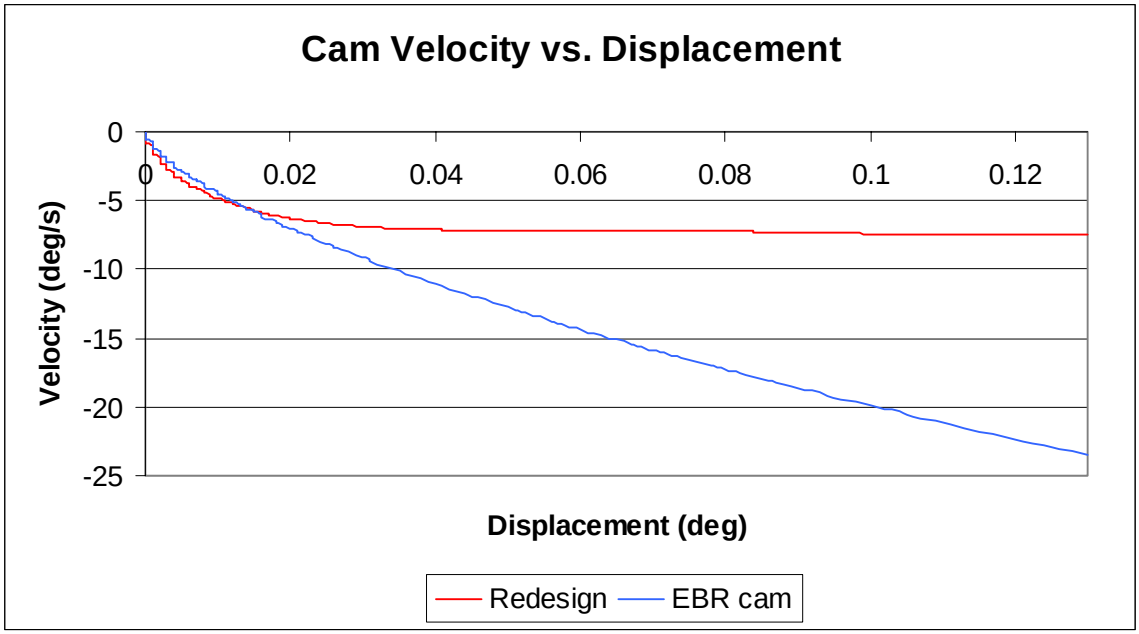

Figure 28: Redesigned vs. Original Vacuum Cam Theoretical Velocity vs. Displacement

We may also note that the velocity of the redesigned cam is slightly higher than the velocity of the initial cam for very small non-zero displacements. It is assumed that the tooling will have reached the nest at the point which the lines cross, and this higher velocity can be safely ignored. The complete s-v-a-j curves for the redesigned vacuum cam can be seen in Figure 29.

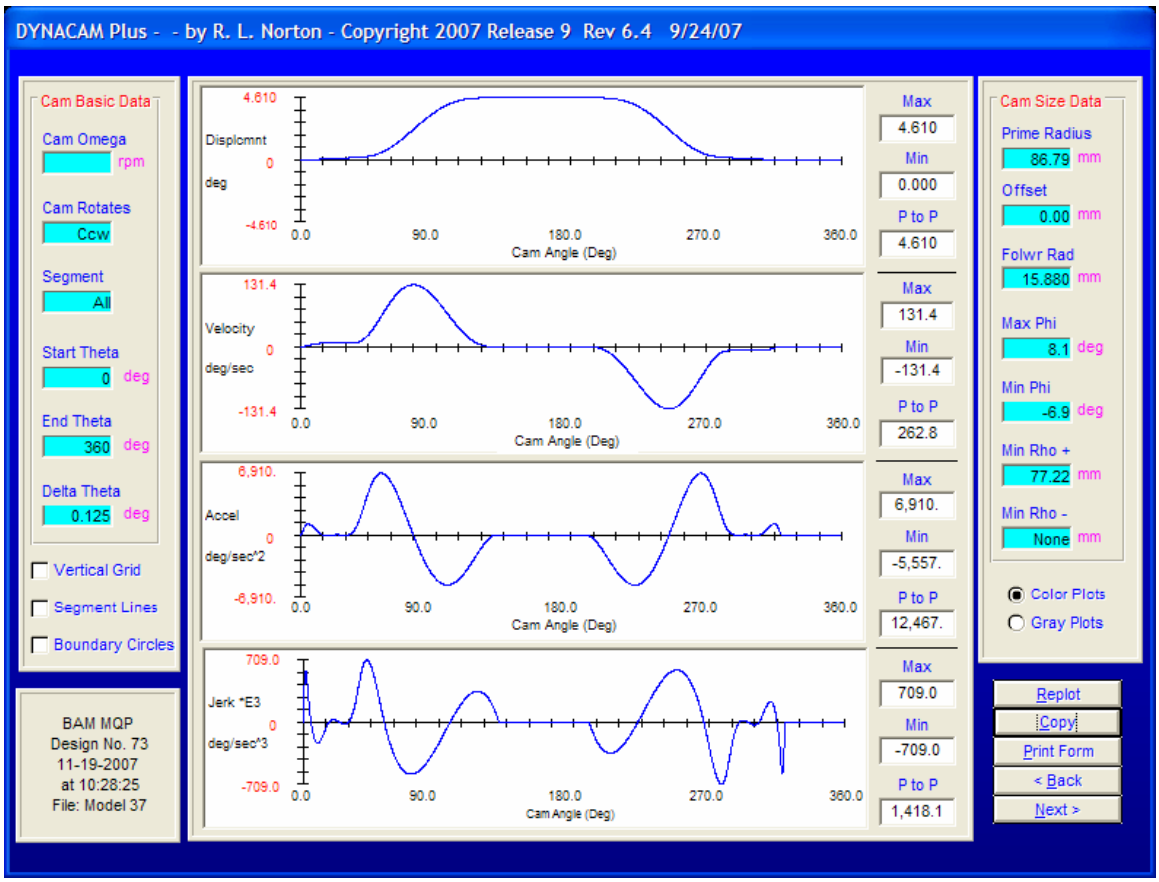

Figure 29: Redesigned Vacuum Cam Parameters (s-v-a-j Curves)

In an attempt to determine the validity of our redesigns before they went to manufacture, we changed our lumped mass and spring parameters to represent the inclusion of the new, thicker shafts, and used dynacam to create a new dynamic solution. We were then able to directly compare the performance of the initial linkages, the linkages with the redesigned cams, and the linkages with both redesigned cams and redesigned shafts. We can see these curves for the vacuum tooling in Figure 30.

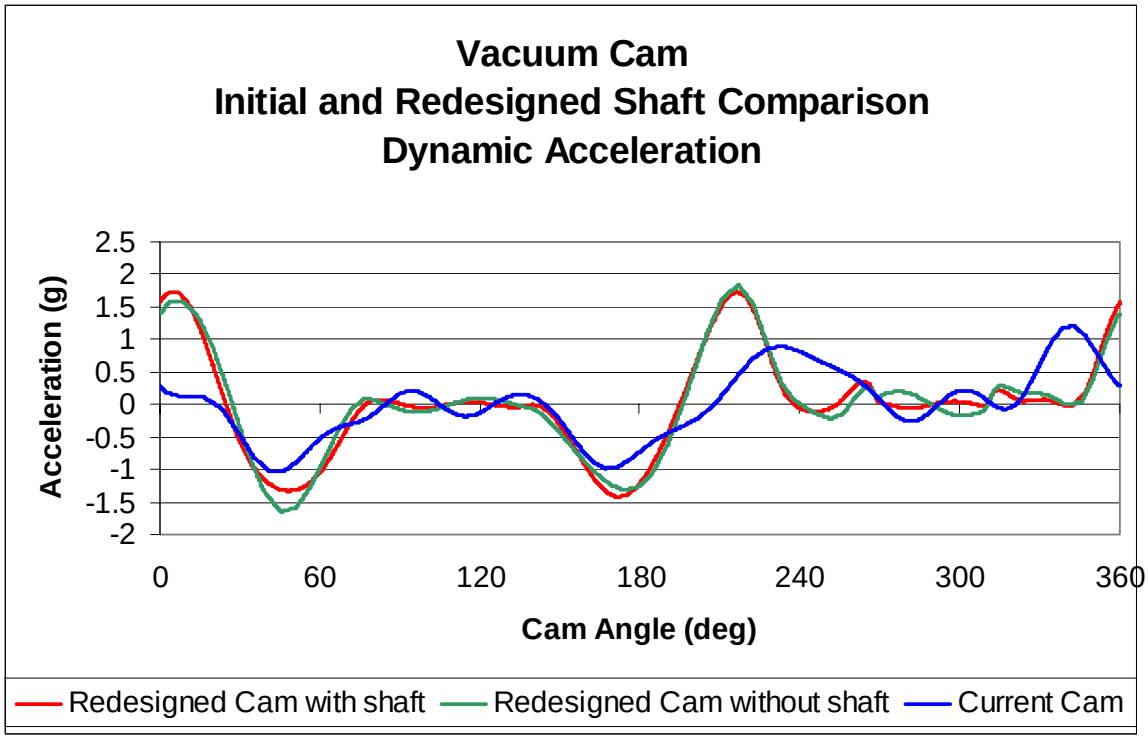

Figure 30: Dynamic acceleration of Vacuum Original Cam vs. Redesigned with and without enlarged Shaft

For the vacuum cam, we can see that the accelerations of the rise and fall have risen, as is expected. The vibrations at both dwells, however, has been substantially lowered by redesigning the cam, and the vibrations and peak accelerations are even lower still when the redesigned shaft is added to the system.

6.2.2. Stripper Cam

The initial stripper cam profile was composed of two segments, a cycloidal rise over 260 degrees and a cycloidal fall over the remaining 100 degrees. This displacement and the resulting velocity, acceleration and jerk can be seen in Figure 31. Note that, for the stripper cam, a rise corresponds to stripper tool moving upward, in the positive direction.

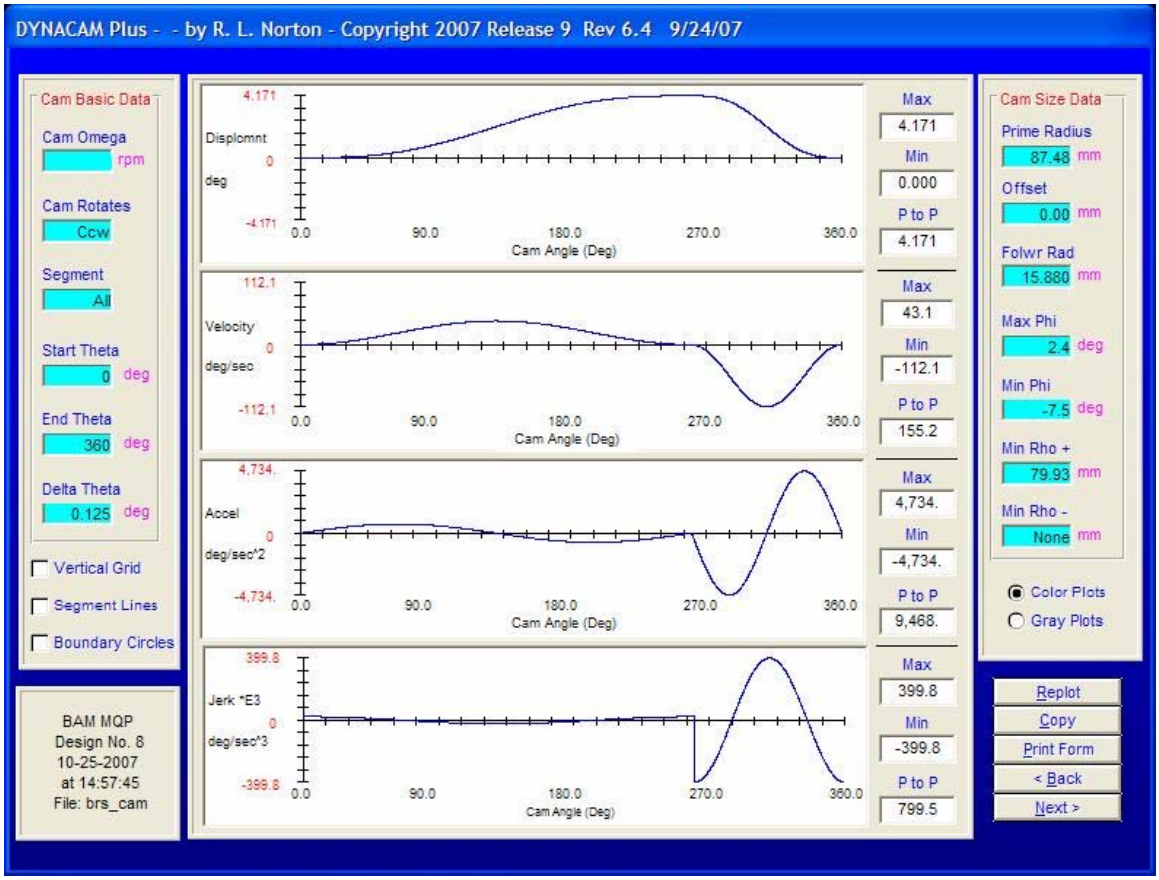

Figure 31: Original Stripper Cam Parameters (s-v-a-j curves)

As there are no hard stops or deliberate points of contact with other parts in the motion of the stripper mechanism, we are not able to reduce the impacts seen in our test data through cam design. Therefore, the focus of the cam redesign was to reduce the acceleration and vibration of the linkage.

Note that after both the rise and the fall, the acceleration returns to zero. This return to zero is unnecessary and its presence increases the peak accelerations and jerk of the cam. By combining the separate rise and fall functions into a single B-spline we immediately eliminated one return to zero by using a single function over the entire cam profile with no internal acceleration constraints. The S-V-A-J curves for the new cam can be seen in Figure 32. Additionally, the use of a spline curve allowed us to create the asymmetric profile.

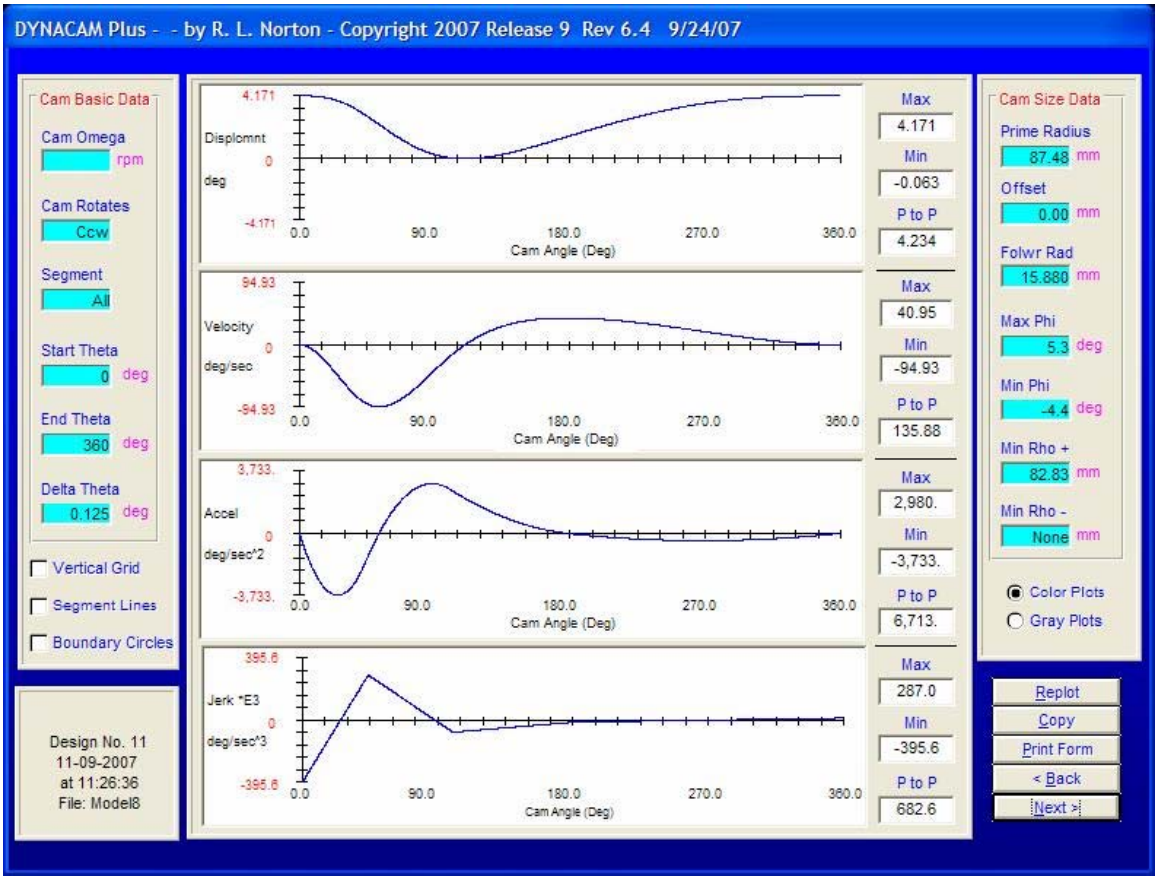

Figure 32: Redesign Iteration Stripper Cam Parameters (s-v-a-j curves)

We can see, under this iteration, one return to zero still exists at the beginning and end of the profile. This results from the restrictions in choosing boundary conditions. In order to solve the equation for a continuous spline, the acceleration at both ends of the segment must be set equal. Any analytic methods to find the ideal boundary condition would be both complicated and tiresome. Using a simplified approach, we created several design iterations. The first iteration had zero acceleration at the ends of the spline. We then compared the profiles and dynamic simulations of these iterations to determine what boundary condition would yield the least peak to peak acceleration value and the least maximum magnitude acceleration value. Furthermore we changed the spline to a 6^{th} degree spline curve which has a continuous 4^{th} order derivative (ping) function and allowed us to pursue a splinedyne cam profile. The final results can be seen in Figures 33 and 34.

Figure 33: Boundary Conditions for Redesigned Stripper Cam

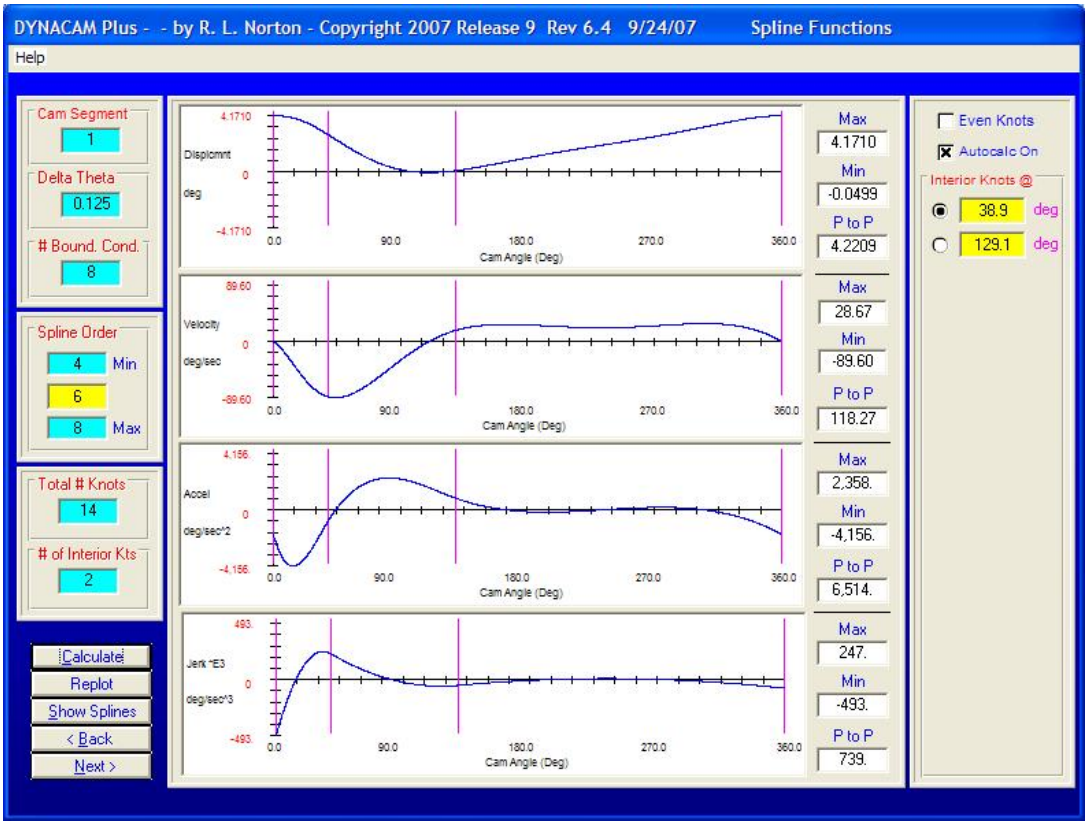

Figure 34: Redesigned Stripper Cam Parameters (s-v-a-j curves)

The redesigned cam does travel below zero displacement. However, as the angular displacements are small, we may assume a linear relationship between the angular displacement and the linear motion of the stripper tool. Using this approximation, an angular displacement of -0.05 degrees, the over travel of the redesigned cam, corresponds to a linear displacement of 0.011 inches, which is well below both the measured and recommended clearance between the vacuum and stripper tools.

By direct comparison, as displayed in Figure 35, we can see that the acceleration of the redesigned cams is a great deal lower than the original stripper cam. Although, the lumped sum parameters of the current station were used to create the dynamic simulation for both cams, the vibrations are also much lower for the redesigned cam as the dynamic simulation curve follows almost exactly with the kinematic trace.

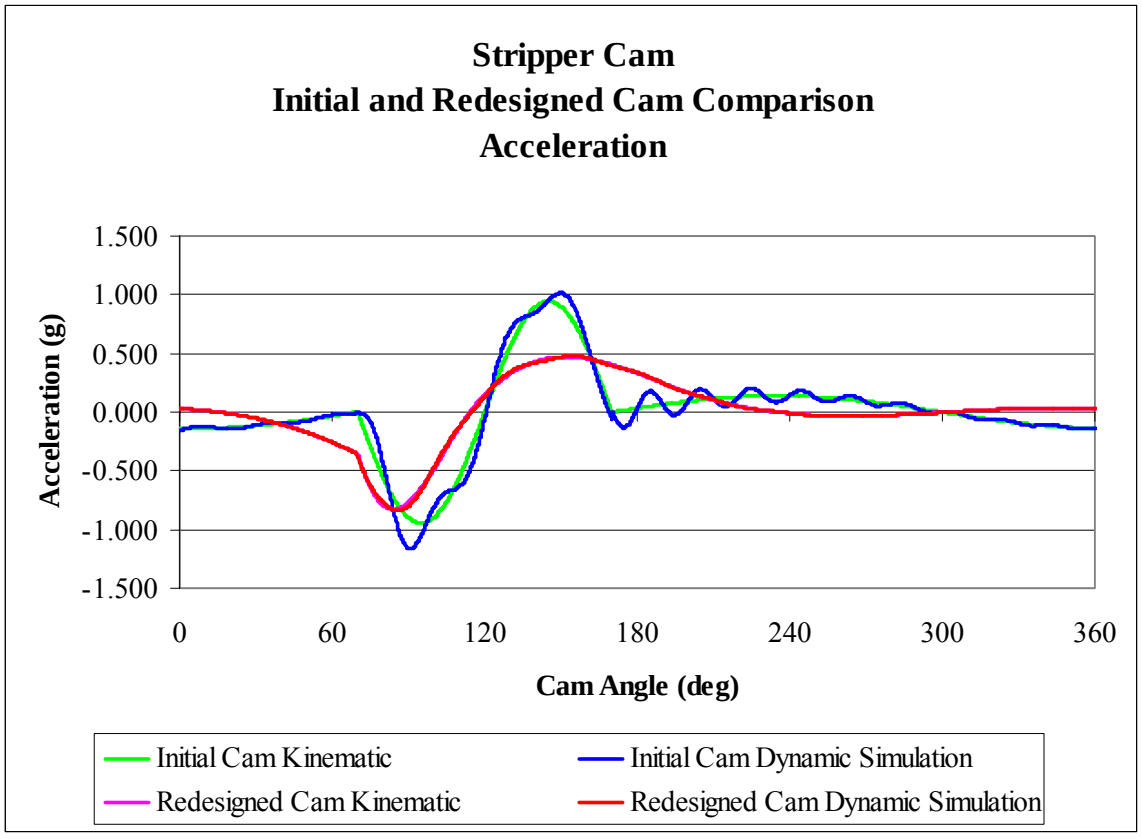

Figure 35: Original vs. Redesigned Stripper Cam Theoretical and Dynamic

Note that for the stripper linkage, there is a drastic reduction in acceleration across nearly the entire cam profile. In addition, the vibrations curve of the redesigned cam almost completely overlays the theoretical curve; the predicted vibrations have fallen to almost zero, even with the initial shaft.

6.3. Air Cylinder Bracket for the Stripper

The existing stripper slide is hardened steel which is impractical to machine. Thus drilling and tapping the end of an existing slide, such that a proper air cylinder mounting bracket could be attached similar to the stabilizer and vacuum cylinders, is not a viable option. Therefore, we chose to machine a temporary mounting bracket so that a cylinder could be mounted in order to obtain test results.

We originally thought of mounting a bracket onto the pivot pin which sticks out of the back side of the slide and is the most accessible. However, this option was not chosen for three reasons. First, the two nuts on the pivot pin are not tightened against the slide in order to reduce friction. Therefore the nuts could not be used to hold the bracket against the slide. Secondly, if a mount was placed between the two nuts which are meant to lock against each other, the pin rotates and so a mount would also have to rotate. Thirdly, the slack resulting from the clearance between the pivot pin and the slide would not be affected by an air cylinder mounted on the pin.

We decided that the most efficacious method of attaching the air cylinder to the slide was a bracket that clamps onto the top of the slide. The device consisted of two aluminum plates, one on either side of the slide, bolted together. One plate, the one to be mounted on the operator's side, had extrusions that mated with the weight saving cutouts made in the slide. This allowed for easier assembly and prevented the mounting bracket from sliding off the top of the slide. We

do not have to worry about the bracket sliding downward, because the cylinder will be pushing up.

The tooling plate was limited in width by the space which exists between the slide and the lever. This plate had four tapped holes which matched four clearance holes on the other plate so the plates can be bolted together. The bolts passed on either side of the slide. The top hole on the other plate was designed so that the piston would make contact with the slide housing. Both plates needed half circle cuts on the bottom to provide clearance for the pivot pin. Figure 36 shows the two plates bolted together and Figure 37 shows them mounted on the slide.

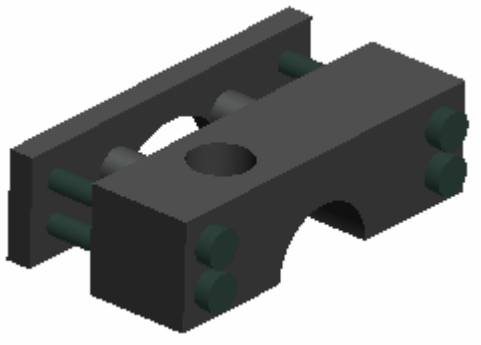

Figure 36 - Air Cylinder Bracket

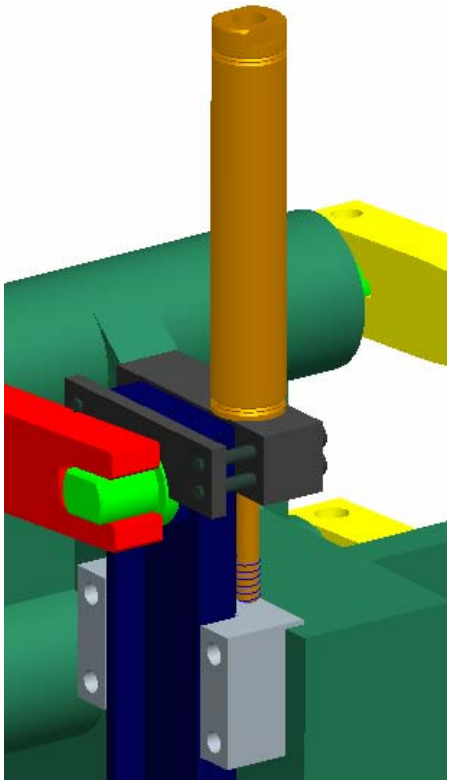

Figure 37 - Air Cylinder Bracket Mounted on Stripper Slide

6.4. Cam Lever Assembly

The cam levers are shown in the drawings to have the conrod, cam follower roller, and the cam spring all on the same side. On the machine we tested, the conrod is attached to the cam lever on the side opposite of the spring and roller. Given that the goal of most of our changes were to stiffen the linkage, we used FEA to find the spring constant of the cam lever in the same manner as before with the conrod attached to the same side as the roller and spring, as seen in Figure 38. The switch to same-side connections roughly doubled the stiffness of the three cam levers as shown in Table 4.

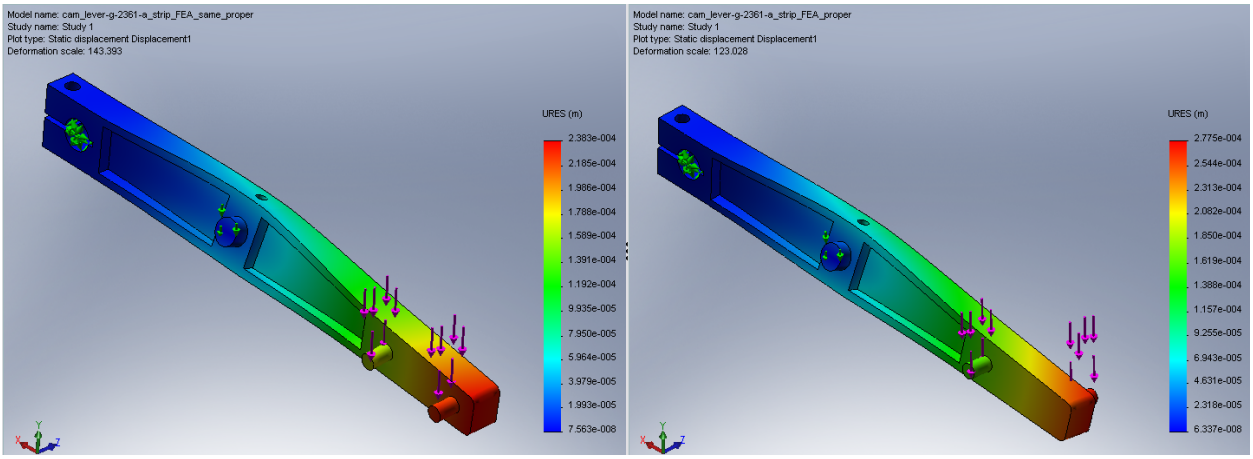

Figure 38: FEA of Cam Lever [Same-side Connections] (left); FEA of Cam Lever [Old Configuration] (right)

Table 4: Percent Increase in Cam Lever Stiffness for Opposite vs. Same Side Conrod Configuration

Cam Lever	k with conrod opposite spring and follower (N/m)	k with conrod on same side (N/m)	% Increase in stiffness
Stripper	978,888	2,103,415	115%
Stabilizer	1,481,790	2,745,210	85%
Vacuum	1,186,060	2,609,333	120%

Thus reversing these connections during set up would seem to be beneficial. However, because the cam levers are not the weakest links in the linkage, they have little effect on the overall spring constant. The percent increase in overall stiffness for the original shaft diameters is shown in Table 5.

Table 5: Percent Increase in Overall Stiffness with Existing Shafts for Opposite vs. Same Side Conrod Configuration

System	k.eff with conrod on opposite side (N/m)	k.eff with conrod on same side (N/m)	% Increase in overall stiffness
Stripper	1,300,000	1,488,000	14.5%
Stabilizer	535,200	553,700	3.5%
Vacuum	300,200	308,500	2.8%

Finally, we analyzed the percent increase in overall stiffness of each linkage with same-side connections after installing new shafts. Because the stiffness of the shaft is near the stiffness of the cam lever, especially for the stripper linkage, the results with the new shafts are more promising. Table 6 shows the results of this analysis.

Table 6: Percent Increase in Overall Stiffness with Improved Shafts for Opposite vs. Same Side Conrod Configuration

System	k.eff with conrod on opposite side – new shafts(N/m)	k.eff with conrod on same side – new shafts(N/m)	% Increase in overall stiffness – new shafts
Stripper	3,318,000	4,898,000	47.6%
Stabilizer	535,200	553,700	3.5%
Vacuum	637,600	676,300	6.1%

Forcing the cam lever to have all of its connections on one side increases the overall stiffness of the stripper linkage by 48%. If the addition of the air cylinder to the back of the stripper tooling slide sufficiently raises the effective mass, causing vibration problems, then the 48% increase in stiffness should be seriously considered.

With the new 1-inch-diameter shaft, the spring constant of the shaft at the follower is slightly more than twice the value of the spring constant of the cam lever. This is not ideal because the cam lever is furthest from the end effector and thus has almost the whole of the effective mass acting on it. If the conrod is attached to the same side, then the cam lever's spring constant is nearly equal to the shafts spring constant. This would justify placing the conrod on the same side, if testing indicates that the cam lever is acting as a spring.

6.5. Vacuum Connecting Rod Air Cylinder

Another area for improvement is the location of the air cylinder on the Vacuum system connecting rod. Air cylinders in general should be located as close as possible to the end effector so that there they are acting on less mass and lower inertial forces are applied to them. By having less mass on the air cylinder the air pressure inside the cylinder can be minimized. By having to accelerate a large mass acting on top of the air cylinder there is a risk of the cylinder compressing undesirably which would affect the position of the end effector as well as create excessive vibrations. To prevent this from happening, adequate air pressure needs to be maintained inside the cylinder. The less mass acting on top of the cylinder, the less air pressure is needed, thus also lowering the cost of energy needed to pressurize the air.

6.6. Stripper Pusher Proposed Redesign

From the high-speed video we noticed that the stripper pushers were not fully engaging the excess material. Instead, the excess material was caught by a corner on the inside of the pusher as seen in Figure 39. Normally the excess material slides inside the slot created between the stripper tool and the pusher but we rarely saw this happen on the high-speed video. More often than not, the material was caught on an edge of the stripper pusher and stripped off the vacuum head.

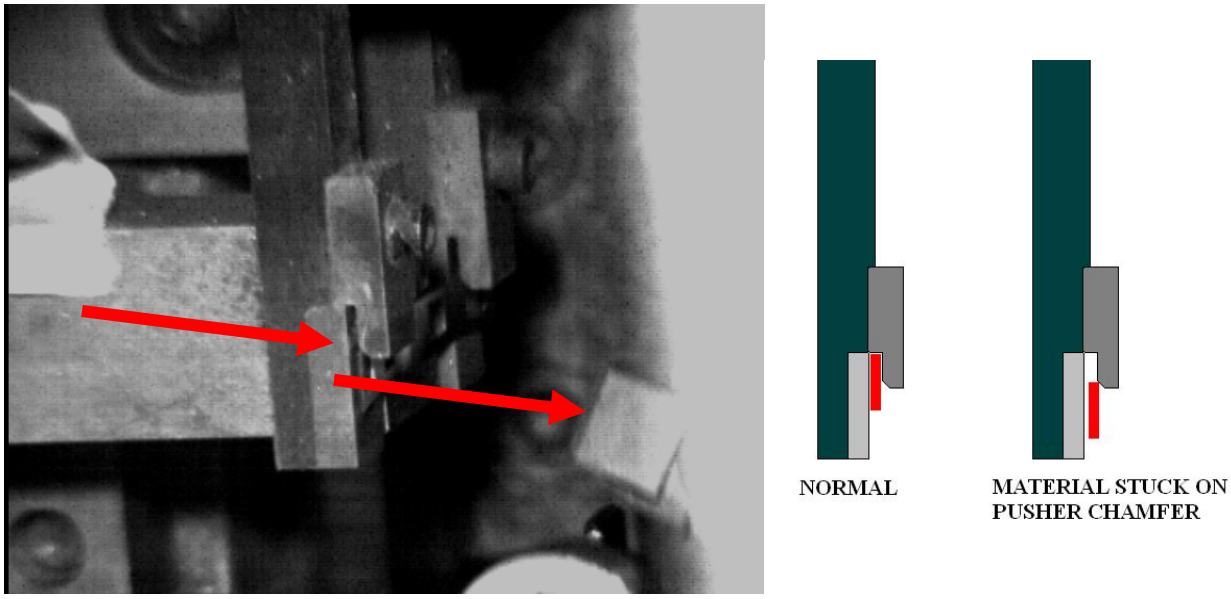

Figure 39: Excess material being stripped from the vacuum head

This caused the material to follow an unpredictable path as it fell down toward the chute. There have been reports from the machine operators that there is significant amount of scrap on the floor for that station. As can be seen from Figure 39, the scrap material is being bent because the ends are touching the stripper while the middle is being held by the vacuum. This bending is what is most likely causing the excess material to get caught on the edge of the stripper pusher. The position of the vacuum head as it dwells relative to the stripper tool causes the bending. The vacuum head dwells behind the stripper tool every time but we do not know if this is designed to be so. What we do know is that the excess material's ends vibrate significantly as the material comes off the nest and when these ends touch the stripper tool there is significant damping and the vibrations stop before the stripper begins its downward motion. If the excess material ends were still vibrating when the stripper begins its downward motion, there would be a possibility that the pushers might miss the ends entirely or only catch one end, resulting in the material not being stripped from the vacuum head. Thus the bending seen on Figure 39 is an acceptable situation considering the alternative.

We believe that if the excess material slides all the way inside the slot created by the stripper tool and the pusher, then the path of the excess material as it falls towards the chute will be more controlled, which will result in less scrap ending up on the floor.

In order to ensure that the excess material slides inside the gap created by the stripper tool and the pusher, we propose a redesign of the pusher. One possible redesign is shown in Figure 40. Figure 40 shows the current pusher cross-section on the left and our proposed redesign on the right. The main goal of the redesign is to reduce the effect of the edge where the excess material gets caught but the ultimate goal is to cause the excess material to slide inside the gap instead of getting caught on an edge. This can be done by changing the slope of the original face. We have only proposed a possible redesign and that redesign can be altered to facilitate machining but the fact remains that the original pusher design needs to be improved.

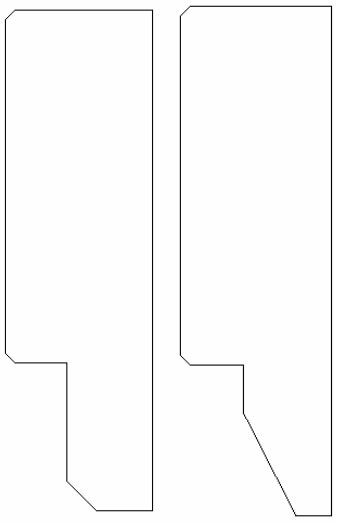

Figure 40: Original pusher design (left) and proposed redesign (right)

7. Implementation and Testing

In order to evaluate the actual improvements which our redesigns made we gathered more experimental data. We replicated the methods and procedures used for the earlier tests (accelerometers placed in the same locations, etc.) so that the results could be compared.

7.1. Improved Cams Alone

The redesigned cams were installed in the machine and we recreated our original accelerometer experiments in order to determine the validity of our redesign. Accelerometer placement, time interval, averaging and trigger placement were all identical. In this way we can directly compare the results of our initial testing with the results generated by our improvements.

Before the tests could continue, mechanics first verified that the new cams did not generate any impacts as a result of tool misalignment. Although a small adjustment had to be made to the conrod of the vacuum linkage, this adjustment is likely a result of the previous cam having been reground and thus being smaller in diameter than the new cam. As expected, the slightly lower displacement of the stripper was still within the clearance between the stripper tool and vacuum head.

7.1.1. Stripper Cam

Accelerometer measurements were taken on both the tooling lever and end effector of the stripper linkage. As we can see in Figure 41, the large impacts have not been eliminated, as was expected. As these impacts do not result from the intended motion of the linkage, the cam was not designed to address this issue. Later analysis in Section 7.3 will discuss the results of the air cylinder used to eliminate these impacts.

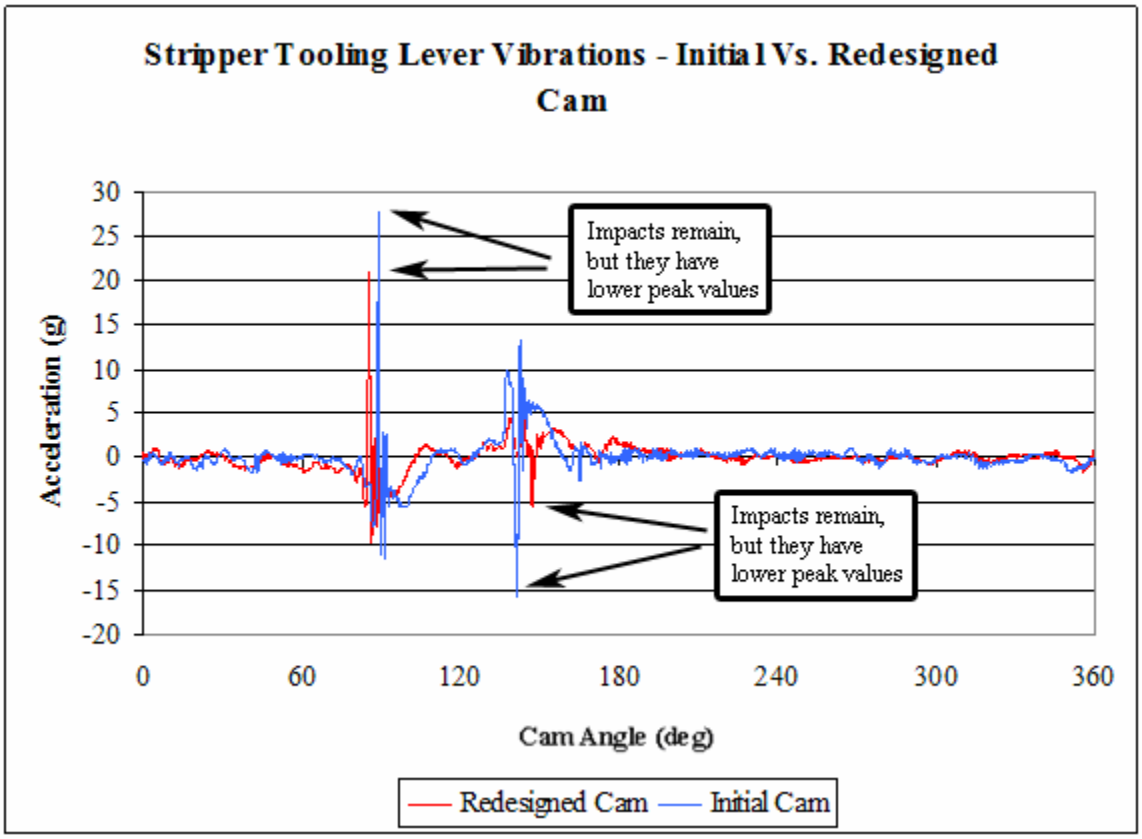

Figure 41: Stripper Tooling Original vs. Redesign Cam Vibrations (B1 in Figure 8)

Comparing the acceleration profiles of the operator lever with the initial and redesigned cams, we can see that the redesigned cam does perform its intended function. Disregarding the impact events, the peak positive acceleration has dropped from six g's to about 4 g's. Even the magnitude of the impacts has decreased as the theoretical acceleration at the time of impact is much lower for the redesigned cam.

We can also see that the vibration has decreased. In order to quantitatively compare the vibrations of the two curves, we can look at the RMS value of the acceleration curve. Note that the RMS value of the intended theoretical acceleration profile has been subtracted from the following values. From Table 7 it is clear that the redesigned cam has decreased vibrations by 32.8%.

Table 7: Stripper Original vs. Redesign Cam Acceleration RMS

RMS Value of Acceleration Curves (g)		
Initial Cam	1.83	100%
Redesigned Cam	1.23	67.2%

7.1.2. Vacuum Cam

The results of the vacuum cam are slightly more ambiguous. As was stated earlier, decreasing the magnitude of the impact comes at the cost of increasing the acceleration profile elsewhere.

We can see from Figure 42 that the peak accelerations of the vacuum head motion have decreased significantly by a factor of about 2, and the magnitude of the impact has been reduced dramatically by a factor of 7. This impact represents a critical point in the linkage motion, when the vacuum head picks up the scrap from the nest. Therefore, by reducing the impact and subsequently the noise of this event, the vacuum head should be able to perform much more consistently and reliably.

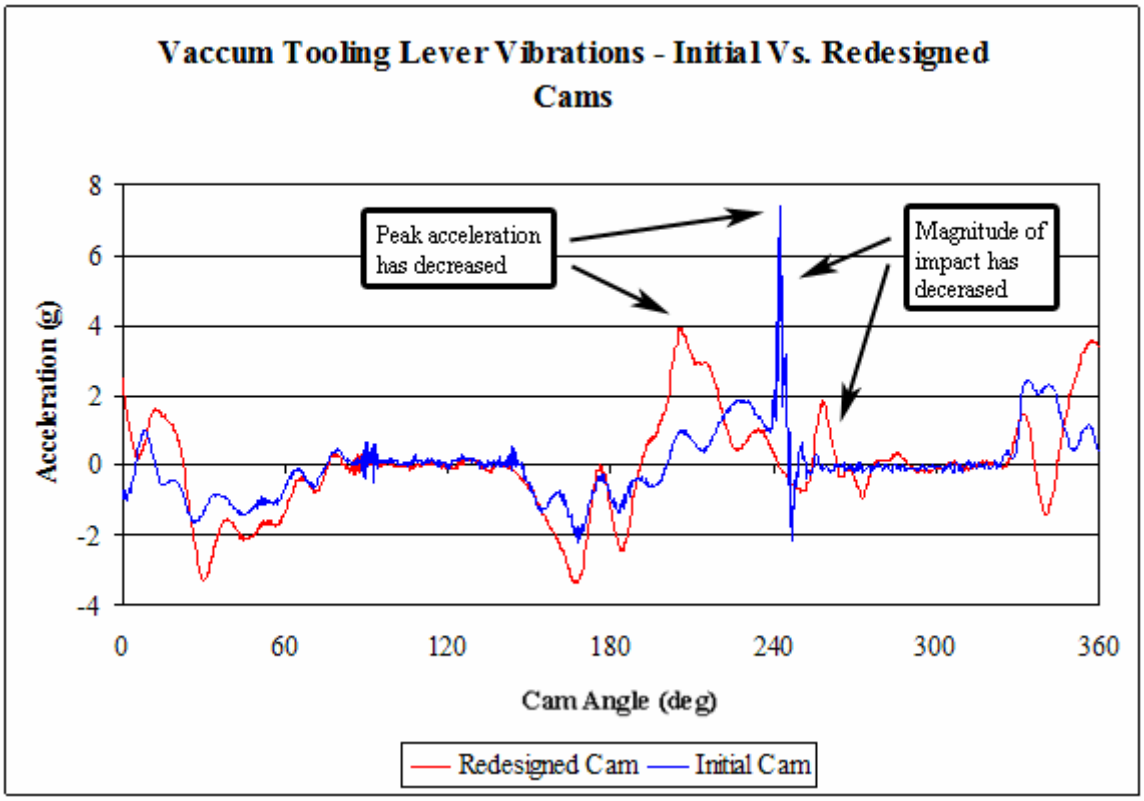

Figure 42: Vacuum Tooling Vibrations Original vs. Redesign Cam (C1 in Figure 8)

Finally, note that, as an unintended consequence, the vibration has increased slightly for the redesigned cam. In particular, at the times of the peak negative magnitude or positive magnitude accelerations, the vibrations are higher than the nominal value. However, the new cam did succeed in removing the unintended impacts, which were much greater than the peaks of the new vibration. We can see in Table 8 that overall vibration has increased by 23.2%. This increase in vibration will be eliminated by the larger torsion shaft, and the effects of this shaft will be discussed later in Section 7.2.

Table 8: Vacuum Original vs. Redesign Cam Acceleration RMS

RMS Value of Acceleration Curve for Vacuum Linkage (g)		
Initial Cam	0.517	100%
Redesigned Cam	0.637	123.2%

7.2. Improved Cams and Shafts

Redesigned shafts of one inch diameter were manufactured for both the stripper and vacuum linkage. These shafts were installed with the redesigned cams still in place. By comparing the results of the data taken with only the redesigned cams installed with the data taken with both the redesigned cams and shafts, we can see the effects that the new shafts have on each linkage.

7.2.1. Vacuum Linkage

The vacuum linkage's performance was improved by substituting the larger diameter shaft. Comparing the vacuum tooling motion, the peak accelerations have not dropped substantially, from about 3.9 g's with the redesigned cams alone down to about 3.7 g's with the redesigned cams and shafts, as shown in Figure 43. Also seen in Figure 43 the second dwell when the vacuum head is against the nest shows significant improvement with the new shaft. With the redesigned shaft, the tooling lever acceleration curve stays under one fourth of a g during this dwell, whereas, with the original shaft, the acceleration has oscillations with peaks of nearly 2 g. This visual improvement is deceptive however because when we took the data with the redesigned shafts the vacuum conrod was set up too short such that there was too much over-travel thus the small bumps in the theoretical acceleration (shown on the blue line at the second dwell in Figure 43) of the vacuum head after the constant slow velocity approach to the nest are not seen because the vacuum head is already against the nest. Essentially the vacuum head is impacting the nest before the low velocity part of the cam profile intended for the impact in our redesigned cam. Thus the lack of vibrations during the dwell in Figure 43 is not attributable to redesigned shaft.

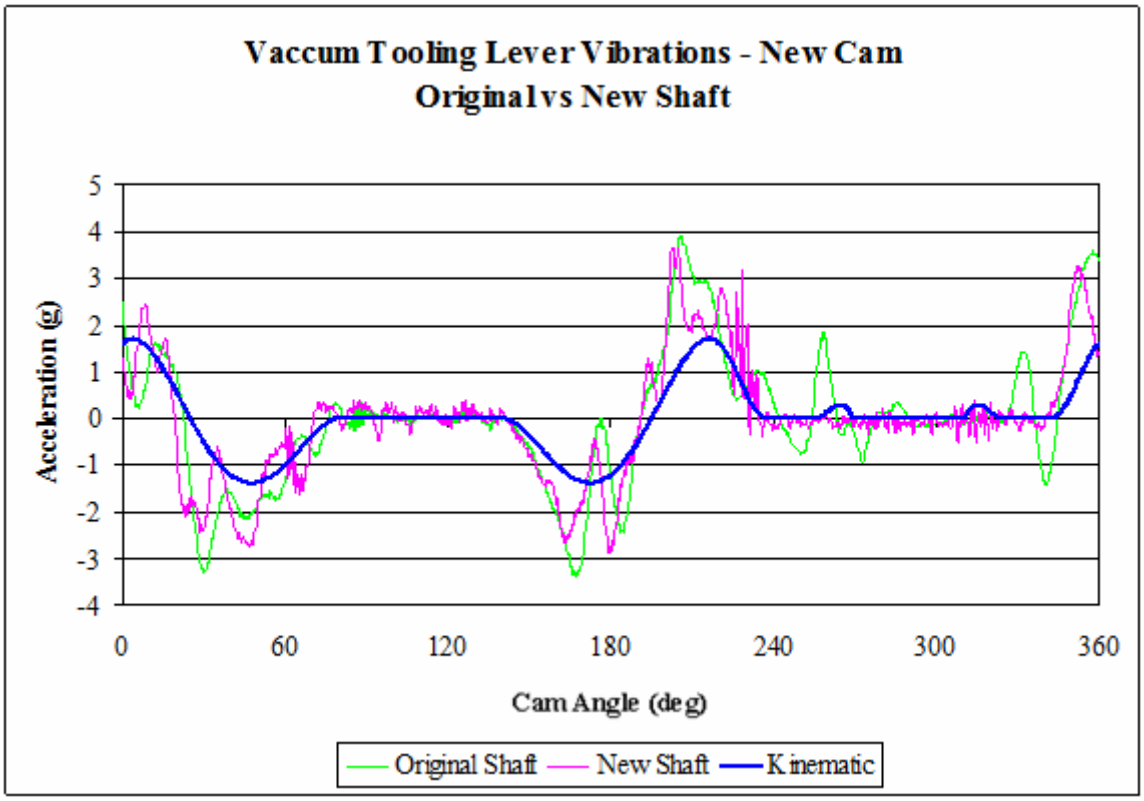

Figure 43: Vacuum Tooling Lever Vibrations Original vs. New Shafts (C1 in Figure 8)

Therefore in order to see the improvement of the linkage made by our redesigned shaft we can look at the back lever and the tooling lever acceleration curves. The acceleration curves for the original shaft show large discrepancies between the tooling lever and the back lever as seen in Figure 44. We did not take these readings simultaneously; we took them on the same day with an unchanged external trigger set up. The data should be perfect and, regardless, the magnitude of the time offset in oscillations is much larger than any likely error. The discrepancies in phase lag and magnitude between the tooling lever and back lever acceleration curves are far greater in with the original shaft than with the redesigned shaft as seen in Figure 44 and Figure 45.

Further improvement is evidenced by the fact that the bumps in theoretical acceleration based on the cam profile are not present in the accelerometer data taken on the back lever with the redesigned shaft. This indicates that the over-travel of the vacuum head is not being absorbed

by the redesigned shaft as it was with the original shaft. With the new shaft the over-travel is being absorbed presumably by the air cylinder in the conrod.

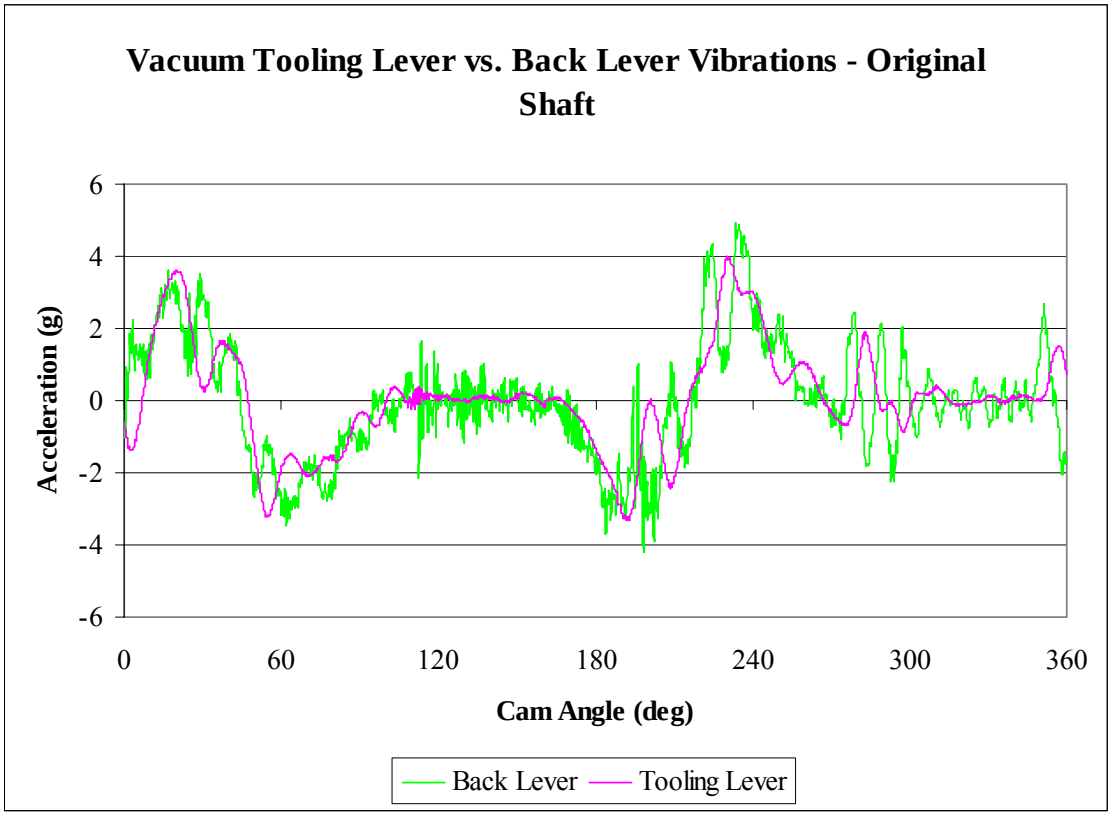

Figure 44: Vacuum Back Lever vs. Tooling Lever Original Shaft (C2 & C1 in Figure 8)

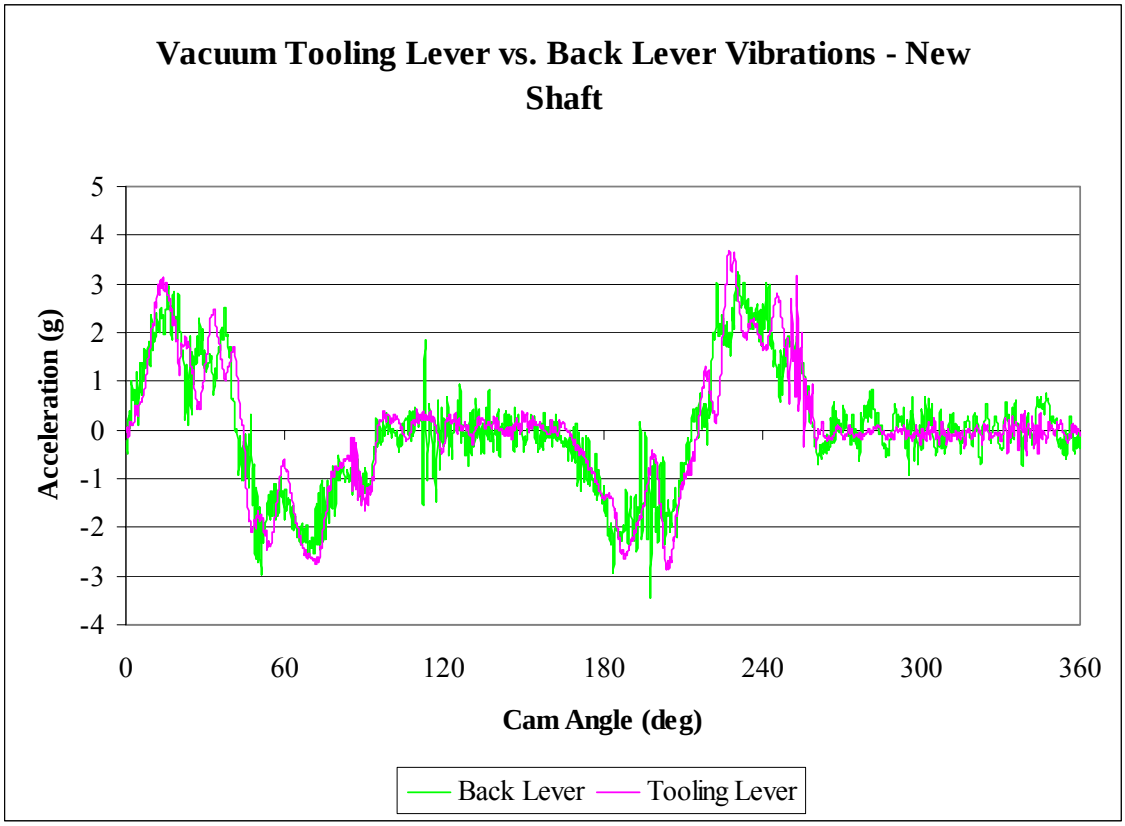

Figure 45: Vacuum Back Lever vs. Tooling Lever Redesigned Shaft (C2 & C1 in Figure 8)

The vibrations of the linkage with the new shaft are much sharper and the frequency of the vibrations is higher. Figure 46 shows the time required for the acceleration curves of the original and redesigned shafts to return to an arbitrary level on one of the spikes in acceleration. This is significant because the less steep a given vibrations and the more time it takes for one spike the are under the curve is larger thus the velocity and the displacement of the lever as a result of the vibrations is larger. Larger vibrational displacement makes the vacuum less reliable. So though the acceleration peaks due to vibrations may not have decreased much the velocity and displacement decreased substantially.

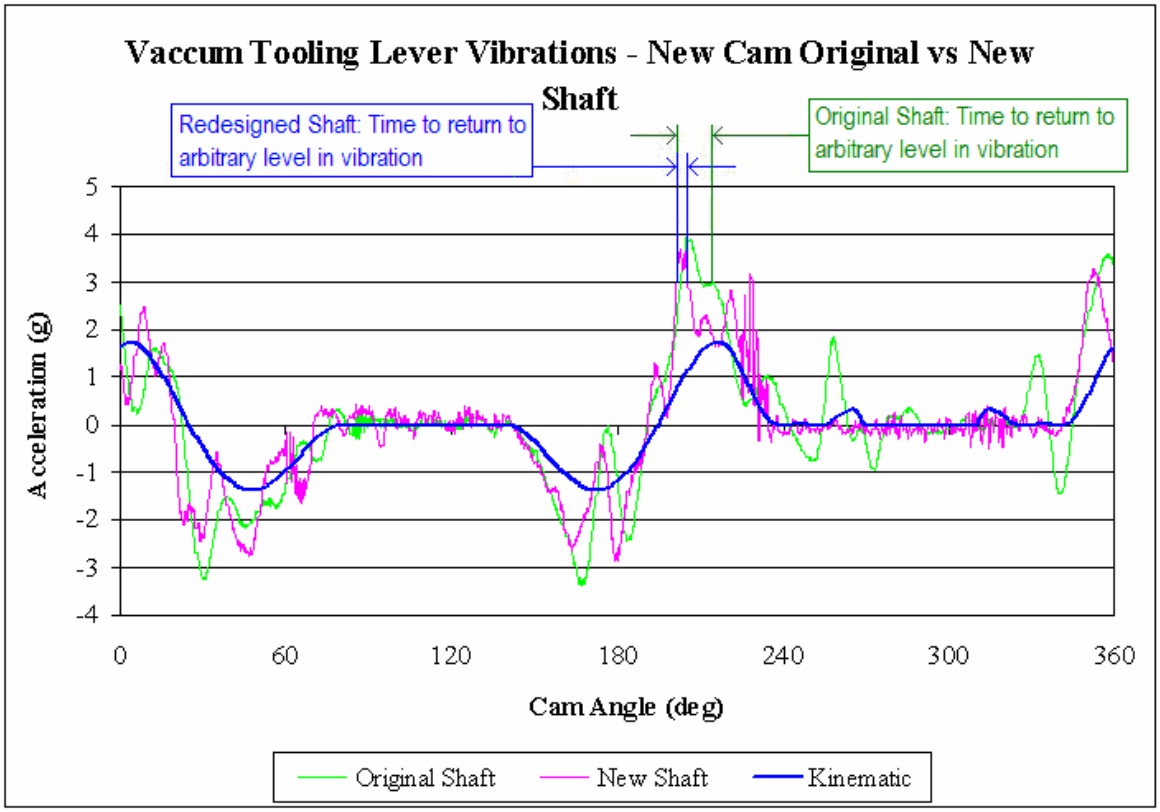

Figure 46: Vacuum Tooling Lever Vibration Frequency Comparison Original vs. New Shafts (C1 in Figure 8)

Although, the peaks in acceleration may not have decreased significantly, the RMS value did. Again, we use the RMS value as an indicator of vibrations; the lower the value, the less noise there is in the data. Note that, as for the RMS values obtained for results presented earlier, the RMS value of the theoretical curve has been subtracted from the RMS value of the data so that we remove the effects of the intended motion. As shown in Table 9, the RMS value increased with the new cams over the old cams by 23.1%. The new shafts brought the value below the original value by 5.2%. Thus the new shaft on the vacuum linkage corrected the one drawback of the new vacuum cam when it was used with the old, less-stiff shaft.

Table 9: RMS of Acceleration Curves of Vacuum Tooling Lever

RMS Value of Acceleration Curve for Vacuum Linkage (g)		
Initial Cam	0.517	100%
Redesigned Cam	0.637	123.1%
Redesigned Cam and Shaft	0.490	94.8%

The results from the redesigned shafts of the vacuum tooling vs the vacuum tooling lever are shown in Figure 47. This test for deviation between the vacuum tooling and tooling lever was performed in order to verify that the force exerted by the air cylinder on the back of the tooling slide was sufficient to keep the linkage slack taken up in one direction. We knew that with the original shafts the force was adequate but with the stiffer shaft that may have changed. Earlier readings taken with the redesigned shaft indicated slight deviations in the acceleration curves of the vacuum tooling from the tooling lever. This data was erroneous however because it was taken when the redesigned vacuum shaft was beginning to bind due to minor inaccuracies in the re-bored shaft holes of the frame. Proper data was taken after the binding had been addressed and corrected. As seen in Figure 47 (which is the proper data) there is only slight deviation, the magnitude of which is nugatory. Thus the force exerted by the air cylinder on the back of the vacuum slide is sufficient at its current pressure.

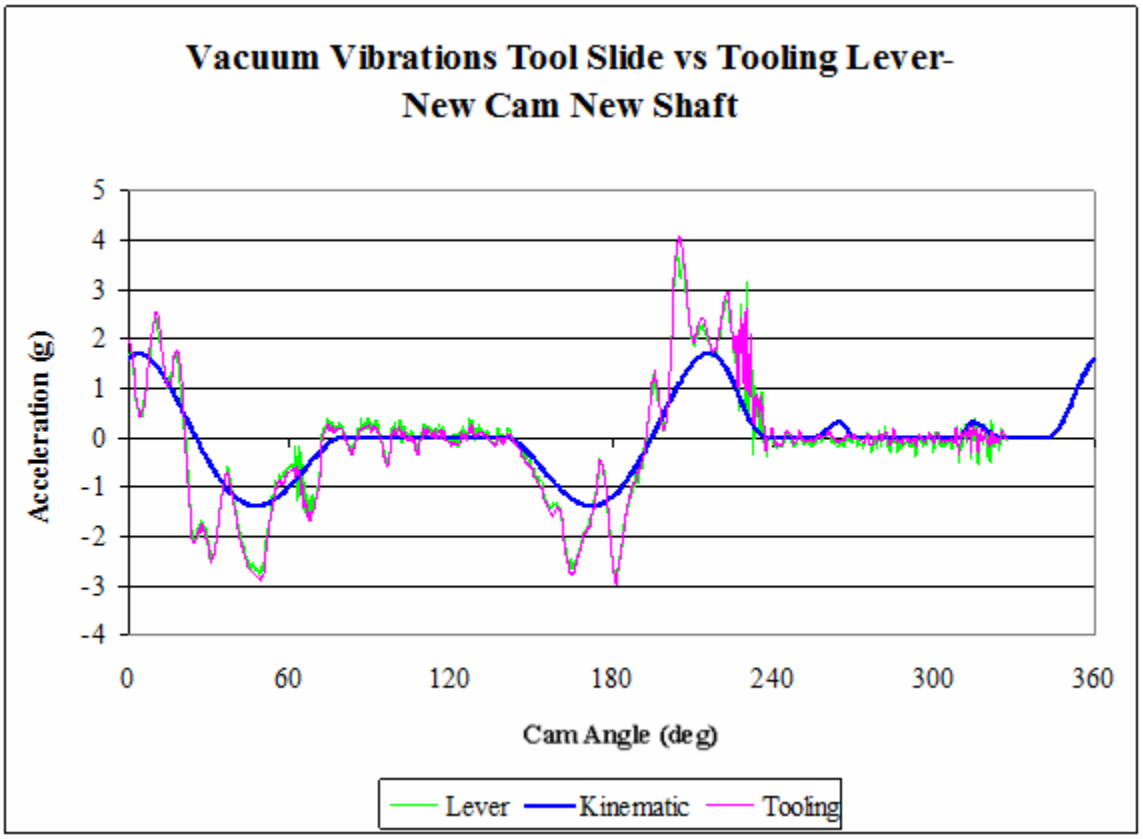

Figure 47: Vacuum Tooling vs. Tooling Lever Vibrations - New cams and Shafts (C4 & C1 in Figure 8)

7.2.2. Stripper Linkage

The introduction of a stiffer shaft did not substantially improve the stripper linkage. As we can see in Figure 48, the acceleration peaks are roughly equal.

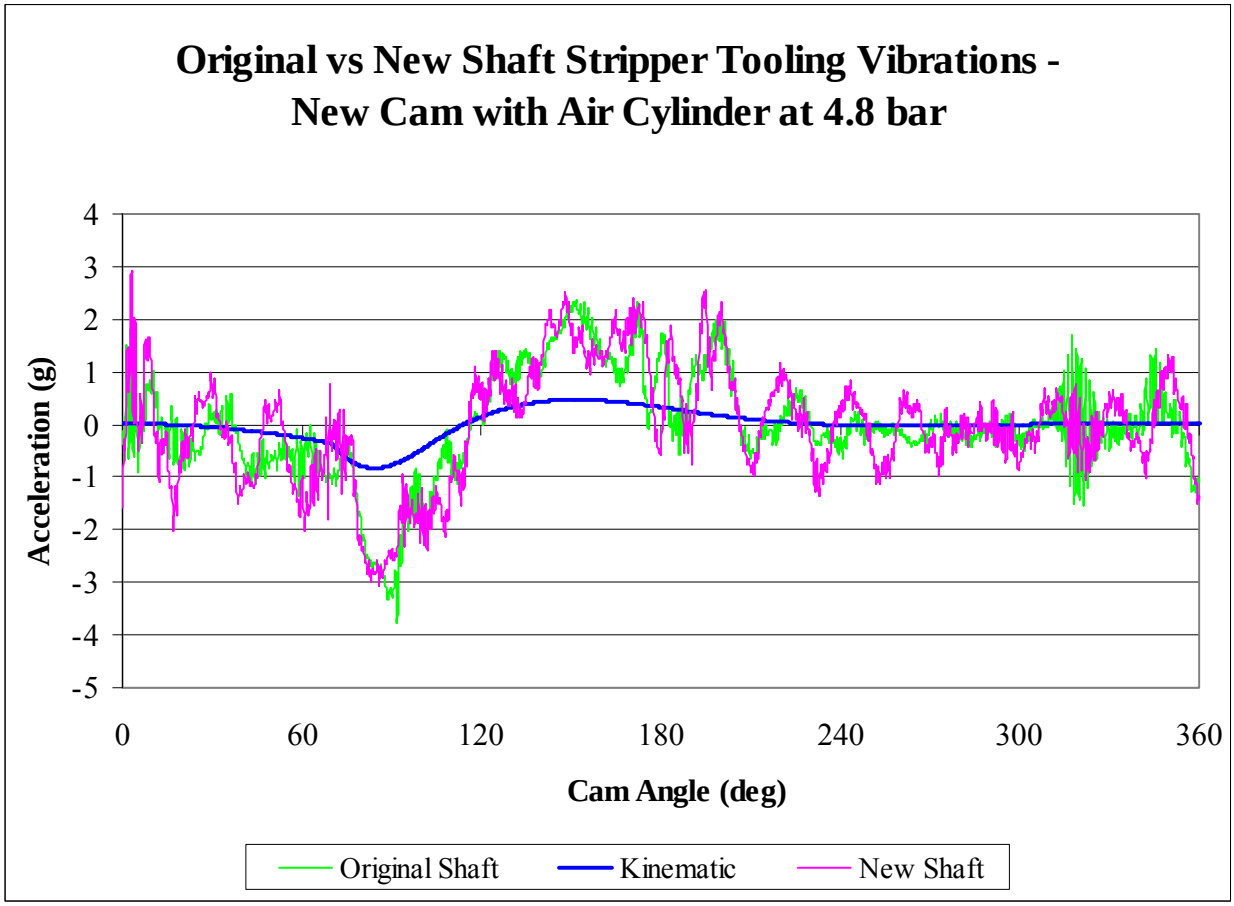

Figure 48: Stripper Tooling Lever Vibrations Original vs. New Shaft

If anything, the new shaft worsened the vibration of the system. The RMS value of the acceleration with the new cam and shaft is 4.3% higher than the RMS value of the acceleration with only the new cam, as shown in Table 10.

Table 10: RMS Values for Stripper Tooling Lever Accelerations

RMS Value of Acceleration Curve for Stripper Linkage (g)		
Initial Design	1.83	100%
Redesigned Cam with Air Cylinder at 4.8 bar	0.749	40.9%
Redesigned Cam and Air Cylinder at 4.8 bar and Redesigned Shaft	0.827	45.2%

We believe the stripper linkage vibration was worsened by the new shaft because the shaft was too stiff. We originally wanted to use a 7/8 inch diameter shaft such that the shaft

would remain the least stiff component in the linkage, assuming the cam lever was set up properly with the conrod on the same side as the spring and follower as discussed in Section 6.4. Even with the cam lever set up as it is currently with the conrod on the side opposite the spring and follower, the stiffness of a 7/8 inch diameter shaft will be twenty six percent greater than the stiffness of the cam lever. With the conrod attached to the cam lever on the same side as the spring and follower the stiffness of the cam lever is more than doubled as discussed in Section 6.4 making it seventy percent stiffer than a 7/8 inch shaft. We choose the 7/8 inch diameter shaft for this reason, because if the conrod placement was changed the shaft would remain the least stiff link, which was desirable because the shaft is closer to the end effector than the cam levers is.

The further away from the end effector and closer to the cam follower, the greater the effective mass acting on each link is because there are more links between it and the end effector. The further from the end effector the most compliant (that is least stiff) link is the worse the vibrations will be.

We were unable to test the linkage with the cam lever set up properly due to time constraints. Knowing that it was probable, we tested for deflection in the cam lever in order to verify that the increased vibrations could be caused by the deflection of the cam lever. If there was negligible deflection then we would know that the cam lever hypothesis was wrong. We mounted accelerometers on the cam lever at the location of the follower and at the end where the conrod is attached as shown in Figure 8, labels B5 and B3. The measurements were taken at the same time so that they would be in phase with each other. The curves showed a slight time offset between the vibrations as shown in Figure 49. This indicates that as the cam motion moves the follower, there is a time delay before the end of the cam lever experiences that motion. During

this time delay, the deflection at the end of the cam lever will be large as it waits to "catch up" with the follower. This large deflection indicates a soft spring. Note that, as further analysis, it would be possible to numerically integrate the acceleration data in order to obtain the actual amount of deflection which occurs. This process, however, is not trivial. As we had limited time for analysis, and the data supports our theory qualitatively if not quantitatively, this integration was not performed.

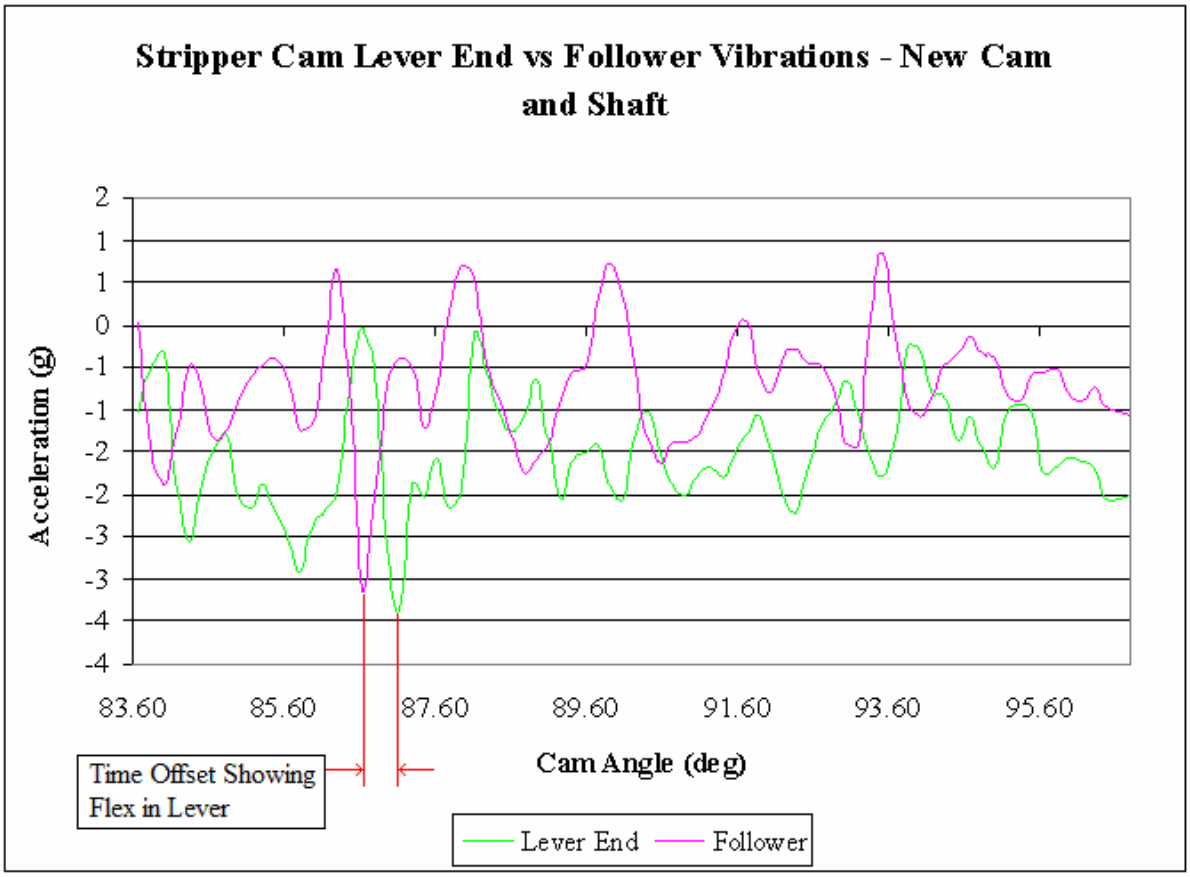

Figure 49: Time Offest in Acceleration curves of Cam Lever at End and at Follower, Showing Flex (B3 & B5 in Figure 8)

7.3. Stripper Linkage Air Cylinder

An air cylinder, Bimba 042 (3/4" bore 2" stroke, single action, spring retracted), was mounted on the top/back of the stripper linkage in order to take up the slack in the linkage in one

direction regardless of the motion of the linkage, eliminating the slack eliminates the intra-linkage impacts, as previously described in Section 5.4.

With the air cylinder connected to an 80-95 psi source (the maximum available on the machine) the tooling slide and lever follow each other precisely as shown in Figure 50. Also shown in the figure is an anomalous spike in acceleration, approximately 10 g with an approximately 5 Hz ring out. Given that the tooling almost follows the theoretical quite well except in this place and given that at this time the acceleration from the cam is nearly zero this spike and ring out was thought to be from extraneous source. With the air cylinder disconnected there is no spike in the same time interval where it occurs with the air cylinder connected at full pressure; thus it is caused by the presence of the functioning air cylinder.

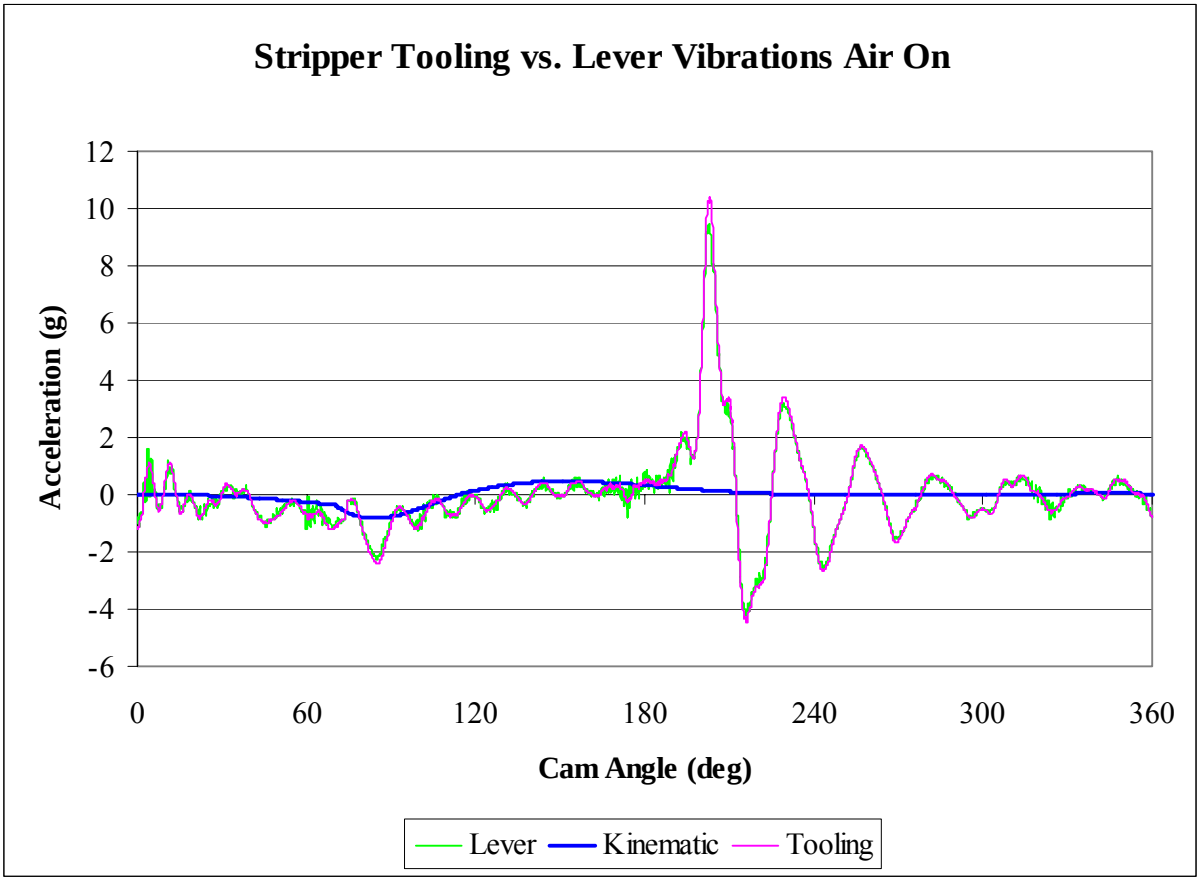

Figure 50: Stripper Tooling vs. Lever Vibrations - Air Cylinder at 6.0 Bar w/ New Cam (B4 & B1 in Figure 8)

It is not a relatively steeply sloped spike, indicating the presence of some damping. This damping lead to the suspicion that the spike was due to either binding in the tooling slide caused by the slightly off center force exerted by the air cylinder or binding in the air cylinder itself. The spike occurs when the stripper is just starting to return upward from its lowest point. At this time the vacuum head is just starting to travel inward toward the nest, thus we also supposed that the spike could have been the result of the vacuum head the stripper forks rubbing. To test these ideas we first mounted an accelerometer on the vacuum head vertically to make absolutely certain that there was not any impact/interference between the vacuum head and stripper tooling. There was not any interference.

Next to determine if any possible binding could be occurring in the cylinder we manually tested the rigidity of our cylinder mounting bracket: it was sufficiently rigid such that the force exerted would not cause the bracket to flex thus the air cylinder become slightly out of vertical which would create a slight force normal to the axis of the cylinder thereby possibly causing it to bind. This was not occurring, thus the only other thing to be binding is the slide, which seemed unlikely and would have been difficult to test so we moved on to other tests.

We next concentrated on determining if the relatively low frequency of 5 Hz was caused by the air cylinder or not. We first did some rough calculations: based on the existing parameters of the cylinder we found that the reservoir volume required for the air cylinder to have fundamental frequency of 5 Hz was between 100 and 160 cubic inches. This is a completely reasonable volume for the actual reservoir to be, thus the air cylinder could have been showing the spike because the cylinder was being excited at one of its natural frequencies.

We chose to test this theory by varying the air pressure to the cylinder. By mounting a pressure regulator in the line to the air cylinder we were able to take accelerometer tests with

various pressures. The accelerometers were mounted on the tooling side lever and the top of the tooling slide the same as before. Readings were taken from 2 to 6 bars by steps of 1 bar and took 25 time-averaged readings at each pressure. Too little pressure did not keep the joint from impacting but too much pressure caused resonant vibrations at the air cylinder's natural frequency of about 5 Hz. Between these two conditions was an optimum operating pressure. of 4.8 bars (70 psi), as seen in Figure 51. The pressure is high enough to keep the linkage slack taken up in one direction with no intra-linkage impacts and the air cylinder is functioning as intended. That pressure is below the level (around 5+ bar) where we start to see oscillations at 5 Hz of as much as 10 g peak magnitude as shown in Figure 50.

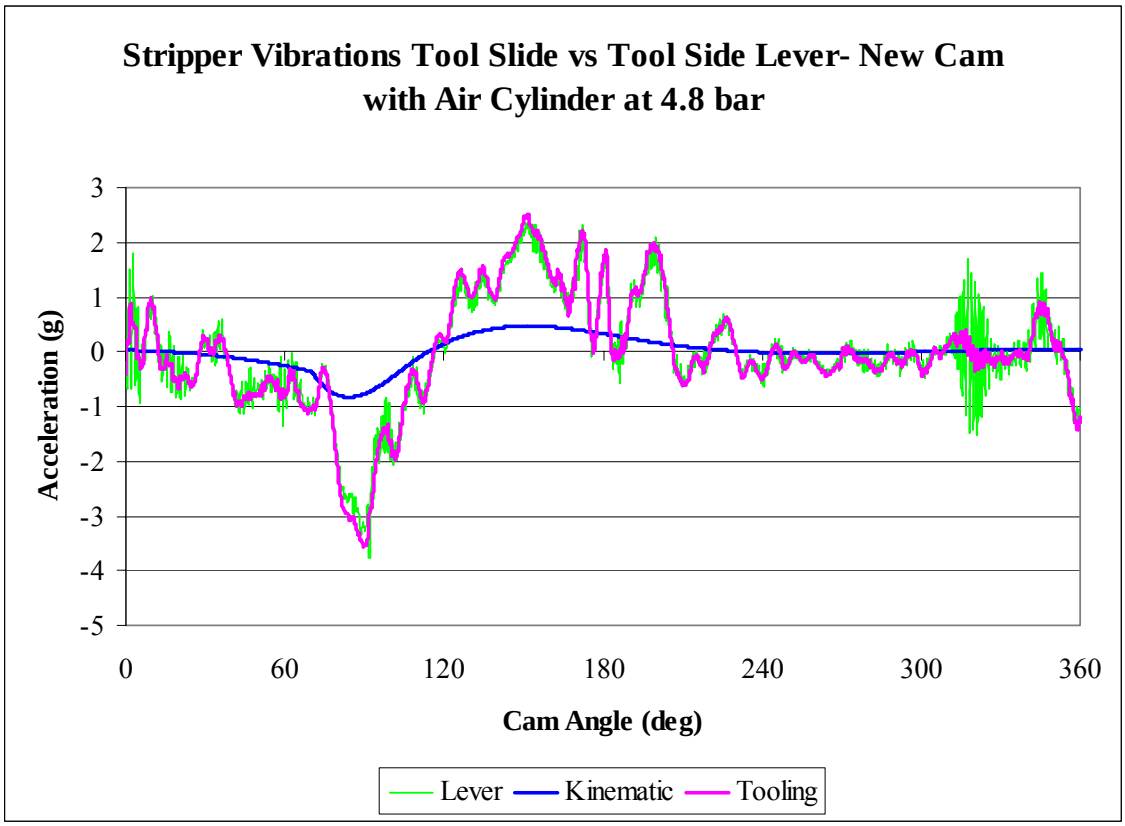

Figure 51: Stripper Tooling vs. Lever Vibrations - Air Cylinder at 4.8 Bar w/ New Cam (B4 & B1 in Figure 8)

With lower pressure such as 2 bar, the RMS average noise is higher, which indicates that the air cylinder does not adequately keep the slack taken up in one direction. This means that the

air cylinder is only helpful if it's at the right pressure, not too high like in Figure 50 and not so low that we see high vibrations like without the air cylinder, as shown in Figure 52.

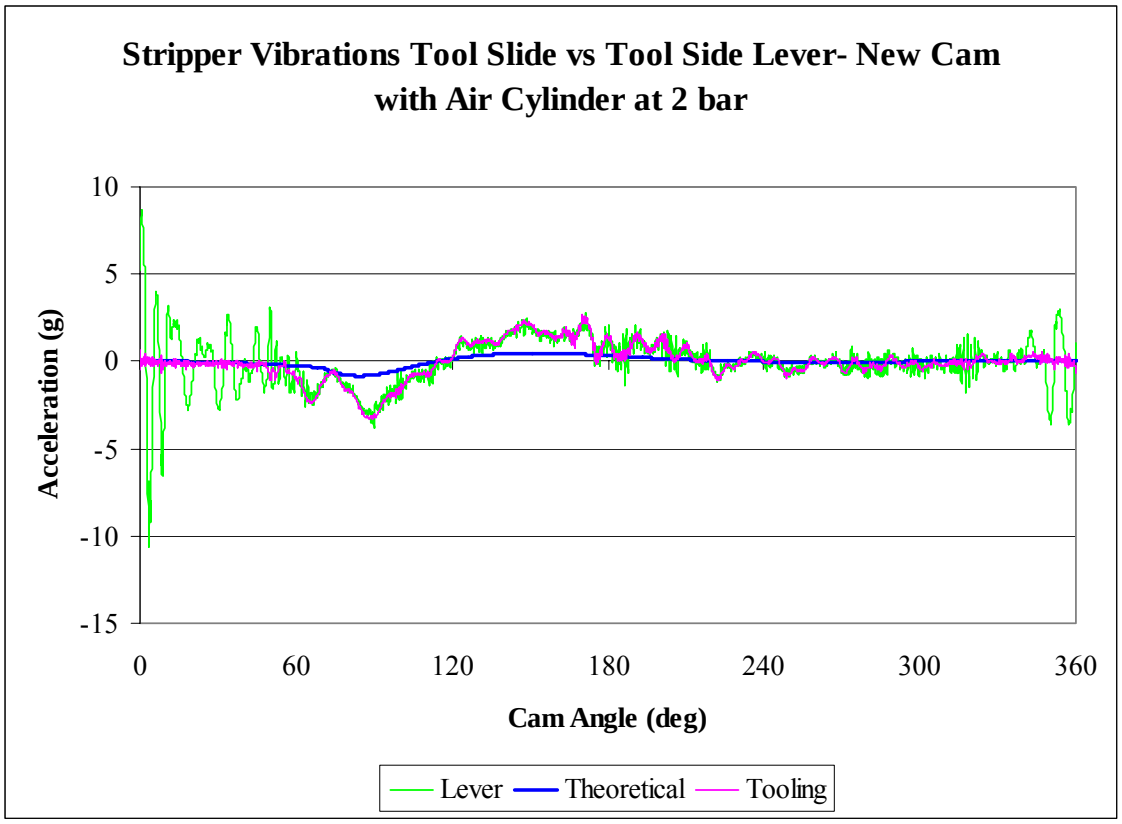

Figure 52: Stripper Tooling vs. Lever Vibrations - Air Cylinder at 2.0 Bar w/ New Cam (B4 & B1 in Figure 8)

The result is that the air cylinder at the proper pressure eliminates the 11-g intra-linkage impact seen in Fifure 52. If the proper pressure is used there is no other detrimental effect seen in the accelerations of the Stripper tooling. Table 11 indicates that with 4.8 bar on the air cylinder the RMS value is 41% of the initial value and 61% of the redesigned cam without the air cylinder.

Table 11: RMS Values for Stripper Tooling Lever Accelerations

RMS Value of Acceleration Curve for Stripper Linkage (g)			
Initial Design		1.83	100%
Redesigned Cam		1.23	67.2%
Redesigned Cam with Air Cylinder	2.0 bar	1.66	90.4%
	6.0 bar	1.67	91.3%
	4.8 bar	0.749	40.9%
Redesigned Cam and Air Cylinder at 4.8 bar and Redesigned Shaft		0.797	43.5%

Overall the new cam and air cylinder reduced the absolute peak acceleration of the stripper tooling lever from 27 g to 3.7 g.

8. Conclusions & Recommendations

We made design changes to two of the three sub-systems on the excess material unload station: the vacuum system and the stripper system. Through redesign, experimentation, and analysis, we are able to present the following conclusions and recommendations for improving this station.

8.1. Vacuum System

Vacuum Stage 1 - (Good) Solution

Our results show that just installing our redesigned cam on the vacuum-system improves its dynamic behavior when properly set up by completely eliminating the impact at excess material pickup. This should improve reliability of function at this station. However, if the new cam is used with the existing 5/8-diameter vacuum-linkage shaft, there will be a 23% increase in RMS average residual vibration over the cycle . Replacing the cam alone nevertheless reduces the severity of impacts at the expense of slightly larger overall vibration. This is a significant improvement and a worthwhile tradeoff but is not the best that can be achieved.

Vacuum Stage 2 - (Better) Solution

In addition to replacing the cam, the vacuum system shaft should be enlarged from its present 5/8-in diameter to one inch. The thicker and stiffer shaft negates the increase in vibrations created by the installation of the redesigned cam, reducing the RMS value of vibration

to below that of the original design. In addition, the stiffer shaft reduces peak accelerations and eliminates the recoil from over-travel windup seen with the original shaft. Using the redesigned cams in combination with the one-inch-diameter shaft gives a 5.2% reduction in average residual vibration as compared to the original cam with the smaller shaft while retaining the advantage of impact elimination.

Vacuum Stage 3 - (Best) Solution

The vacuum system is further improved if, in addition to the two changes noted above, the cam lever is set up such that the conrod is attached on the same side of the lever as the follower and air spring. Attaching the conrod on the same side of the lever as the follower and air spring gives a 6% additional increase in the stiffness of the vacuum system as a whole. This increase in stiffness will further reduce vibrations.

8.2. Stripper system

Stripper Stage 1 - (Good) Solution

Installing the redesigned stripper cam improves that linkage's dynamic behavior significantly; it reduces peak accelerations by eliminating unnecessary returns to zero acceleration in the cam profile and also reduces vibrations and intra-linkage impacts. Just replacing the cam gives a 33% reduction in vibrations.

Stripper Stage 2 - (Better) Solution

In addition to replacing the stripper cam, adding an air cylinder mounted on the back of the stripper slide will completely eliminate the intra-linkage impacts by taking up the linkage slack in one direction. This air cylinder eliminates unintended impact accelerations in the stripper

motion and reduces overall vibration from 25 g to 4 g. This air cylinder will also decrease tool and roller follower wear, allow highly worn links to be used longer (because clearance is removed), increase the reliability of the stripper system, and decrease the amount of scrap material that misses the chute. Including this air cylinder pressurized to 4.8 bar in addition to installing the new cam gives a total reduction of 59% in vibrations and completely eliminates impacts in this linkage.

The stripper pusher inserts should also be reworked. The chamfer on their leading edge should be made steeper and made to start further out on the leading edge as shown in Figure 53, reproduced here. This will make the stripper better able to catch the material in the vertical slot and make the material fall into the chute more reliably.

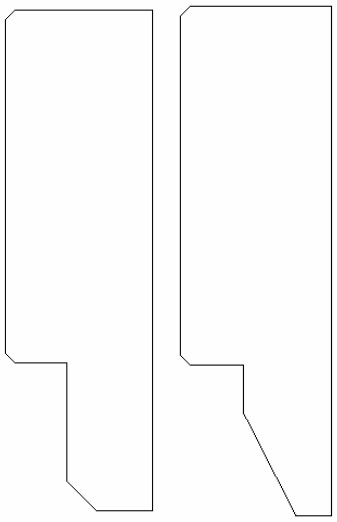

Figure 53: Original pusher design (left) and proposed redesign (right)

Stripper Stage 3 - (Best) Solution

The shaft of the stripper linkage can be enlarged to a 7/8-inch diameter. The tested 1-inch diameter shaft was slightly detrimental to the system; it increased the RMS acceleration over that of the new cam and air cylinder used with the existing shaft and did not significantly decrease

peak accelerations. However, even with the slightly increased vibrations seen with the 1-inch shaft, the system still had a 54.8% reduction in vibrations as compared to the original system. Based on our engineering analysis, we believe our initial shaft design of 7/8 inch diameter should perform much better than the tested one inch shaft but we do not have test data to confirm this at present.

In combination with the shaft replacement it is important that the cam lever of the stripper linkage be set up such that the conrod is attached on the same side of the lever as are the follower and air spring. This, in combination with the new shaft, will increase the stiffness of the overall effective spring constant of the stripper system by 48%. But, just enlarging the stripper shaft, without also moving the conrod attachment to the same side as the other items will compromise the result, so these changes should only be made in combination.

As a side note, the dynamic behavior of the stabilizer linkage would also be improved by attaching its conrods on the same side of its cam lever as the other attachments.

Appendix A: Stiffness Model Calculations

Stripper Linkage

Back Lever

$m_l := .42403\,kg$ $\quad k_l := 9.97805\,10^6\,\frac{N}{m}$

$r_l := 92.08\,mm$ $\quad I_l := 1.1487\cdot 10^3\cdot kg\cdot mm^2$

Slide Lever (tooling lever)

$m_{sl} := .44133\,kg$ $\quad k_{sl} := 9.89903\,10^6\,\frac{N}{m}$

$r_{sl} := 104.87\,mm$ $\quad I_{sl} := 1.720\,10^3\,kg\cdot mm^2$

Shaft

$r_s := \frac{5}{16}\,in$ $\quad F_s := 500\,N$ $\quad x_s := r_l$ $\quad m_s := .27167\,kg$

$J_s := \frac{\pi}{2}\cdot r_s^4$ $\quad G_s := 80.8\cdot 10^9\,Pa$ $\quad L_s := 184.66\,mm$

$\phi := \frac{F_s\cdot x_s\cdot L_s}{J_s\cdot G_s}$ $\quad \phi = 0.017\,rad$ angular deflection in radians

G = shear mod of elasticity for material

$k_s := \frac{F_s}{x_s\cdot \sin(\phi)}$ $\quad k_s = 3.218\times 10^5\cdot\frac{N}{m}$

$k_{st} := \frac{G_s\cdot J_s}{L_s} = 2.728\times 10^3\,J$ $\quad I_m := 8.901\,kg\cdot mm^2$

$\omega := \sqrt{\frac{k_{st}}{I_m}} = 2.786\times 10^3\cdot\frac{rev}{s}$

Cam Lever

$k_{cl} := 978888\frac{N}{m}$

$m_{cl} := .96546\,kg$

$r_{cl} := 301.02\,mm$ $\quad I_{cl} := 1.001\cdot 10^4\,kg\cdot mm^2$

$a := 127\,mm$ ground to follower

$b := 174.02\,mm$ follower to conrod

$r_{cl} - a = 0.174\,m$

Connection Rod

$m_{cr} := .479475kg + 2 \cdot .0887 \cdot kg = 0.657kg$ $d_{cr} := 15.88mm$ $E_{cr} := 70 \cdot 10^{9} Pa$

$L_{cr} := 552.196mm$ $A_{cr} := d_{cr}^{2} \cdot \sqrt{3}$ $A_{cr} = 4.368 \times 10^{-4} m^{2}$

$k_{cr} := \frac{E_{cr} \cdot A_{cr}}{L_{cr}}$ $k_{cr} = 5.537 \times 10^{7} \cdot \frac{N}{m}$

Tooling

$m_t := 1.84332701bm = 0.836kg$ $E_{steel} := 206.8 \cdot 10^{9} Pa$

$A_t := 400mm^{2}$ $L_t := 120mm$

$k_t := \frac{E_{steel} \cdot A_t}{L_t}$ $k_t = 6.893 \times 10^{8} \cdot \frac{N}{m}$

Effective Masses

$m_{t.eff} := m_t$ $m_{t.eff} = 0.836kg$

$m_{cr.eff} := m_{cr}$ $m_{cr.eff} = 0.657kg$

$m_{cl.eff} := \frac{I_{cl}}{r_{cl}^{2}}$ $m_{cl.eff} = 0.11kg$

$m_{sl.eff} := \frac{I_{sl}}{r_{sl}^{2}}$ $m_{sl.eff} = 0.156kg$

$m_{l.eff} := \frac{I_l}{r_l^{2}}$ $m_{l.eff} = 0.135kg$

$m_f := 0.0993kg$

$m_b := m_{t.eff} + m_{sl.eff}$

$m_a := m_{l.eff} + m_{cr.eff} + m_{cl.eff}$

$m_b = 0.993\,kg$

$m_{ab} := m_a + \left(\frac{r_{sl}}{r_l}\right)^2 \cdot m_b$

$m_a = 0.903\,kg$

$m_{ab} = 2.19\,kg$

$m_{eff} := \left(\frac{r_{cl}}{a}\right)^2 \cdot m_{ab} + m_f$

$m_{eff} = 12.404\,kg$

$k_b := \left(\frac{1}{k_{sl}} + \frac{1}{k_t}\right)^{-1}$

$m_{eff} = 27.346\,lb$

$k_a := \left[\left(\frac{1}{k_s}\right) + \left(\frac{1}{k_l}\right) + \left(\frac{1}{k_{cr}}\right) + \left(\frac{1}{k_{cl}}\right)\right]^{-1}$

$k_{ab} := \left[\frac{1}{k_a} + \frac{1}{\left[\left(\frac{r_{sl}}{r_l}\right)^2 \cdot k_b\right]}\right]^{-1}$

$k_{ab} = 2.311 \times 10^5 \frac{kg}{s^2}$

$k_{eff} := \left(\frac{r_{cl}}{a}\right)^2 \cdot k_{ab}$

$k_{eff} = 1.299 \times 10^6 \cdot \frac{N}{m}$ $\quad k_{eff} = 7.415 \times 10^3 \cdot \frac{lbf}{in}$

$k_{tf} := k_t \cdot \left(\frac{r_{sl}}{r_l}\right)^2 \cdot \left(\frac{r_{cl}}{a}\right)^2$ $\quad k_{slf} := k_{sl} \cdot \left(\frac{r_{sl}}{r_l}\right)^2 \cdot \left(\frac{r_{cl}}{a}\right)^2$

$k_{sf} := k_s \cdot \left(\frac{r_{cl}}{a}\right)^2$ $\quad k_{lf} := k_l \cdot \left(\frac{r_{cl}}{a}\right)^2$ $\quad k_{crf} := k_{cr} \cdot \left(\frac{r_{cl}}{a}\right)^2$ $\quad k_{clf} := k_{cl} \cdot \left(\frac{r_{cl}}{a}\right)^2$

Summary

$$\begin{pmatrix} k_{tf} \\ k_{slf} \\ k_{sf} \\ k_{lf} \\ k_{crf} \\ k_{clf} \\ k_{eff} \end{pmatrix} = \begin{pmatrix} 5.023 \times 10^9 \\ 7.214 \times 10^7 \\ 1.808 \times 10^6 \\ 5.606 \times 10^7 \\ 3.111 \times 10^8 \\ 5.499 \times 10^6 \\ 1.299 \times 10^6 \end{pmatrix} \cdot \frac{N}{m} \qquad \begin{pmatrix} k_{tf} \\ k_{slf} \\ k_{sf} \\ k_{lf} \\ k_{crf} \\ k_{clf} \\ k_{eff} \end{pmatrix} = \begin{pmatrix} 2.868 \times 10^7 \\ 4.119 \times 10^5 \\ 1.032 \times 10^4 \\ 3.201 \times 10^5 \\ 1.776 \times 10^6 \\ 3.14 \times 10^4 \\ 7.415 \times 10^3 \end{pmatrix} \cdot \frac{lbf}{in}$$

Vacuum Linkage

Back Lever

$m_l := .8244\,kg$ $\quad k_l := 4.52489\times 10^6\,\frac{N}{m}$

$r_l := 173.04\,mm$ $\quad I_l := 7492.7075\,kg\cdot mm^2$

Slide Lever (tooling lever)

$m_{sl} := .5285\,kg$ $\quad k_{sl} := 5.52792\times 10^6\,\frac{N}{m}$

$r_{sl} := 136.58\,mm$ $\quad I_{sl} := 3244.3476\,kg\cdot mm^2$

Shaft

$r_s := \frac{5}{16}\cdot in$ $\quad L_s := 179.83\,mm$ $\quad F_s := 500\,N$ $\quad x_s := r_l$

$m_s := 0.2582\,kg$ $\quad G_s := 80.8\cdot 10^9\,Pa$ $\quad J_s := \frac{\pi\cdot r_s^4}{2}$

$$\phi := \frac{F_s\cdot x_s\cdot L_s}{J_s\cdot G_s} = 0.031$$

$$k_s := \frac{F_s}{x_s\cdot\sin(\phi)} = 9.358\times 10^4\cdot\frac{N}{m}$$

$k_{st} := \frac{G_s\cdot J_s}{L_s} = 2.802\times 10^3\,J$ $\quad I_m := 8.4679\,kg\cdot mm^2$

$\omega := \sqrt{\frac{k_{st}}{I_m}} = 2.895\times 10^3\cdot\frac{rev}{s}$

Cam Lever

$k_{clm} := 1.18606\,10^6\,\frac{N}{m}$ $\quad m_{cl} := 1.064\,kg$ $\quad k_{cl} := k_{clm}$

$r_{cl} := 287.655\,mm$ $\quad I_{cl} := 3.28696651\,10^4\,kg\cdot mm^2$ $\quad a := 127\,mm$ ground to follower

$k_{cl} = 1.186\times 10^6\cdot\frac{N}{m}$ $\quad b := 0.161\,m$ follower to conrod

$r_{cl} - a = 0.161\,m$

Connection Rod

$m_{cr} := .41148\,kg$ $\quad d_{cr} := 15.88\,mm$ $\quad E_{cr} := 71.7\cdot 10^9\,Pa$

$L_{cr} := 415.843mm$ $A_{cr} := d_{cr}^2 \cdot \sqrt{3}$ $A_{cr} = 4.368 \times 10^{-4} m^2$

$k_{cr} := \frac{E_{cr} \cdot A_{cr}}{L_{cr}}$ $k_{cr} = 7.531 \times 10^7 \cdot \frac{N}{m}$

Air Cylinder

$m_{ac} := .16209kg$

$d_{cylinder} := 20mm$ $L_{cylinder} := 10mm$

$d_{tube} := 0.004m$ $L_{tube} := 1m$

$P := 4530Pa$

$x := 0.00718mm$

$A_{cylinder} := \frac{\pi \cdot d_{cylinder}^2}{4} = 314.159mm^2$

$k_{ac} := \frac{P \cdot A_{cylinder}}{x} = 1.982 \times 10^5 \frac{kg}{s^2}$

Tooling

$m_t := 0.943662688kg$ $E_{steel} := 206.8 10^9 Pa$

$A_t := 400mm^2$ $L_t := 120mm$

$k_t := \frac{E_{steel} \cdot A_t}{L_t}$ $k_t = 6.893 \times 10^8 \cdot \frac{N}{m}$

Effective Masses

$m_{t.eff} := m_t$ $m_{t.eff} = 0.944kg$

$m_{cr.eff} := m_{cr}$

$m_{cl.eff} := \frac{I_{cl}}{r_{cl}^2}$

$m_{cl.eff} = 0.397kg$

$$m_{sl.eff} := \frac{I_{sl}}{r_{sl}^{2}}$$

$m_{sl.eff} = 0.174kg$

$$m_{l.eff} := \frac{I_{l}}{r_{l}^{2}}$$

$m_{l.eff} = 0.25kg$

$$m_{ac.eff} := m_{ac}$$

$$m_{b} := m_{t.eff} + m_{sl.eff}$$

$$m_{a} := m_{l.eff} + m_{cr.eff} + m_{cl.eff} + m_{ac.eff}$$

$$m_{ab} := m_{a} + \left(\frac{r_{sl}}{r_{l}}\right)^{2} \cdot m_{b}$$

$m_{ab} = 1.917kg$

$$m_{eff} := \left(\frac{r_{cl}}{a}\right)^{2} \cdot m_{ab}$$

$m_{eff} = 9.836kg$

$m_{eff} = 21.685lb$

$$k_{b} := \left(\frac{1}{k_{sl}} + \frac{1}{k_{t}}\right)^{-1}$$

$$k_{a} := \left[\left(\frac{1}{k_{s}}\right) + \left(\frac{1}{k_{l}}\right) + \left(\frac{1}{k_{cr}}\right) + \left(\frac{1}{k_{cl}}\right) + \left(\frac{1}{k_{ac}}\right)\right]^{-1}$$

$$k_{ab} := \left[\frac{1}{k_{a}} + \frac{1}{\left[\left(\frac{r_{sl}}{r_{l}}\right)^{2} \cdot k_{b}\right]}\right]^{-1}$$

$k_{a} = 5.949 \times 10^{4} \frac{kg}{s^{2}}$

$k_{b} = 5.484 \times 10^{6} \frac{kg}{s^{2}}$

$k_{s} = 9.358 \times 10^{4} \frac{kg}{s^{2}}$

$$k_{eff} := \left(\frac{r_{cl}}{a}\right)^{2} \cdot k_{ab}$$

$k_{eff} = 3 \times 10^{5} \cdot \frac{N}{m}$

$$k_{tf} := k_{t} \cdot \left(\frac{r_{sl}}{r_{l}}\right)^{2} \cdot \left(\frac{r_{cl}}{a}\right)^{2} \qquad k_{slf} := k_{sl} \cdot \left(\frac{r_{sl}}{r_{l}}\right)^{2} \cdot \left(\frac{r_{cl}}{a}\right)^{2} \qquad k_{acf} := k_{ac} \cdot \left(\frac{r_{cl}}{a}\right)^{2}$$

$$k_{sf} := k_s \cdot \left(\frac{r_{cl}}{a}\right)^2 \qquad k_{lf} := k_l \cdot \left(\frac{r_{cl}}{a}\right)^2 \qquad k_{crf} := k_{cr} \cdot \left(\frac{r_{cl}}{a}\right)^2 \qquad k_{clf} := k_{cl} \cdot \left(\frac{r_{cl}}{a}\right)^2$$

Summary

$$\begin{pmatrix} k_{tf} \\ k_{slf} \\ k_{sf} \\ k_{lf} \\ k_{crf} \\ k_{clf} \\ k_{acf} \\ k_{eff} \end{pmatrix} = \begin{pmatrix} 2.203 \times 10^{9} \\ 1.767 \times 10^{7} \\ 4.801 \times 10^{5} \\ 2.321 \times 10^{7} \\ 3.864 \times 10^{8} \\ 6.085 \times 10^{6} \\ 1.017 \times 10^{6} \\ 3 \times 10^{5} \end{pmatrix} \cdot \frac{N}{m} \qquad \begin{pmatrix} k_{tf} \\ k_{slf} \\ k_{sf} \\ k_{lf} \\ k_{crf} \\ k_{clf} \\ k_{acf} \\ k_{eff} \end{pmatrix} = \begin{pmatrix} 1.258 \times 10^{7} \\ 1.009 \times 10^{5} \\ 2.741 \times 10^{3} \\ 1.326 \times 10^{5} \\ 2.206 \times 10^{6} \\ 3.474 \times 10^{4} \\ 5.806 \times 10^{3} \\ 1.713 \times 10^{3} \end{pmatrix} \cdot \frac{lbf}{in}$$

Stabilizer Linkage

Back Lever

$m_l := .90798\,kg$ $\qquad k_l := 3.04878\times 10^6\,\frac{N}{m}$

$r_l := 198.9\,mm$ $\qquad I_l := 10855.569\,kg\cdot mm^2$

Slide Lever (tooling lever)

$m_{sl} := .3053987\,kg$ $\qquad k_{sl} := 2.4727992\times 10^7\,\frac{N}{m}$

$r_{sl} := 73.78\,mm$ $\qquad I_{sl} := 555.4404\,kg\cdot mm^2$

Shaft

$r_s := \frac{5}{16}\cdot in$ $\qquad m_s := 0.1337613\,kg$

$F_s := 500\,N$ $\qquad x_s := r_l$

$J_s := \frac{\pi}{2}\cdot r_s^4$ $\qquad G_s := 80.8\cdot 10^9\,Pa$ $\qquad L_s := 101.35\,mm$

$\phi := \frac{F_s\cdot x_s\cdot L_s}{J_s\cdot G_s}$ $\qquad \phi = 0.02\,rad$ angular deflection in radians

G = shear mod of elasticity for material

$k_s := \frac{F_s}{x_s\cdot\sin(\phi)}$ $\qquad k_s = 1.257\times 10^5\cdot\frac{N}{m}$

$k_{st} := \frac{G_s\cdot J_s}{L_s} = 4.971\times 10^3\cdot J$ $\qquad I_m := 4.55\,kg\cdot mm^2$

$\omega := \sqrt{\frac{k_{st}}{I_m}} = 5.261\times 10^3\cdot\frac{rev}{s}$

Cam Lever

with maluable cast iron

$k_{clm} := 1.4817910^6\,\frac{N}{m}$ $\qquad k_{clm} = 1.482\times 10^6\cdot\frac{N}{m}$

$m_{cl} := 1.0916879\,kg$ $\qquad k_{cl} := k_{clm}$ $\qquad a := 127\,mm$ ground to follower

$b := 0.156\,m$ follower to conrod

$r_{cl} := 282.905mm$ $I_{cl} := 2.99344301 \cdot 10^{4} kg \cdot mm^2$ $r_{cl} - a = 0.156m$

Connection Rod

$m_{cr} := .479475kg$ $d_{cr} := 15.88mm$ $E_{cr} := 70 \cdot 10^{9} Pa$

$L_{cr} := 519.18mm$ $A_{cr} := d_{cr}^{2} \cdot \sqrt{3}$ $A_{cr} = 4.368 \times 10^{-4} m^2$

$k_{cr} := \frac{E_{cr} \cdot A_{cr}}{L_{cr}}$ $k_{cr} = 5.889 \times 10^{7} \cdot \frac{N}{m}$

Tooling

$m_t := 1.0674079kg + .05923231kg$ $E_{steel} := 206.8 \cdot 10^{9} Pa$

$A_t := 400mm^2$ $L_t := 120mm$

$k_t := \frac{E_{steel} \cdot A_t}{L_t}$ $k_t = 6.893 \times 10^{8} \cdot \frac{N}{m}$

Effective Masses

$m_{t.eff} := m_t$ $m_{t.eff} = 1.127kg$

$m_{cr.eff} := m_{cr}$

$m_{cl.eff} := \frac{I_{cl}}{r_{cl}^{2}}$ $m_{cl.eff} = 0.374kg$

$m_{sl.eff} := \frac{I_{sl}}{r_{sl}^{2}}$ $m_{sl.eff} = 0.102kg$

$m_{l.eff} := \frac{I_l}{r_l^{2}}$ $m_{l.eff} = 0.274kg$

$m_b := m_{t.eff} + m_{sl.eff}$

$m_a := m_{l.eff} + m_{cr.eff} + m_{cl.eff}$

$m_{ab} := m_a + \left(\frac{r_{sl}}{r_l} \right)^{2} \cdot m_b$

$m_{ab} = 1.297\,kg$

$$m_{eff} := \left(\frac{r_{cl}}{a}\right)^2 \cdot m_{ab}$$

$m_{eff} = 6.436\,kg$

$$k_b := \left(\frac{1}{k_{sl}} + \frac{1}{k_t}\right)^{-1}$$

$m_{eff} = 14.188\,lb$

$$k_a := \left[\left(\frac{1}{k_s}\right) + \left(\frac{1}{k_l}\right) + \left(\frac{1}{k_{cr}}\right) + \left(\frac{1}{k_{cl}}\right)\right]^{-1}$$

$$k_{ab} := \left[\frac{1}{k_a} + \frac{1}{\left[\left(\frac{r_{sl}}{r_l}\right)^2 \cdot k_b\right]}\right]^{-1}$$

$k_{ab} = 1.077\times 10^5 \frac{kg}{s^2}$

$$k_{eff} := \left(\frac{r_{cl}}{a}\right)^2 \cdot k_{ab}$$

$k_{eff} = 5.346\times 10^5 \cdot \frac{N}{m}$

$k_{eff} = 3.053\times 10^3 \cdot \frac{lbf}{in}$

$$k_{tf} := k_t \cdot \left(\frac{r_{sl}}{r_l}\right)^2 \cdot \left(\frac{r_{cl}}{a}\right)^2 \qquad k_{slf} := k_{sl} \cdot \left(\frac{r_{sl}}{r_l}\right)^2 \cdot \left(\frac{r_{cl}}{a}\right)^2$$

$$k_{sf} := k_s \cdot \left(\frac{r_{cl}}{a}\right)^2 \qquad k_{lf} := k_l \cdot \left(\frac{r_{cl}}{a}\right)^2 \qquad k_{crf} := k_{cr} \cdot \left(\frac{r_{cl}}{a}\right)^2 \qquad k_{clf} := k_{cl} \cdot \left(\frac{r_{cl}}{a}\right)^2$$

Summary

$$\begin{pmatrix} k_{tf} \\ k_{slf} \\ k_{sf} \\ k_{lf} \\ k_{crf} \\ k_{clf} \\ k_{eff} \end{pmatrix} = \begin{pmatrix} 4.707\times 10^8 \\ 1.688\times 10^7 \\ 6.236\times 10^5 \\ 1.513\times 10^7 \\ 2.922\times 10^8 \\ 7.353\times 10^6 \\ 5.346\times 10^5 \end{pmatrix} \cdot \frac{N}{m}$$

$$\begin{pmatrix} k_{tf} \\ k_{slf} \\ k_{sf} \\ k_{lf} \\ k_{crf} \\ k_{clf} \\ k_{eff} \end{pmatrix} = \begin{pmatrix} 2.688\times 10^6 \\ 9.641\times 10^4 \\ 3.561\times 10^3 \\ 8.639\times 10^4 \\ 1.669\times 10^6 \\ 4.199\times 10^4 \\ 3.053\times 10^3 \end{pmatrix} \cdot \frac{lbf}{in}$$

Appendix B: Frame Safety of Factor Calculations

frame material: class 40 cast iron low temp anneal

$\sigma_{yeild} := 324 \cdot 10^6 Pa$ $\sigma_{ult} := 448 \cdot 10^6 Pa$

Maximum Force

based on 100g accelerations

$m_{opeff} := 0.993 kg$ $m_{beff} := .903 kg$

$m_t := m_{beff} + m_{opeff}$

$a_{omax} := 100 g$ $a_{bmax} := 100 g$

$f_b := (a_{bmax} + 1g) \cdot m_{beff}$ $f_b = 894.396 N$

$f_o := (a_{omax} + 1g) \cdot m_{opeff}$ $f_o = 983.538 N$

$F_a := m_{opeff} \cdot a_{omax} + m_{beff} \cdot a_{bmax} + m_t \cdot g$

$F_a = 1.878 \times 10^3 N$ $F_a = 422.176 lbf$

Geometry

$width := 2 \cdot 25.4 mm$

effective width = width where bushings are acting.

$r_s := \frac{25.4}{2} mm$ $r_o := \frac{44.45}{2} mm$

for tear out failure

$r_i := \frac{\left(1 + \frac{3}{8}\right)}{2} in$ $r_i = 0.017 m$

$\frac{21.69}{2} = 10.845$

$10.845 + 3.185 = 14.03$

$wallthickness := r_o - r_i$ $wallthickness = 4.763 mm$

$\frac{30.25}{2} = 15.125$

$3.185 + 15.125 = 18.31$

$A_{to} := width \cdot 2 \cdot \sqrt{r_o^2 - r_i^2}$ $A_{to} = 1.397 \times 10^{-3} m^2$

$A_{tension} := 2 \cdot width \cdot (r_o - r_i)$ $A_{tension} = 4.839 \times 10^{-4} m^2$

Fatigue

$S_{ut} := 65\,ksi$

load := "axial" surface := "as_cast"

R := 0.9999 T := 72 $ksi := 10^3 psi$

$$S'_e := \begin{cases} \text{return } 0.5 \cdot S_{ut} \text{ if } S_{ut} \le 200 \cdot ksi \\ 100 \cdot ksi \text{ otherwise} \end{cases}$$

$S'_e = 32.5\,ksi$

Load

$$C_{load} := \begin{cases} \text{return } 1 \text{ if load} = \text{"bending"} \\ \text{return } 1 \text{ if load} = \text{"torsion"} \\ \text{return } 0.7 \text{ if load} = \text{"axial"} \end{cases}$$

$C_{load} = 0.7$

Surface

$C_{surf} := 1$

Temperature

$$C_{temp} := \begin{cases} \text{return } 1 \text{ if } T \le 840 \\ 1 - 0.0032 \cdot (T - 840) \text{ otherwise} \end{cases}$$

$C_{temp} = 1$

Reliability

$$C_{reliab} := \begin{cases} \text{return } 1.000 \text{ if } R = 0.50 \\ \text{return } 0.897 \text{ if } R = 0.90 \\ \text{return } 0.814 \text{ if } R = 0.99 \\ \text{return } 0.753 \text{ if } R = 0.999 \\ \text{return } 0.702 \text{ if } R = 0.9999 \\ \text{return } 0.659 \text{ if } R = 0.99999 \end{cases}$$

$C_{reliab} = 0.659$

Size

$A_{95} := A_{to}$

$$d_{equiv} := \sqrt{\frac{A_{95}}{.0766}}$$

$$C_{sizeto} := 0.869 \left(\frac{d_{equiv}}{m} \right)^{-0.097}$$

$C_{sizeto} = 1.055$

Size

$A_{95} := A_{tension}$

$d_{equiv} := \sqrt{\frac{A_{95}}{.0766}}$

$C_{sizet} := 0.869\left(\frac{d_{equiv}}{m}\right)^{-0.097}$ $C_{sizet} = 1.111$

$C_{size} := \min\left(C_{sizet}, C_{sizeto}, 1\right)$ $C_{size} = 1$

$S_e := C_{load} \cdot C_{size} \cdot C_{surf} \cdot C_{temp} \cdot C_{reliab} \cdot S'_e$ $S_e = 14.992\,ksi$

$\tau_{frame} := \frac{F_a}{A_{to}}$ $\tau_{frame} = 1.344 \times 10^6\,Pa$

$\sigma_t := \frac{F_a}{A_{tension}}$ $\sigma_t = 3.881 \times 10^6\,Pa$

$\sigma_x := \frac{\sigma_t}{Pa}$ $\sigma_z := 0$

$\tau_{xz} := 0$ $\tau_{xy} := \frac{\tau_{frame}}{Pa}$

$\sigma_y := 0$ $\tau_{yz} := 0$

$$S := \begin{pmatrix} \sigma_x & \tau_{xy} & \tau_{xz} \\ \tau_{xy} & \sigma_y & \tau_{yz} \\ \tau_{xz} & \tau_{yz} & \sigma_z \end{pmatrix}$$

$C_2 := \sigma_x + \sigma_y + \sigma_z$

$$C_1 := \left|\begin{pmatrix} \sigma_x & \tau_{xy} \\ \tau_{xy} & \sigma_y \end{pmatrix}\right| + \left|\begin{pmatrix} \sigma_x & \tau_{xz} \\ \tau_{xz} & \sigma_z \end{pmatrix}\right| + \left|\begin{pmatrix} \sigma_y & \tau_{yz} \\ \tau_{yz} & \sigma_z \end{pmatrix}\right| \qquad C_1 = -1.808 \times 10^{12}$$

$C_0 := |S|$

$C_0 = 0$

$C := \begin{pmatrix} -C_0 \\ C_1 \\ -C_2 \\ 1 \end{pmatrix}$ $\begin{pmatrix} \sigma_3 \\ \sigma_2 \\ \sigma_1 \end{pmatrix} :=$ polyroots (C)

$$\begin{pmatrix} \sigma_3 \\ \sigma_2 \\ \sigma_1 \end{pmatrix} = \begin{pmatrix} -4.202 \times 10^5 \\ 0 \\ 4.301 \times 10^6 \end{pmatrix}$$

$\sigma_1 = 4.301 \times 10^6$ $\sigma_2 = 0$ $\sigma_3 = -4.202 \times 10^5$

$$S = \begin{pmatrix} 3.881 \times 10^6 & 1.344 \times 10^6 & 0 \\ 1.344 \times 10^6 & 0 & 0 \\ 0 & 0 & 0 \end{pmatrix}$$

$\tau_{13} := \frac{|\sigma_1 - \sigma_3|}{2}$ $\tau_{21} := \frac{|\sigma_2 - \sigma_1|}{2}$ $\tau_{32} := \frac{|\sigma_3 - \sigma_2|}{2}$

$\tau_{13} = 2.361 \times 10^6$ $\tau_{21} = 2.151 \times 10^6$ $\tau_{32} = 2.101 \times 10^5$

all stresses are in Pa

$\tau_{max} := \max(\tau_{13}, \tau_{21}, \tau_{32})$

$\sigma_{vm} := \sqrt{\sigma_1^2 + \sigma_2^2 + \sigma_3^2 - \sigma_1 \cdot \sigma_2 - \sigma_2 \cdot \sigma_3 - \sigma_1 \cdot \sigma_3}$

$\sigma_{vm} = 4.526 \times 10^6$ Pa

$$\sigma_{vm2} := \sqrt{\frac{(\sigma_x - \sigma_y)^2 + (\sigma_y - \sigma_z)^2 + (\sigma_z - \sigma_x)^2 + 6 \cdot (\tau_{xy}^2 + \tau_{yz}^2 + \tau_{xz}^2)}{2}}$$

$\sigma_{vm2} = 4.526 \times 10^6$ Pa

$scf := 4$

Assume a Geometric and material defect stress concentration factor of 5

$S_e = 1.499 \times 10^4 \cdot psi$

$K_{safety} := \frac{S_e}{scf \cdot \sigma_{vm} \cdot Pa}$ $K_{safety} = 5.71$ $S_e = 1.034 \times 10^8 \, Pa$

$K_s := \frac{.5 \cdot S_e}{scf \cdot \tau_{max} \cdot Pa}$ $K_s = 5.473$ $\frac{S_e}{7.7 \cdot 10^5 Pa} = 134.244$

Minimum Safety factor from Maximum realistic loading conditions outward with diameter of 1 3/8 for a shaft diameter of 1 inch

$k_f := \frac{375N}{1.74 \cdot 10^{-5} m} = 2.155 \times 10^7 \cdot \frac{N}{m}$

$k_f = 1.231 \times 10^5 \cdot \frac{lbf}{in}$

$K_{sFEA} := \frac{S_e}{3.655 \cdot 10^6 Pa} = 28.281$

$Kmin_{sFEA} := \frac{S_e}{1.71 \cdot 10^7 Pa} = 6.045$

$Kmin_{sFEA} := \frac{S_e}{2.026 \cdot 10^7 Pa} = 5.102$

$Kmin_{sFEA} := \frac{S_e}{3.059 \cdot 10^7 Pa} = 3.379$

$Kmin_{sFEA} := \frac{S_e}{1.198 \cdot 10^7 Pa} = 8.628$

Minimum Safety factor from Maximum realistic loading conditions outward with diameter of 1 3/8 for a shaft diameter of 1 inch With air cylinder forces considered

$$Kmin_{sFEA} := \frac{S_e}{1.895 \cdot 10^7 \, Pa} = 5.455$$

$$Kmin_{sFEA} := \frac{S_e}{2.377 \cdot 10^7 \, Pa} = 4.349$$

$$Kmin_{sFEA} := \frac{S_e}{3.334 \cdot 10^7 \, Pa} = 3.1$$

$$Kmin_{sFEA} := \frac{S_e}{1.196 \cdot 10^7 \, Pa} = 8.643$$

Appendix C: FEA Procedure Using Solidworks

To get an accurate calculation of the spring constant for the levers, the boundary conditions, constraints, and loading conditions should accurately represent the types of loading on the levers. The following steps explain how to perform an accurate finite element analysis on the levers to determine the displacement under the loading and, ultimately, the spring constant.

Step 1: Load the ProE part into SolidWorks

Open the file from SolidWorks and make sure to import material properties, sketch/curve entities, and geometry from hidden sections on the window that pops up.

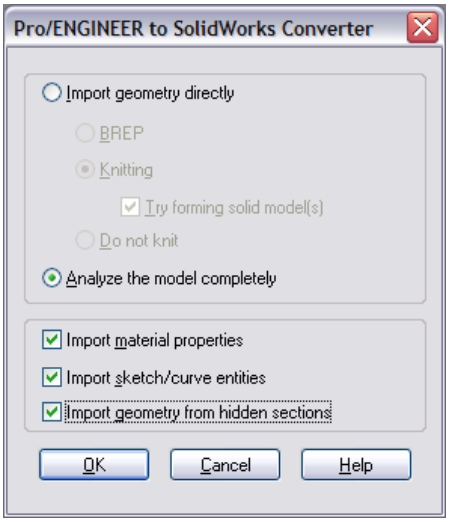

Import the model as a body.

Step 2: Create a Study

Open COSMOSWorks by going to Tools>Add Ins and check the box next to COSMOSWorks.

Right-click on the name of the part and create a Static Study from the COSMOSWorks toolbar:

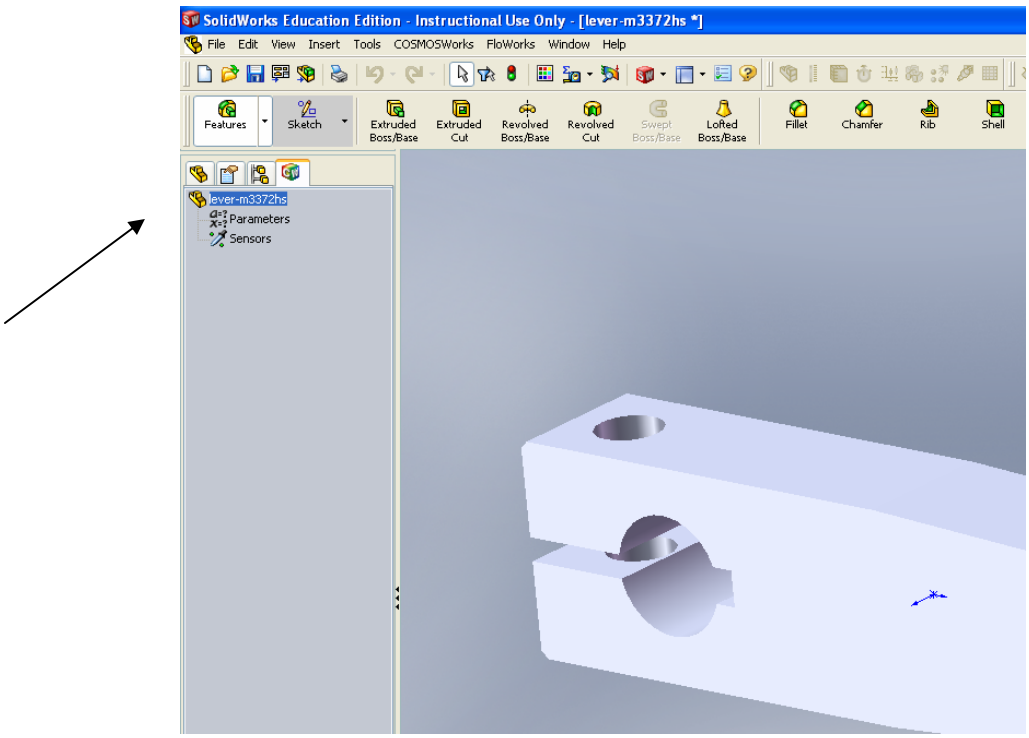

Step 3: Apply Material

Under the Study, right-click on Solids and apply the material to the part:

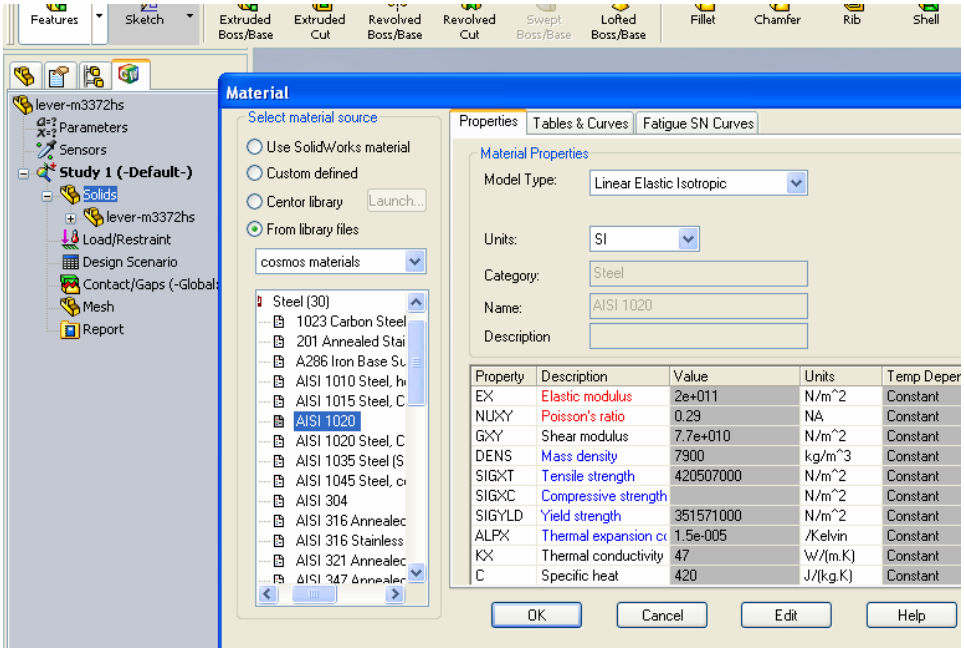

Step 4: Apply Restraints and Loading

One end of our lever is attached to a shaft. The lever does not rotate around the shaft due to a key so we use a fixed restraint on that end of the lever. To create a fixed restraint, right-click on Load/Restraint and select Restraints. Then make sure the Fixed is selected as a type of restraint and then select the two inside faces of the hole which contact the shaft, as shown below in green.

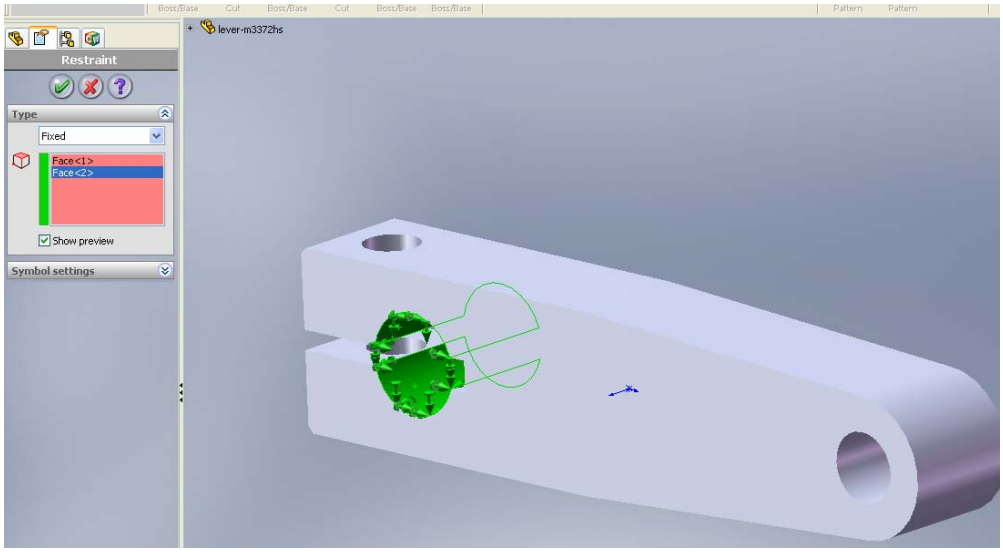

The force acting on this lever is transmitted through a pin so the pin feature needs to be created on the lever. To apply a load, a point and a coordinate system also needs to be created. After these features are created, apply a load by right-clicking on Load/Restraint and selecting Bearing Load. Apply this load on the outside surface of the pin and direct the load in the proper direction by selecting the coordinate system. Also make a note of what value you select for the force because this force will be used along with the displacement to calculate the spring constant.

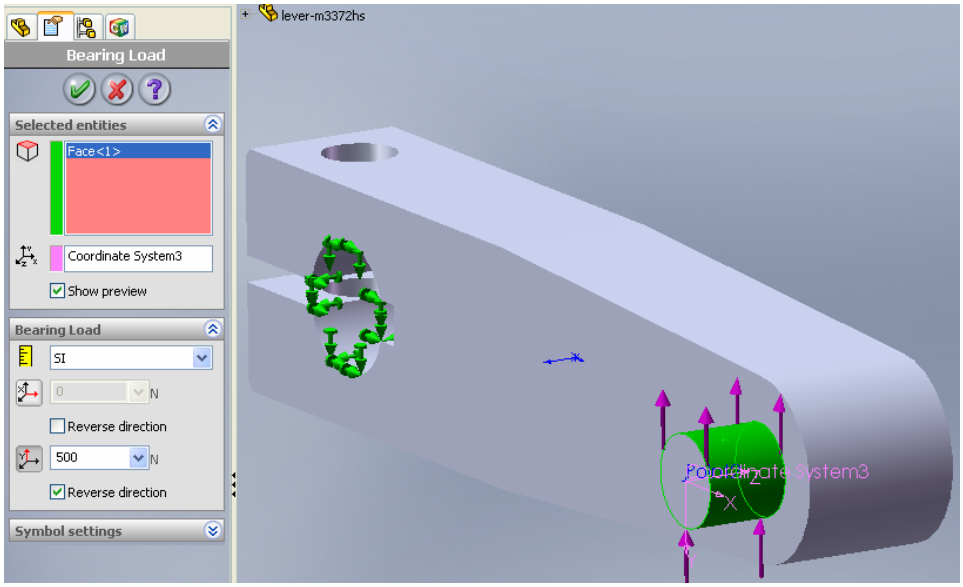

Step 5: Run the Analysis

After applying restraints and loading conditions, run the analysis by right-clicking on Mesh and selecting “Mesh and Run”. After the analysis is complete, there are several options that become available for viewing the results. To view the displacement results, right-click on Results and select “Define Displacement Plot”. Then Select the resultant displacement and units of displacement and select ok to see a plot similar to the one below:

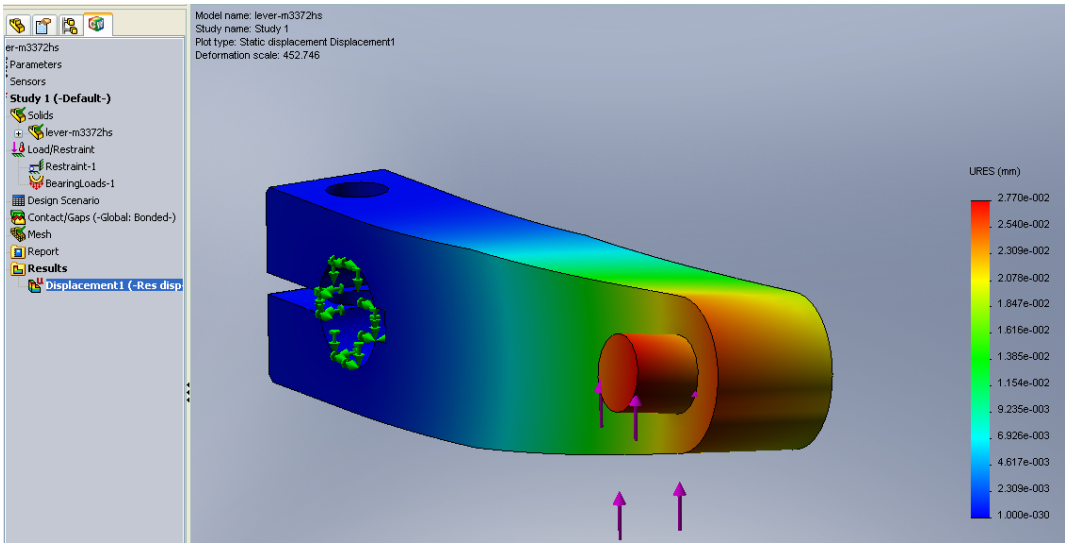

Use the maximum displacement value and the force that was applied to calculate the spring constant of the lever.

Cam Lever Restraints and Loading

The cam levers are under different loading than the lever above. The figure below shows the cam lever restraints and loadings.

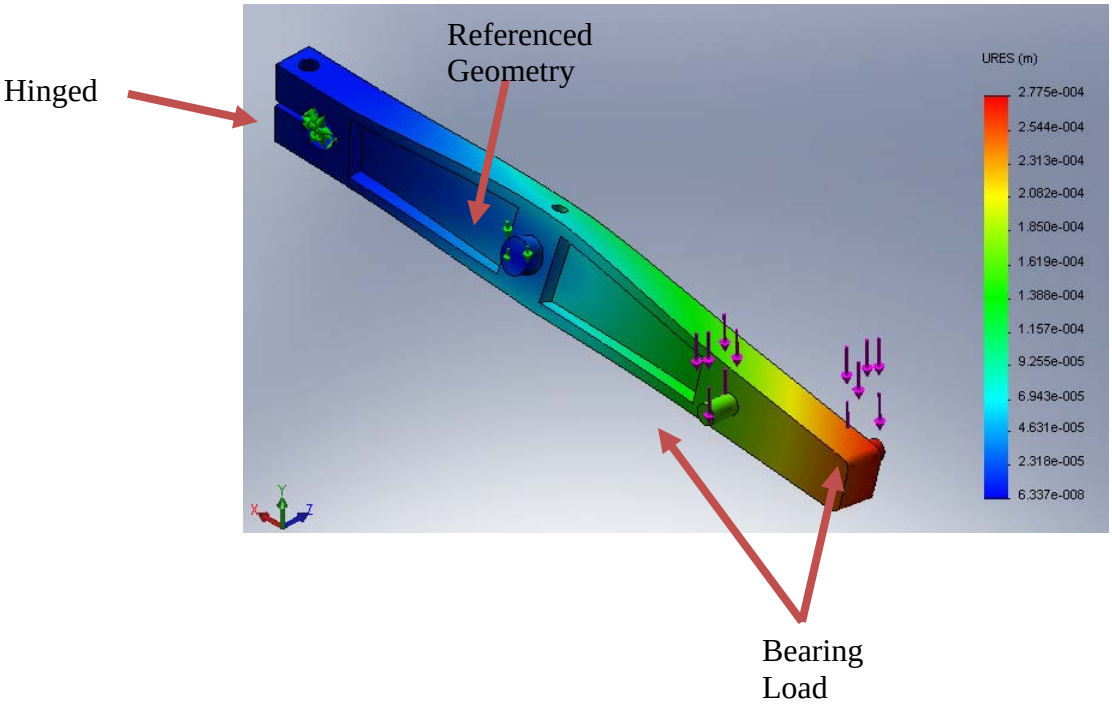

Hinged: This restraint allows rotation of the lever about only one axis. This is like having a lever connected to a support but the lever is free to rotate. This accurately represents the connection of the lever in reality which is connected to a grounded support but is free to rotate about that support.

Referenced Geometry: This restraint allows rotation about any axis but prevents translation in the vertical plane. This restraint accurately represents the connection of the roller follower to the cam. The cam is connected to the follower at a point and it keeps it from translating vertically

except to follow the cam profile. Because this is a static analysis, the follower does not translate vertically but is free to deform in any direction under the loading.

Bearing Load: This is the loading on the lever due to the air spring keeping the follower on the cam and due to the connecting rod.

To find the spring constant for the cam levers, the displacement (call it d1) is found with no load from the connecting rod and with only the load from the air spring (call it F1). Then the displacement (call it d2) is found with the addition of the connecting rod load (call it F2). The spring constant is F2/(d2-d1).